AD-A190 198 RESEARCH INVESTIGATION DIRECTED TOWARD EXTENDING THE USEFUL RANGE OF THE ELECTROMAGNETIC SPECTRUM(U) COLUMBIA RADIATION LAB NEW YORK G W FLYNN ET AL 1/2

UNCLASSIFIED 31 DEC 87 DAAG29-85-K-0049 F/G 17/5 NL

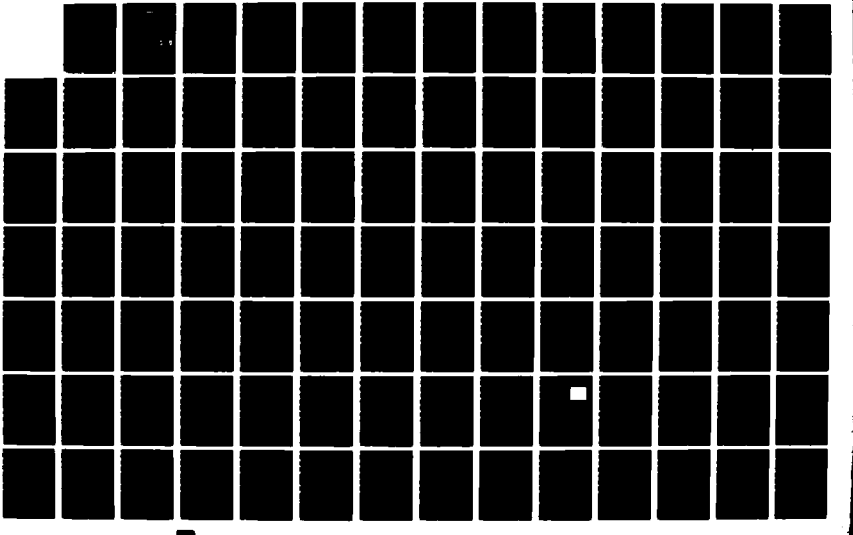

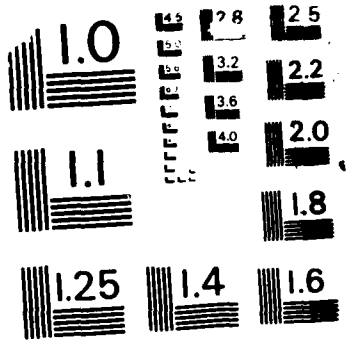

CRL

COLUMBIA UNIVERSITY

DEPARTMENTS OF PHYSICS,
CHEMISTRY, ELECTRICAL ENGINEERING

★ ANNUAL REPORT NO. 37

October 1, 1986–September 30, 1987

CONTRACT DAAG29-85-K-0049

APPROVED FOR PUBLIC RELEASE: DISTRIBUTION UNLIMITED

TO:

THE JOINT SERVICES TECHNICAL ADVISORY COMMITTEE

REPRESENTING: THE U.S. ARMY RESEARCH OFFICE
THE OFFICE OF NAVAL RESEARCH
THE AIR FORCE OFFICE OF SCIENTIFIC RESEARCH

COLUMBIA RADIATION LABORATORY, NEW YORK, NEW YORK 10027

★ December 31, 1987

COLUMBIA RADIATION LABORATORY

RESEARCH INVESTIGATION DIRECTED TOWARD EXTENDING THE USEFUL RANGE OF THE ELECTROMAGNETIC SPECTRUM

Progress Report No. 37

October 1, 1986 through September 30, 1987

Contract DAAG29-85-K-0049

Object of the Research:

Basic research in the fields of quantum electronics; electromagnetic propagation, detection and sending; and solid state electronics.

The research reported in this document was made possible through support extended the Columbia Radiation Laboratory, Columbia University, by the Joint Services Electronics Program (U.S. Army Research Office, Office of Naval Research, and the Air Force Office of Scientific Research) under Contract DAAG29-85-K-0049.

Submitted By: George W. Flynn and Richard M. Osgood, Jr.
Co-Directors

Coordinated By: Karen Wingate, Departmental Administrator
Cynthia Leslie, Administrative Aide
Barbara Blegen, Secretary

COLUMBIA UNIVERSITY
Columbia Radiation laboratory
Department of Physics
New York, New York 10027

December 31, 1987

RESEARCH SUPPORT

The research reported in this document was made possible through support extended to the Columbia Radiation Laboratory, Columbia University, by the **Joint Services Electronics Program** (U.S. Army Research Office, Office of Naval Research, and the Air Force Office of Scientific Research) under Contract DAAG29-85-K-0049.

Portions of this work were also supported by:

Air Force Office of Scientific Research

Contract AFOSR-84-00138
Contract AFOSR-30602-85-C-0072
Contract AFOSR-88-0014
Contract F-49620-85-C-0067

Army Research Office

Contract DAAG29-85-K-0210

National Science Foundation

Grant NSF-CHE 85-17460
Grant NSF-ECE 82-19636
Grant NSF-CDR 84-21402
Grant NSF-CHE 85-13553
Grant NSF-PYI-ECS-85-52572

Office of Naval Research

Contract N00014-78-C-0154
Contract N00014-78-C-0517
Contract N00014-86-K-0694

Department of Energy

Contract DE-AC02-78-ER-04940

Semiconductor Research Corporation

Project SRC-85-02-055

The support of these agencies is acknowledged in the text.

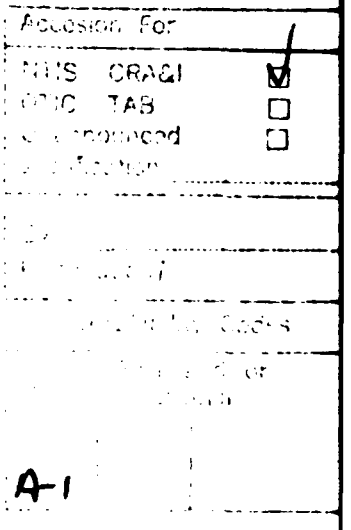

SECURITY CLASSIFICATION OF THIS PAGE

REPORT DOCUMENTATION PAGE

1a. REPORT SECURITY CLASSIFICATION Unclassified	1b. RESTRICTIVE MARKINGS
2a. SECURITY CLASSIFICATION AUTHORITY	3. DISTRIBUTION / AVAILABILITY OF REPORT Approved for Public Release; Distribution Unlimited
2b. DECLASSIFICATION / DOWNGRADING SCHEDULE	
4. PERFORMING ORGANIZATION REPORT NUMBER(S) Annual Report No. 37	5. MONITORING ORGANIZATION REPORT NUMBER(S)
6a. NAME OF PERFORMING ORGANIZATION Columbia University Radiation Laboratory 6b. OFFICE SYMBOL (*If applicable*)	7a. NAME OF MONITORING ORGANIZATION Department of the Army
6c. ADDRESS (*City, State, and ZIP Code*) Columbia Radiation Laboratory Columbia University New York, NY 10027	7b. ADDRESS (*City, State, and ZIP Code*) U.S. Army Research Office Research Triangle Park, NC 27709
8a. NAME OF FUNDING / SPONSORING ORGANIZATION Department of the Army 8b. OFFICE SYMBOL (*If applicable*)	9. PROCUREMENT INSTRUMENT IDENTIFICATION NUMBER DAAG29-85-K-0049
8c. ADDRESS (*City, State, and ZIP Code*) U.S. Army Research Office Research Triangle Park, NC 27709	10. SOURCE OF FUNDING NUMBERS PROGRAM ELEMENT NO. / PROJECT NO. / TASK NO. / WORK UNIT ACCESSION NO.

11. TITLE (*Include Security Classification*)
RESEARCH INVESTIGATION DIRECTED TOWARD EXTENDING THE USEFUL RANGE OF THE ELECTROMAGNETIC SPECTRUM

12. PERSONAL AUTHOR(S)
George W. Flynn, Richard M. Osgood, Jr.

13a. TYPE OF REPORT	13b. TIME COVERED	14. DATE OF REPORT (*Year, Month, Day*)	15. PAGE COUNT
Annual	FROM 10/1/86 TO 9/30/87	December 31, 1987	

16. SUPPLEMENTARY NOTATION

17. COSATI CODES			18. SUBJECT TERMS (*Continue on reverse if necessary and identify by block number*)
FIELD	GROUP	SUB-GROUP	photon-number-squeezed light theory of light detection excess noise factor

19. ABSTRACT (*Continue on reverse if necessary and identify by block number*)

The usual semiclassical theory of light detection has been demonstrated to be valid only in the absence of feedback from detector to source. A revised theory has been developed that is valid even in the presence of such feedback. Research has begun on the possibility of using various heterostructures (including quantum-well devices) that might serve as solid-state versions of the space-charge-limited Franck-Hertz experiment (this experiment produced the first source of cw photon-number-squeezed light, reported in 1985.)

20. DISTRIBUTION / AVAILABILITY OF ABSTRACT	21. ABSTRACT SECURITY CLASSIFICATION
☒ UNCLASSIFIED/UNLIMITED ☐ SAME AS RPT ☐ DTIC USERS	unclassified
22a. NAME OF RESPONSIBLE INDIVIDUAL George W. Flynn	22b. TELEPHONE (*Include Area Code*) (212) 280-3265 / 22c. OFFICE SYMBOL

DD FORM 1473, 84 MAR 83 APR edition may be used until exhausted. All other editions are obsolete.

SECURITY CLASSIFICATION OF THIS PAGE

Block 18 continued--Subject Terms (Key Words)

feedback
sub-Poisson light
superlattice avalanche photodiodes
$Cu+Cl_2$
Time-Of-Flight
ion ejection
Excimer
Ge
ions
threshold
low energy ion beam
sputtering of silicon dioxide
gallium arsenide MESFET
Collisions
Carbon Dioxide
Deuteruim
Infrared Absorption
Pyruvic Acid
Photodissociation
Surface
Femtosecond
Interface
Binaphthyl
Liquid
Adsorption
Structure
Capacitance Measurement
Schottky Capacitance
Interface States
$NiSi_2$-Si
Optical Coherent Transients
Sodium Vapor
Ultrafast Modulation Spectroscopy
Four-Wave Mixing
Photon Echo Modulation Spectroscopy
In Situ Processing
cosmic-ray noise
Cerenkov radiation
Laser Induced Desorption
mass spectrometer
$CuCl_x$
Si
Quadropole mass spectrometer
photoionic emission
low temperature processing
silicon oxidation
germanium nitride
gate leakage current
Hot Atoms
Hydrogen
Diode Laser
Excimer Laser
Energy Transfer
Chlorine atoms
Picosecond
Second-Harmonic
Isomerization
Water
Erythrosin
Isotherm
Capacitance
Negative Capacitance
Schottky Barrier
Metal-semiconductor Interface
Impact Ionization
Photon Echoes
Spectroscopy
Non-linear Optics
Time-Delayed Four-Wave Mixing
Etching
Photoelectron Emission

Block 19 continued--Abstract

Research has been conducted in the design of superlattice modulator devices, specifically GaAs/AlGaAs superlattice structures. Three aspects of superlattice design have been explored: carrier energy bands and band edge wave functions, barrier-layer thickness, and impurity doping effects.

Ejection of ion and neutral species has been studied for the $Cu+Cl_2+$ laser system using a Time-of-Flight detection technique. The system was investigated under various laser fluence (0-130 mJ/cm^2) and varying Cl_2 surface coverage (0.5-500L). Ion ejection occurs for the 193 nm system (Cu^+, Cl^+, $CuCl^+$) and the 248 nm system (Cu^+, Cl^+).

Si and Ge ion ejection was observed to occur from clean silicon and germanium surfaces upon excimer laser irradiation at fluences (0-150 mJ/cm^2) well below that necessary to cause the thermionic emission or melting of the substrate. Quadrupole mass spectrometric techniques were employed to characterize the translational energy and angular variation of the ion products. Laser intensity dependent measurements were performed at 193, 248 and 351 nm to elucidate the laser fluence and photon energy threshold behavior of each of the charged species.

An understanding of the mechanisms behind the low energy ion beam oxidation of silicon has been achieved. Extensive experiments exploring the effects of beam energy, dose, substrate temperature, beam composition, and substrate orientation have been performed. A new implantation-sputtering model has been created to explain the observed phenomena. Computer simulation utilizing this model has led to excellent prediction of experimental results.

The sputtering yield of silicon dioxide by low energy argon

ions has been experimentally measured. A simple assumption extendable to other oxide systems has led to the use of existing theory to quantitatively predict the yield.

Germanium has been nitrided using a low energy ion beam, and metal-insulator-semiconductor devices have been fabricated and tested.

The use of photochemically deposited excess arsenic on GaAs surfaces in GaAs MESFET fabrication has been shown to reduce gate leakage current.

Investigation of interface states at metal-semiconductor junctions has been actively performed. Considerable progress has been made in the development of measurement techniques, data accumulation and theoretical tools. Experimentally, a new technique has been developed to measure the diode interface capacitance. This technique overcomes the difficulties that usually arise from the large diode conductance, so that measurement capabilities have been improved. Using this technique, the properties of forward-bias capacitance on several different types of Schottky diodes have been studied. A variety of data corresponding to different temperatures and frequencies were collected. A model for data interpretation is currently being constructed, which may help to extract the density and some other quantities of interface states. A "negative capacitance" has been discovered in these experiments. This phenomenon was explained by considering the loss of interface charge at occupied states below the Fermi level due to the hot carrier effect. A modification to the Shockley-Read statistics was proposed to simulate the capacitance. Results have shown good agreement with the experimental observations.

Second Harmonic Generation at the Air-Liquid Interface is being used as a surface-sensitive probe of the structure and energetics in a variety of liquid systems, including neat water and solutions. In addition to initiating studies of reaction dynamics at the surface, femtoscond experiments of chemical

reactions in the bulk liquid are being implemented.

Recently, a number of Broadband Incoherent Four Wave mixing experiments have been carried out making relaxation time measurements in the picosecond regime and verifying the viability of this technique by comparison of the results with the previous work done with short pulses. Current experiments extend the application of this technique to the femtosecond regime where measurements of the relaxation rates in glasses doped with semiconductor micro-crystallites are being made.

Transient time-delayed four-wave mixing (TDFWM) experiments have been performed on the Na D doublet using a novel angled-beam geometry. Petahertz superposition-state modulations have been observed in the integrated TDFWM signal as a function of the time delay. As the time delay is varied, the lowest order mixing signal modulates with a period of 980 attoseconds--corresponding to the sum frequency of the two Na D lines. Higher diffraction order mixing signals contain modulation components at integral multiples of the doublet sum frequency.

A new, nonperturbative analysis of the interaction of Incoherent Light with matter has been proposed by R. Friedberg and S. R. Hartmann. Experiments are underway to verify this theory.

Recent experiments on objects which have previously been called diffraction-free beams are better thought of as line images. Improved methods for generating line images have been suggested and demonstrated.

High energy collisions between H atoms and carbon dioxide molecules have been studied using diode lasers. Quantum state resolved final state rotational distributions have been determined for several different vibrational states. The isotope effect, which occurs when deuterium is substituted for hydrogen,

has been observed to lead to increased excitation of high rotational levels. Temperature dependent studies have been used to determine the dependence of excitation cross section on initial state.

An experimental apparatus has been set up for the direct monitoring of chlorine atom concentrations using infrared diode lasers. Calibration of the spectral region near 11 microns, where Cl atoms absorb, has been performed by monitoring vibrationally excited transitions in the molecule OCS.

TABLE OF CONTENTS

PUBLICATIONS AND REPORTS

K. B. Eisenthal, K. Bhattacharyya, and E. V. Sitzmann, "Study of Chemical Reactions by Surface Second Harmonic Generation: p-Nitrophenol at the Air-Water Interface," **J. Chem. Phys.** 87(1987):1442.

T. Kreutz, J. O'Neill, and G. Flynn, "IR Diode Laser Study of Vibrational Energy Distribution in CO_2 Produced by UV Excimer Laser Photofragmentation of Pyruvic Acid," **J. Chem. Phys.** 87(1987):4598-4605.

A. Hewitt, J. Hershberger, G. Flynn, and R. Weston, Jr., "Rotationally Resolved Isotope Effect in the Hot Atom Collisional Excitation of CO_2 $(00^0 1)$ by Time-Dependent Diode Laser Spectroscopy," **J. Chem. Phys.** 87(1987):1894.

T. Kreutz, J. O'Neill, and G. Flynn, "Diode Laser Absorption Probe of V-V Energy Transfer in CO_2," **J. Phys. Chem.** 91(1987):5540-5543.

S. S. Todorov, C. F. Yu, and E. R. Fossum, "Direct Formation of Dielectric Thin Films on Silicon by Low Energy Ion Beam Bombardment," **Vacuum** 36(1986):929-932.

C. F. Yu, S. S. Todorov, and E. R. Fossum, "Characterization of Ultra-Thin SiO_2O_2 Films Formed by Direct Low Energy Ion Beam Oxidation," **J. Vac. Sci. Technol.** A5(4)(1987):1569-1571.

D. V. Rossi, E. R. Fossum, G. D. Pettit, P. D. Kirchner, and J. M. Woodall, "Reduced Reverse Bias Current in Al-GaAs and $In_{0.75}Ga_{0.25}As$-GaAs Junctions Containing an Interfacial Arsenic Layer," **J. Vac. Sci.Technol.** B5(1987):982-984.

S. S. Todorov and E. R. Fossum, "Growth Mechanism of Thin Oxide Films Under Low Energy Oxygen Ion Bombardment," to be published in **J. Vac. Sci. Technol.**

S. S. Todorov and E. R. Fossum, "Sputtering of Silicon Dioxide Near Threshold," to be published in **Appl. Phys. Lett.**

S. S. Todorov and E. R. Fossum, "Oxidation of Silicon by a Low Energy Ion Beam: Model and Experiment," to be published in **Appl. Phys. Lett.**

S. S. Todorov, "Interactions of Low Energy Oxygen Ions with Silicon Surfaces," Ph. D. diss., Columbia University, 1987.

S. R. Hartmann, "Using Incoherent Light to Generate Coherent Excitations," Proceedings of the International Laser Science Conference ILS-II, Seattle, Washington, 1986, to be published in **Am. Inst. Phys. Conf. Proc.**

D. DeBeer, S. R. Hartmann and R. Friedberg, "Comment on Diffraction Free Beams," to be published in **Phys. Rev. Lett.**

R. Friedberg and S. R. Hartmann,"A Diagramatic Technique for Calculating Radiation of Coherently or Incoherently Excited Two-level Atoms," to be published in **J. Phys. B.**

H. S. Cho and P. R. Prucnal, "New Formalism of the Kronig-Penney Model with Application to Superlattices," **Phys. Rev. B** 36(1987):3237-3242.

W. Holber, J. O. Chu, D. Gaines, A. Nahata, and R. M. Osgood, "Laser Assisted Plasma Etching," ECS Proceedings, 1986.

C. F. Yu, M. T. Schmidt, D. V. Podlesnik, and R. M. Osgood, "Optically-Induced, Room-Temperature Oxidation of Gallium Arsenide," **Mat. Res. Soc. Symp. Proc.** 75(1987):251-255.

P. D. Brewer and R. M. Osgood,"Large Area Laser-Assisted Etching of Electronic Materials," **SPIE** 611(1986):62.

R. W. Ade, E. E. Harstead, T. Cacouris, E. R. Fossum, P. R. Prucnal, and R. M. Osgood, "Direct Connection of Optical Fibers to Integrated Circuits," IEPS Proceedings, San Diego, 1986.

C. F. Yu, M. T. Schmidt, D. V. Podlesnik, and R. M. Osgood, Jr., "Wavelength Dependence of Optically Induced Oxidation of GaAs (100)," **J. Vac. Sci. Technol.** B5(1987):1087-1091.

W. Holber, D. Gaines, C. F. Yu, R. M. Osgood, "Laser Desorption of Polymer in a Plasma Reactor," to be published in **Appl. Phys. Lett.**

D. V. Podlesnik, "Light-Guided Etching for III-V Semiconductor Device Fabrication," Proceedings of the European Solid State Device Research Conference, Bologna, Italy, (1987): 462-470.

C. F. Yu, M. T. Schmidt, D. V. Podlesnik, E. S. Yang, and R. M. Osgood, Jr., "Ultraviolet-Light-Enhanced Reaction of Oxygen with Gallium Arsenide Surfaces," to be published in **J. Vac. Sci. Tech.**

X. Wu, H. L. Evans, E. S. Yang and P. S. Ho, "An improved Differential Voltage Technique for Capacitance Measurement," to be published in **Solid State Electronics.**

M. T. Schmidt, D. V. Podlesnik, H. L. Evans, C. F. Yu, E. S. Yang, and R. M. Osgood, Jr., "The Effect of a Thin UV-Grown Oxide on Metal-GaAs Contacts," to be published in **J. Vac. Sci. Technol.**

M. C. Teich, Review of R. P. Feynman's book entitled, "Surely You're Joking, Mr. Feynman! Adventures of a Curious Character," **Phys. Today** 39, #9(1986):61.

J. H. Shapiro, P. Kumar, G. Saplakoglu, M. C. Teich, and B. E. A. Saleh, "Theory of Light Detection in the Presence of Feedback," **J. Opt. Soc. Am. B** 3(1986):66.

M. C. Teich, K. Matsuo, and B. E. A. Saleh, "Excess Noise Factor and Gain Distributions for Superlattice Avalanche Photodiodes," **J. Opt. Soc. Am. A** 3(1986):39.

F. Capasso and M. C. Teich, "Conversion of Poisson Photons into Sub-Poisson Photons by the Action of Electron Feedback," **Phys. Rev. Lett.** 57(1986):1417-1420.

M. C. Teich, K. Matsuo, and B. E. A. Saleh, "Excess Noise Factors for Conventional and Superlattice Avalanche Photodiodes and Photomultiplier Tubes," **IEEE J. Quant. Electron** QE-22(1986):1184-1193.

M. C. Teich, F. Capasso, and B. E. A. Saleh, "Photon-Number-Squeezed Recombination Radiation in Semiconductors," **J. Opt. Soc. Am. B** 4(1987):1663-1666.

J. H. Shapiro, G. Saplakoglu, S. T. Ho, P. Kumar, B. E. A. Saleh, and M. C. Teich, "Theory of Light Detection in the Presence of Feedback," **J. Opt. Soc. Am. B** 4(1987):1604-1620.

M. C. Teich and B. E. A. Saleh, "Approximate Photocounting Statistics of Shot-Noise Light with Arbitrary Spectrum," **J. Mod. Opt.** 34(1987):1169-1178.

B. E. A. Saleh and M. C. Teich, "Can the Channel Capacity of a Lightwave Communication System be Increased by the Use of Photon-Number-Squeezed Light," **Phys. Rev. Lett.** 58(1987):2656-2659.

M. C. Teich, R. A. Campos, and B. E. A. Saleh, "Statistical Properties of Clustered Cosmic-Ray Events at Ground Level Determined from Photomultiplier-Tube Background Registrations," **Phys. Rev. D**(1987):2649-2665.

Lectures and Presentations

K. B. Eisenthal, Columbia Chemical Physics Seminar, Columbia University, New York, NY, November 1987.

E. R. Fossum, "Characterization of Ultra-Thin SiO_2 Films Formed by Direct Low Energy Ion Beam Oxidation," AVS Meeting, Baltimore, MD, October 1986.

E. R. Fossum, "Progress in Understanding Low Energy Ion Beam Oxidation of Silicon," SISC, San Diego, CA, December 1986.

E. R. Fossum, "Room Temperature Growth of Silicon Dioxide Using a Low Energy Ion Beam," MRS Fall Meeting, Boston, MA, December 1986.

E. R. Fossum, "Reduced Leakage Current in Al-GaAs Schottky Diodes with an Arsenic Interfacial Layer, PCSI Salt Lake City, Utah, January 1987.

E. R. Fossum, "Comparison of the Properties of Thermal and Ion Beam Oxides," MRS Spring Meeting, Anaheim, CA, April 1987.

E. R. Fossum, "Growth Mechanism of Thin Oxide Films Under Low Energy Oxygen Ion Bombardment," 31st Electron, Ion, and Photon Beam Conference, Woodland Hills, CA, May 1987.

E. R. Fossum, "Thin Oxide Growth Using Low Energy Ion Beam Bombardment," European MRS Meeting, Strasbourg, France, June 1987.

E. S. Yang, "Schottky Contact Characterization of Thin, Excimer Laser Grown GaAs Oxides," Materials Research Society, Fall 1987 Symposium, Boston, MA, November 30-December 4, 1987.

E. S. Yang, "Schottky Contact Characterization of Thin, Excimer Laser Grown GaAs Oxides," IBM, Yorktown Heights, NY; IBM Fishkill, NY; Bell Labs, Murray Hill, NJ; Bellcore, Red Bank, NJ; 1986-1987.

G. W. Flynn, Symposium on Vibrational Energy Transfer Kinetics, Lasers 1986 Meeting, Orlando, Florida, November 3, 1986.

G. W. Flynn, Symposium on Photodissociation Dynamics, American Physical Society Meeting, New York, NY, March 16, 1987.

G. W. Flynn, The Consolidated Edison Lecture, Columbia University, New York, NY, April 1, 1987.

G. W. Flynn, Symposium on Recent Advances in laser Spectroscopy, Polytechnic University, Brooklyn, NY, May 15, 1987.

G. W. Flynn, Symposium on Time Dependent Used of Infrared Diode Lasers, Boston, MA, June 4, 1987.

G. W. Flynn, "Dynamics of Molecular Collisions," Oglebay Park, WV, July 14, 1987.

G. W. Flynn, Keynote Address, The American Scientific Glassblowers Society, 32nd Annual Symposium, Boston, MA, July 30, 1987.

G. W. Flynn, Plenary Lecture, Third International Laser Science Conference, Atlantic City, NJ, November 4, 1987.

G. W. Flynn, Emory University, Atlanta, GA, October 7, 1986.

G. W. Flynn, Boston College, Boston, MA, January 12, 1987.

G. W. Flynn, University of Cincinatti, Cincinatti, OH, February 6, 1987.

G. W. Flynn, University of Virginia, Charlottesville, VA, March 6, 1987.

G. W. Flynn, Massachusetts Institute of Technology, Cambridge, MA, March 10, 1987.

S. R. Hartmann, "Femtosecond Relaxation Using Time Delayed Four Wave Mixing," Workshop on High Speed Optical Processes and Opto-Electronic Devices Based on Compound Semiconductors, Ann Arbor, MI, May 27-29, 1987.

S. R. Hartmann, "Ultrafast Relaxation and Spectroscopy Using Noisy Broad Band or Quiet Narrow Band Laser Sources," Nonlinear Spectroscopy Workshop, UCLA Conference Center at Lake Arrowhead, CA, March 13-15, 1987.

D. V. Podlesnik, "Room Temperature Chemical Reactions Enhanced by Photogenerated Carriers," McDonnell-Douglas, Elmsford, NY, October 1986.

R. M. Osgood, "Lasers and Electronics," Dupont, Wilmington, DL, October 1986.

R. M. Osgood, "Laser Assisted Plasma Etching," Electrochemical Society Meeting, San Diego, CA, October 1986.

R. M. Osgood, "Laser Processing for Microelectronics," Leos Traveling Lecture, Dallas, TX, October 1986.

C. F. Yu, "Characterization of Ultrathin SiO_2 Films Formed by Direct Low-Energy Ion Beam Oxidation," American Vacuum

Society Meeting, Baltimore, MD, October 1986.

R. M. Osgood, et al., Materials Research Society Meeting, Boston, MA, December 1986.

R. M. Osgood, "Overview of laser Processing," IBM Seminar, Hopewell Junction, NY, December 1986.

R. M. Osgood, "Laser Processing for Microelectronics," Leos Traveling Lecture, Providence, RI, January 6, 1987; MIT, Cambridge, MA, January 7, 1987, IEEE, Boston, MA, January 8, 1987; ESI, Portland, OR, January 12, 1987; UCLA, Los Angeles, CA, January 14, 1987; Spectra Physics, CA, January 15, 1987.

R. M. Osgood, "Processing Electronic Materials," National Academy of Sciences, Washington, D.C., January 23, 1987.

D. V. Podlesnik, et al., "Optically Induced Periodic Structures," Southwest Optics, Albuquerque, NM, February 9, 1987.

R. M. Osgood, "Overview of Laser Chemical Processing," Engineering Foundation, Santa Barbara, CA, February 23, 1987.

R. M. Osgood, "Photogenerated Laser-Induced Chemistry," German Physical Society, Bad Honnef, Germany, March 5, 1987.

R. M. Osgood, "Physics of Laser Induced Etching," American Physical Society, New York, NY, March 16, 1987.

R. M. Osgood, "Microelectronics Research at Columbia," Workshop on Electronic Cooling, Columbia University, New York, NY, April 10, 1987.

R. M. Osgood, "Photocarrier-Induced Surface Chemistry: Fundamentals and Applications," American Chemical Society, Denver, CO, April 27, 1987.

R. M. Osgood, "Lasers at the Frontiers of Materials Science and Engineering," Plenary Session, CLEO/IQEC, Baltimore, MD, April 30, 1987.

G. V. Treyz, et al., "Gas Diffusion Limitations in the Laser-induced Etching of High-Aspect Ratio Trenches in Silicon," CLEO/IQEC, Baltimore, MD, April 30, 1987.

A. W. Willner, et al., "Inhibition of Laser-Induced Photochemical Reactions in Semiconductors by Background Illumination," CLEO/IQEC, Baltimore, MD, April 30, 1987.

R. M. Osgood, "Photochemical Processing," DARPA GaAs Technology Review, Washington D.C., April 30, 1987.

R. M. Osgood, "Photocarrier-Induced Etching," Bell Labs Seminar, Murray Hill, NJ, May 13, 1987.

R. M. Osgood, "Laser Processing for Microelectronics," Leo's Traveling Lecture, University of Maryland, Baltimore, MD, May 19, 1987.

R. M. Osgood, "Laser Processing for Microelectronics," Leo's Traveling Lecture, University of Maryland, Cleveland, OH, NASA-Lewis Research Center, May 20, 1987.

R. M. Osgood, "The Role of Photogenerated Carriers in Laser-Surface Interactions," European Materials Research Society, Strasbourg, France, June 4, 1987.

R. M. Osgood, "Single Photon Laser Assisted Surface Chemistry," The Gordon Conference, Andover, NH, August 13, 1987.

J. A. O'Neill, "Total Internal Reflection Spectroscopy of Adsorbed Molecules," The Gordon Conference, Andover, NH, August 13, 1987.

C. F. Yu, "Laser Enhanced Oxidation of Semiconductor Surfaces," American Chemical Society, New Orleans, LA, September 2, 1987.

R. M. Osgood, "Laser for Opto- and Microelectronics," American Chemical Society, New Orleans, LA, September 2, 1987.

R. M. Osgood, "Photon Induced Surface Science," Allied Signal Corporation Seminar Series, Morristown, NJ, September 22, 1987.

Columbia Resonance Seminars

Meetings are held periodically at Columbia University, New York, New York during the academic year and are open to all members of the New York scientific community. Guest speakers are invited to discuss work in the general area of the research in the Columbia Radiation Laboratory.

P. Berman, Physics Department, New York University, "Collisionally Aided Coherent Emission at an Optical Frequency," October 3, 1986.

Y. Prior, The Weizmann Institute of Science, Israel, "Novel Aspects in Four Wave Mixing," October 17, 1986.

R. Friedberg, Columbia University, "Interaction of Noisy Light and Matter--Density Matrix Evolution," October 24, 1986.

B. Aull, MIT Lincoln Laboratories, "Multiple Quantum Well Structures for Electro-optic Devices," October 29, 1986.

F. Pollak, Brooklyn College, "Modulation Spectroscopy of Superlattices, Quantum Wells and Heterostructures," November 5, 1986.

A. Szabo, National Research Council, Canada, "Photon Echo Modulation and Dephasing in Ruby," November 7, 1986.

D. J. Wolford, IBM, "Electronic States in Semiconductors Under High Pressure," November 19, 1986.

R. Slusher, AT&T Bell Laboratories, "Squeezing the Vacuum: Recent Results and Applications," November 26, 1986.

J. Tsang, IBM, "Subpicosecond Raman and Photoluminescence Studies of Carrier Dynamics in GaAs," February 4, 1987.

C. Shank, AT&T Bell Labs, "Investigation of Ultrafast Processes With Six Femtosecond Pulses," February 25, 1987.

M. Drake, Exxon Research & Engineering Co., "Molecular Dynamics in Restricted Geometries," March 18, 1987.

R. Feenstra, IBM, "Scanning Tunneling Microscopy of Cleaved Semiconductor Surfaces," March 25, 1987.

A. Sanchez, MIT Lincoln Laboratories, "Ti:Al_2O_3 Tunable Solid State Laser Technology," April 1, 1987.

I. QUANTUM GENERATION AND DETECTION OF RADIATION

A. NOISE IN THE GENERATION, PARTITION, AND DETECTION OF LIGHT

(M.C. Teich, B. Saleh)
(JSEP work unit 1, 1985 - 1988)
(Principal Investigator: M.C. Teich (212) 280-3117)

We have made substantial progress in understanding the generation of photon-number-squeezed (sub-Poisson) light from both theoretical and experimental points of view, in evaluating the noise properties of conventional and superlattice avalanche photodiodes, and in understanding the behavior of cosmic-ray noise in optical systems.

Photon-number-squeezed light, it appears, may have many uses. It may have application in increasing the distance between repeaters in lightwave communication systems, in spectroscopy, in interferometry, and in gravitational-wave detection. In the course of the work carried out under this contract, we reported the first successful generation of cw photon-number-squeezed light using a Franck-Hertz apparatus excited by a space-charge-limited electron beam.[1] We also investigated the possibilities of using external feedback *from* detector-to-source, instead of space charge, to create quiet electron excitations.[2]

1. Conversion of Poisson Photons into Sub-Poisson Photons by the Action of Electron Feedback -- The use of an external-feedback system for generating such light was first suggested by experiments in which feedback was used to produce sub-Poisson electrons.[3] Both the experiment of Walker and Jakeman[3] and the experiment of Machida and Yamamoto[3] involved laser (Poisson) photons illuminating a photodetector and an electronic negative feedback path from the detector to the source. In the former experiment, the feedback directly controlled the photons at the output of the laser whereas in the

latter experiment, the feedback controlled the current at the input to the laser. Nevertheless, the principle involved in the two experiments is the same.[4] Unfortunately, these simple configurations could not generate usable sub-Poisson photons since the feedback current is generated from the annihilation of the in-loop photons. However, under special circumstances, an external-feedback system can be used to produce sub-Poisson photons, such as when correlated photon pairs are available[5] or a quantum nondemolition measurement may be made. The resultant light may only be weakly sub-Poisson in such cases because these multiphoton processes involve a series of detections and/or a weak nonlinear effect.

We developed a new approach for converting Poisson photons into sub-Poisson photons via single-photon transitions.[2] There does not appear to be any fundamental limit that would impede the technique from being used to produce an arbitrarily intense cw light source that is also arbitrarily sub-Poisson. It makes use of the action of an electron current configured in a feedback loop. Consider, for example, an optical system in which a photon emitter illuminates a detector/source combination, in a closed-loop circuit. Two alternative configurations are shown in Figure 1. The character of the photon emitter is immaterial; we have chosen it to be a light-emitting diode (LED) for simplicity but it could be a laser. In Figure 1(a) the photocurrent derived from the detection of light from the LED photon emitter is negatively fedback to the LED input. It has been established both theoretically[4,6] and experimentally[3] that, in the absence of the block labeled "source," sub-Poisson electrons will flow in a circuit such as this. This conclusion will sometimes be correct in the presence of this block, which can act as only an added impedance to the electron flow. Incorporating this element into the system critically alters its character, however, since it permits the sub-Poisson electrons flowing in the circuit to be converted into photon-number-squeezed photons by means of electron transitions. The key to achieving this effect is the replacement of the detector used in other feedback configurations

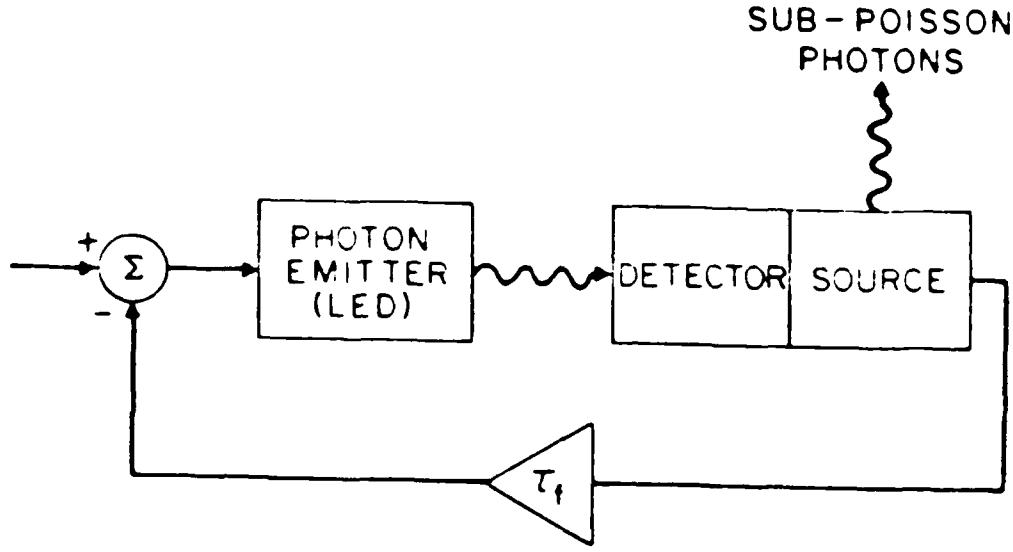

(a)

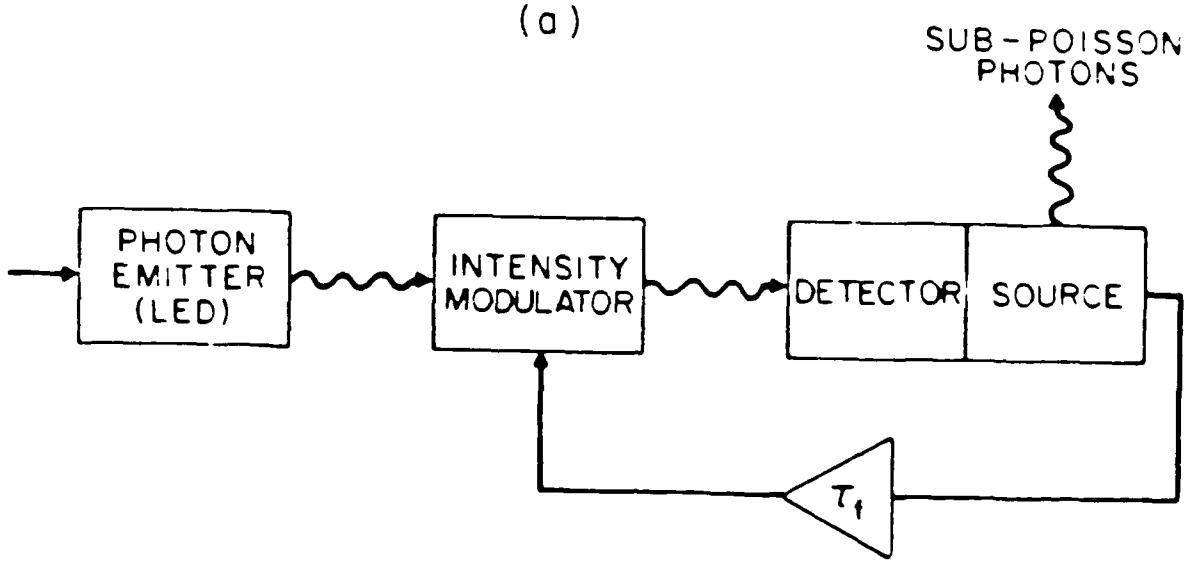

(b)

Fig. 1 : Generation of sub-Poisson photons by means of negative feedback. The feedback produces sub-Poisson electrons in the detector/source which, in turn, generate sub-Poisson photons. (a) Negative feedback modulating the photon-emitter input current. (b) Negative feedback modulating the photon-emitter output light. Wavy lines represent photons; solid lines represent electron current. τ_f signifies the feedback time constant.

with a structure that acts simultaneously as a detector and a source. The electrons simply emit sub-Poisson photons and continue on their way. In the absence of the feedback path, of course, the electrons would simply emit Poisson photons. Thus, the introduction of the electron feedback converts Poisson photons into sub-Poisson photons. The configuration in Figure 1(b) is similar except that the (negative) feedback current modulates (gates) the light intensity at the output of the LED rather than the current at its input.

In Figure 2 we illustrate two possible solid-state detector/source configurations. The basic structure consists of a reverse-biased p^+in^+ diode where the p^+ and n^+ heavily-doped regions have a wider bandgap than the high-field,light-absorbing/emitting i region. Two light-generation schemes are explicitly considered here: single-photon dipole electronic transitions between the energy levels of the quantum wells [Fig. 2(a)] and impact excitation of electroluminescent centers in the i region by drifting electrons [Fig. 2(b)].

The ability of configurations such as these to generate sub-Poisson light requires a number of interrelations among various characteristic times associated with the system.[7] The degree to which a light source is sub-Poisson (its Fano factor) has been estimated to be $Fn \approx 0.968$ for both the quantum-well device and the electroluminescent structure.[2] These estimates provide a significant potential improvement over the value observed in the space-charge-limited Franck-Hertz experiment.[1] Lower values of the Fano factor can be achieved in structures that exhibit higher radiative efficiency. As indicated earlier, there is no fundamental limit that impedes this scheme from being used to produce an arbitrarily sub-Poisson cw light source of arbitrarily high intensity.

2. Semiclassical Theory of Light Detection in the Presence of Feedback -- The usual formulations of the quantum and semiclassical theories of photodetection presume open-loop configurations, i.e., that there are no feedback paths leading

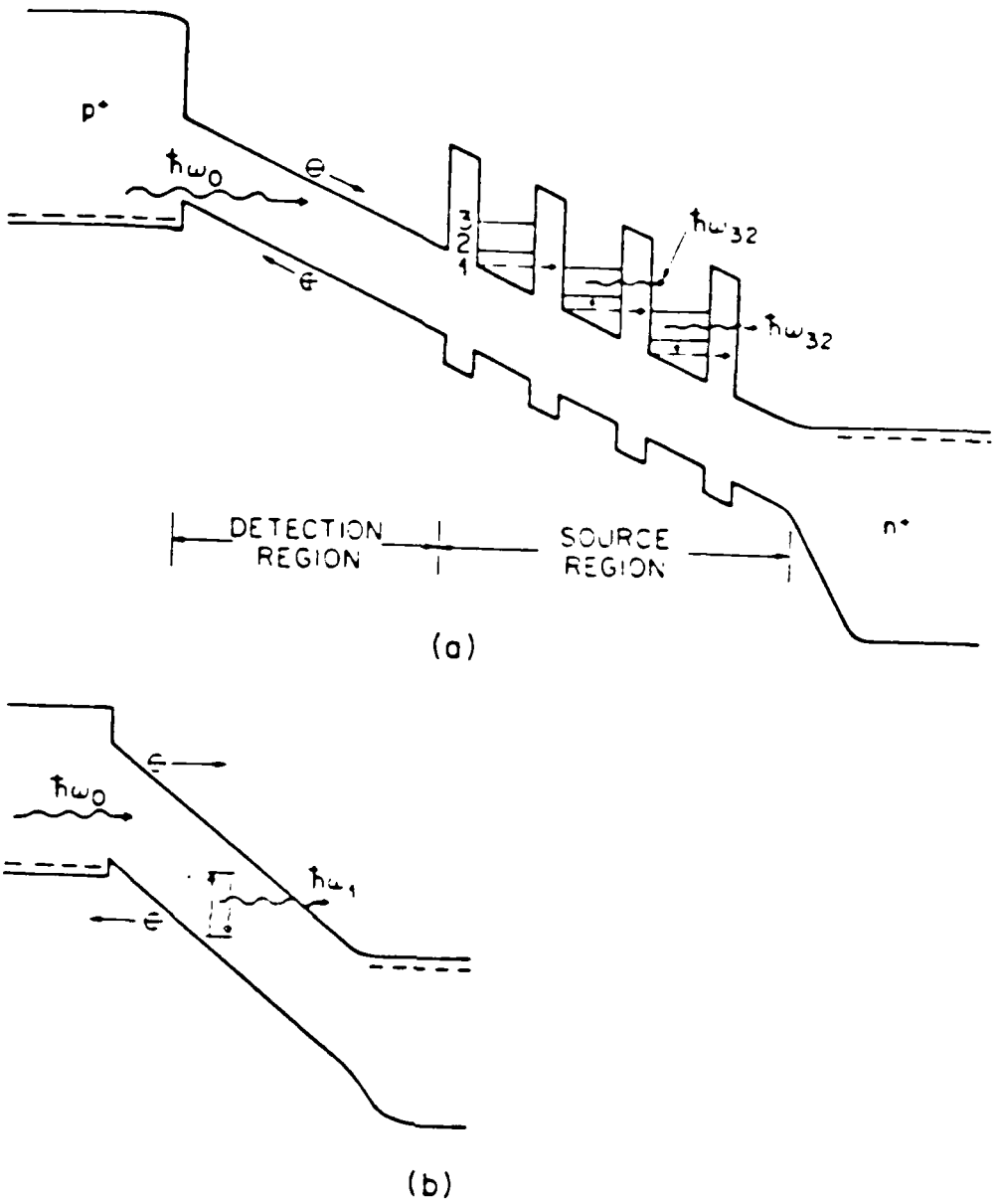

Fig. 2: (a) Band diagram of the quantum-well detector/source. The energy of the incident photon emitted by the LED is denoted $\hbar\omega_o$. The absorbing region (detection region) is of $Ga_{0.47}In_{0.53}As$ or GaAs, typically 1 μm thick. In the source region, the wells are $Ga_{0.47}In_{0.53}As$ or GaAs in the thickness range 150 - 300 Å. The barrier layers are of $Al_{0.48}In_{0.58}As$ (in the case of $Ga_{0.47}In_{0.53}As$ wells) or AlAs (in the case of GaAs wells) and should be in the thickness range 20 - 50 Å to achieve tunneling times < 1 psec. Photons of energy $\hbar\omega_{32}$ are emitted via transitions from level 3 to 2. The p^+ and n^+ widegap regions are of $Al_{0.48}In_{0.52}As$ (or AlAs). The interface between the i and n^+ regions is compositionally graded. (b) Energy-band diagram of a detector/source with electroluminescent centers that are impact-excited by energetic photoelectrons, emitting photons with energy $\hbar\omega_1$.

from the output of the photodetector to the light beam impinging on that detector. In such configurations, the qualitative and quantitative distinctions between the quantum and semiclassical theories are well understood. In the quantum theory, photocurrent and photocount randomness arise from the quantum noise in the illumination beam whereas in the semiclassical theory the fundamental source of randomness is associated with the excitations of the atoms forming the detector. Nevertheless, the quantum theory subsumes the semiclassical theory in a natural way.

The clarity of understanding associated with open-loop photodetection configurations has been extended to closed-loop systems in which there is a feedback path leading from the output of the detector back to the light beam at the detector input. We have shown that the unmistakable signatures of nonclassical light associated with open-loop detection do not carry over to closed-loop systems. Nevertheless, open-loop nonclassical light can be generated with closed-loop photodetection if photon pairs are available or, alternatively, if the in-loop photons are not destroyed.[4-7]

This research was also supported by the National Science Foundation, Grant NSF-CDR 84-21402.

3. Excess Noise Factor and Gain Distributions for Superlattice Avalanche Photodiodes -- We have elucidated the noise properties[8-11] and time response[8] of superlattice avalanche photodiodes (SAPD's) and compared their properties with those of the conventional avalanche photodiode.[11] SAPD's promise a reduction in the feedback noise associated with conventional two-carrier avalanche devices. The expression for the excess noise factor F_e of the two-carrier SAPD in the presence of residual hole ionization has been obtained.[9] F_e depends on the average overall gain of the device $\langle M \rangle$, the electron impact-ionization probability per stage P, and the ratio $k_s = Q/P$ where Q is the hole-ionization probability per stage. It turns out that even a small amount of residual hole ionization can lead

to a large excess noise factor, thereby limiting the usefulness of the device.

Theoretical results have been obtained for the gain distribution and electron-counting distribution of the single-carrier SAPD (in the absence of residual hole ionization).[10] The gain distribution assumes single-electron injection whereas the electron counting distribution assumes Poisson electron injection and is therefore used for calculating the bit error rate (BER) of an optical communication system. The single-carrier SAPD receiver has been found to always perform better than the single-carrier conventional avalanche photodiode receiver, for all values of the gain. It has been demonstrated that the BER advantage can attain several orders of magnitude, even though the excess noise factors for the two devices lie within a factor of two.

The (single-photon) impulse response function for the SAPD was derived in the absence of residual hole ioniztion, when the effects of random transit time are incorporated into the carrier multiplication process.[8] For a five-stage quaternary device, the gain-bandwidth product is calculated to be in the vicinity of 600 GHz which is quite large. These results were extended to the CAPD, which turns out to be a special case of the SAPD (in the limit of an infinite number of stages with infinitessimal gain per stage).[11]

This research was also supported by the National Science Foundation Grant NSF-ECE 82-19636.

4. Behavior of Cosmic-ray Noise in Optical Systems -- We have also carried out a detailed study of the effects of noisy dark events, such as those arising from cosmic rays, on an optical system.[12] The light arises from high-energy cosmic rays that reach an optical-fiber system at the surface of the earth and, by means of Cerenkov radiation and fluorescence, produce visible photons. These photons may be generated in the detector (e.g., at the faceplate of a PMT), in the optical fiber, or in optical components of the system. They are unwanted because they

introduce errors into data transmitted on a fiber-optic telecommunication system. In the detector, they result in photoelectrons which are a clustered source of noise above and beyond the usual thermally generated Poisson dark events. We have established the statistical nature of this kind of dark noise in photodetectors, and shown that it is indeed distinctly noisier than the Poisson distribution. We have also developed a suitable theoretical model to describe the phenomenon, based on the Poisson-driven Yule-Furry birth process (PDYF). The fit of theory to data is excellent over 5 1/2 orders of magnitude of the photoelectron probability distribution.[12]

This research was also supported by the National Science Foundation Grant NSF-CDR 84-21402.

References:

1 M. C. Teich and B. E. Saleh, J. Opt. Soc. Am. B2, 275 (1985).

2 F. Capasso and M. C. Teich, Phys. Rev. Lett. 57, 1417 (1986).

3 J. G. Walker and E. Jakeman, Proc. Soc. Photo-Opt. Instrum. Eng. 492, 274 (1985); S. Machida and Y. Yamamoto, Opt. Commun. 57, 290 (1986).

4 J. H. Shapiro, G. Saplakoglu, S. T. Ho, P. Kumar, B. E. A. Saleh, and M. C. Teich, J. Opt. Soc. Am. B 4, 1604 (1987).

5 B. E. A. Saleh and M. C. Teich, Opt. Commun. 52, 429 (1985).

6 J. H. Shapiro, M. C. Teich, B. E. A. Saleh, P. Kumar, and G. Saplakoglu, Phys. Rev. Lett. 56, 1136 (1986).

7 M. C. Teich, B. E. A. Saleh, and J. Perina, J. Opt. Soc. Am. B1, 366 (1984); M. C. Teich and B. E. A. Saleh, Prog. Opt. 26, 1 (1988), in press.

8 K. Matsuo, M. C. Teich, and B. E. A. Saleh, IEEE Trans. Electr. Dev. ED-32, 2615 (1985); IEEE J. Light. Tech. LT-3, 1223 (1985).

9 M. C. Teich, K. Matsuo, and B. E. A. Saleh, IEEE J. Quant. Electr. QE-22, 1184 (1986).

10 M. C. Teich, K. Matsuo, and B. E. A. Saleh, IEEE Trans. Elect. Dev. ED-33, 1475 (1986).

11 M. C. Teich, K. Matsuo, and B. E. A. Saleh, IEEE Trans. Elect. Dev. ED-33, 1511 (1986).

12 M. C. Teich, R. Campos, and B. E. A. Saleh, Phys. Rev. D 36, 2649 (1987).

B. DESIGN OF MULTIPLE QUANTUM WELL STRUCTURES FOR INTEGRATED ABSORPTIVE LOSS OPTICAL MODULATORS

(H. Cho, P. R. Prucnal)
(JSEP work unit 1, 1985 - 1988)
(Principal Investigator: P. R. Prucnal (212) 280-3119)

1. Background -- Optical fibers as communication interconnects for VLSI chips offer advantages such as small size, immunity to EMI/EMP, freedom from capacitive loading, and significantly increased bandwidth. However, the potential bandwidth of fiber optics has not yet been realized due to the speed limitations in the opto-electronic transmitters and receivers, and electronic signal processing elements. The optical generation of data can be efficiently performed by using a mode-locked laser to create high speed optical pulses and an electro-optic modulator driven by electronic data, which acts as a gate for the optical pulses. This technique alleviates the necessity of electronically pulsing the optical source at high speeds, and enables data to be encoded into bits less than 100 ps in duration.[1-2]

A novel coupling technique consisting of the insertion of a fiber into a high aspect ratio hole (created via a 'cold' laser-assisted etching process) on the chip's surface has been demonstrated.[3] A modulator employing the same coupling technique is proposed (Figure 1). Here the etched hole penetrates the substrate from the back side, stopping at a surface grown MQW structure. The light is intensity modulated by the electro-absorption effect in response to an applied electric field, and collected by a fiber mounted above the front surface.

Research is being conducted in the design of superlattice modulator devices, specifically GaAs/AlGaAs superlattice structures. Three aspects of superlattice design have been explored: carrier energy bands and band edge wave functions, barrier-layer thickness, and impurity doping effects.

INTEGRATED ABSORPTIVE-LOSS MODULATOR

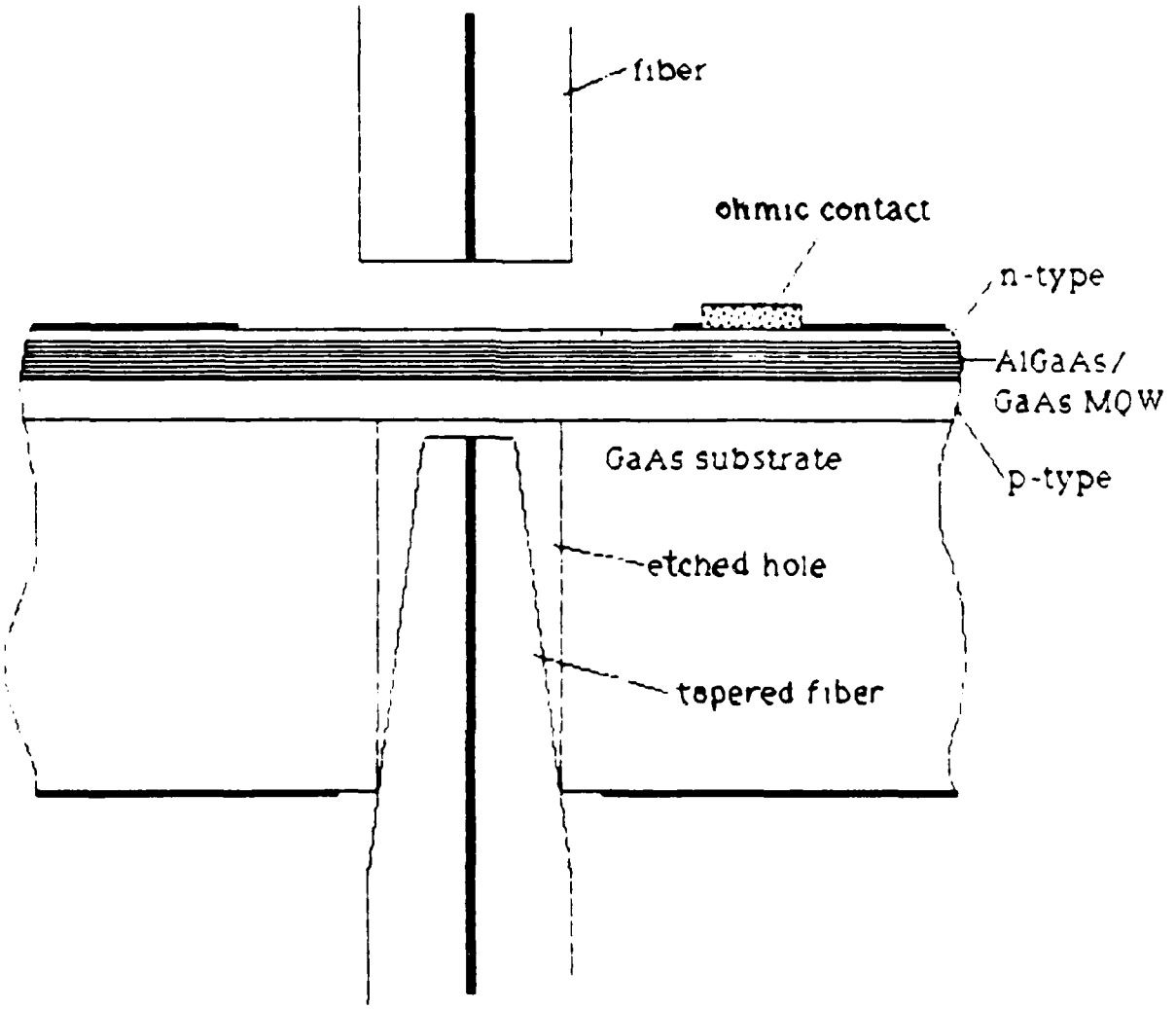

Figure 1

2. New Formalism of the Kronig-Penney Model -- A new formalism of the Kronig-Penney model has been developed which is considerably simpler than the conventional one.[4] This new formalism yields not only the carrier energy bands but also the wave functions at the edges of each band. Although it is formulated to be applied to superlattices, it also is applicable to bulk materials.

3. Critical Barrier-Layer Thickness -- The critical barrier-layer thickness (the thickness above which superlattice structures behave as uncoupled quantum wells and below which they behave as coupled well structures) of GaAs/AlGaAs superlattices has been found as a function of design parameters such as Al concentration.[5] The calculated critical barrier-layer thickness has been shown to be valid and accurate. Its application to the design of modulators, lasers, and other uncoupled well structures has been discussed.

4. Impurity Doping -- The effect of impurity doping on the shift of electron and hole subbands has been formulated by applying perturbation theory. The electron energy shift due to the impurity doping has been found to be on the order of 10 meV for Nd = $10^{18} cm^{-3}$, x=0.3, and layer thicknesses of 100Å. This formalism is expected to be applicable to superlattices with doping levels up to 10^{18} cm^{-3}.

This research was also supported by the National Science Foundation under Grant NSF-CDR 84-21402.

References:

1 P. R. Prucnal, M. A. Santoro, S. K. Sehgal, "Ultra-Fast All-Optical Synchronous Multiple Access Fiber Networks," IEEE J. Select Areas Com., in press.

2 P. R. Prucnal, D. J. Blumenthal, S. K. Sehgal, M. A. Santoro, "A 10 GHz All-Optical Network Using a Mode-Locked Source," in preparation.

3 P. R. Prucnal, E. R. Fossum, R. M. Osgood, "Integrated Fiber

Optic Coupler for VLSI/VHSIC Interconnections," Opt. Letters, 11, #2, 109-111(1986).

4 H. Cho and P. R. Prucnal, "New Formalism of the Kronig-Penney Model with Application to Superlattices," Phys. Rev. B. Vol. 36 No. 6, 3237-3242 (1987).

5 H. Cho and P. R. Prucnal, "Critical Barrier-Layer Thickness of GaAs/AlGaAs Superlattices," J. Appl. Phys. in submission.

II. PHYSICAL AND PHOTOCHEMICAL PROPERTIES OF ELECTRONIC MATERIALS

A. LOW-COVERAGE LASER INDUCED DESORPTION FOR Cl ON COPPER

(L. Chen, V. Liberman, J. A. O'Neill, R. Osgood)
(JSEP work unit 4, 1985 - 1988)
(Principal Investigator: R. M. Osgood (212) 280-4462)

1. Introduction -- The spontaneous chemical reaction which occurs at room temperature between copper and chlorine has been studied extensively by Chuang[1], and Winters[2]. Their results indicate that a chlorinated surface layer with an average stoichiometry of $CuCl_x$ ($0 \leq X \leq 2$) is formed as the Cl_2 coverage increases from 10L to 10^{10} L. Also, the surface composition is found to depend strongly on the rate of diffusion of chlorine into the bulk. Under conditions where $x<1$, the surface layer consists of Cu and CuCl while at exposures where $x>1$, the coexistence of CuCl and $CuCl_2$ is detected.

This report describes the pulsed UV laser desorption of neutral and ionic spheres from a copper surface which has been exposed to Cl_2. In the present study, chlorine coverages vary from less than 1L to several hundred L per laser pulse. The desorption results presented here for the low Cl_2 coverage differ significantly from the high chlorine coverage results studied elsewhere. It is believed that the fundamental desorption mechanisms are quite different for the low and the high coverage regimes.

2. Experimental -- The results presented below are obtained from two types of copper samples: a single crystal Cu and a polycrystalline copper layer of 1.5 microns on 500 Å of titanium. The sample preparation involves cleaning and etching the copper sample with 5% solution of sulfuric acid. The small amount of oxide formed on the sample surface during loading is

subsequently removed upon chlorination and irradiation of the surface with the excimer laser.

The chlorine is introduced by a pulsed molecular beam incident on the surface at an angle of 45^{o} with the copper sample. The excimer laser is also incident on the surface at a 45^{o} angle, making a 90^{o} angle with the molecular beam. Desorbed products are detected with a quadrupole mass spectrometer located along the surface normal. The typical pressure in the UHV chamber is $1X10^{-9}$ torr while the pressure in the mass spectrometer chamber is $1X10^{-10}$ torr. Experiments are performed at various Cl_2 coverages (0.5-500L), laser wavelengths (193, 248 and 351 nm) and at different laser fluences (0-130 mj/cm^2).

In order to estimate how much of the mass signal is due to the gas phase photodissociation above the sample surface, a parallel beam experiment is performed. The excimer laser beam is split with one part directly incident on the sample surface and the other part passing above the surface and parallel to it. This experiment, performed with the laser and the molecular beam synchronized with each other, shows no significant signal contribution from the gas phase photofragmentation.

3. Results -- At low laser fluences (below the melting threshold), illumination of copper samples without the presence of chlorine yields no particle signal. At higher incident fluences ($2J/cm^2$), above the Cu melting threshold, a strong Cu signal is observed (Figure 1). The average translational energy of this copper species is corresponding to T=4875 K, which exceeds the boiling point of copper (2868 K). The observed high energy can be explained by the laser vaporization of Cu surface and the subsequent transfer of energy to the Cu atoms from the dense superheated vapor formed above the surface.[3]

In the remainder of this section of the report, we will describe the Time-of-Flight results for the Cu + Cl_2 + laser system, where the different laser wavelengths are 193 nm, 248 nm and 351 nm.

a. $Cu+Cl_2+193nm$ -- The mass spectrum for the 193

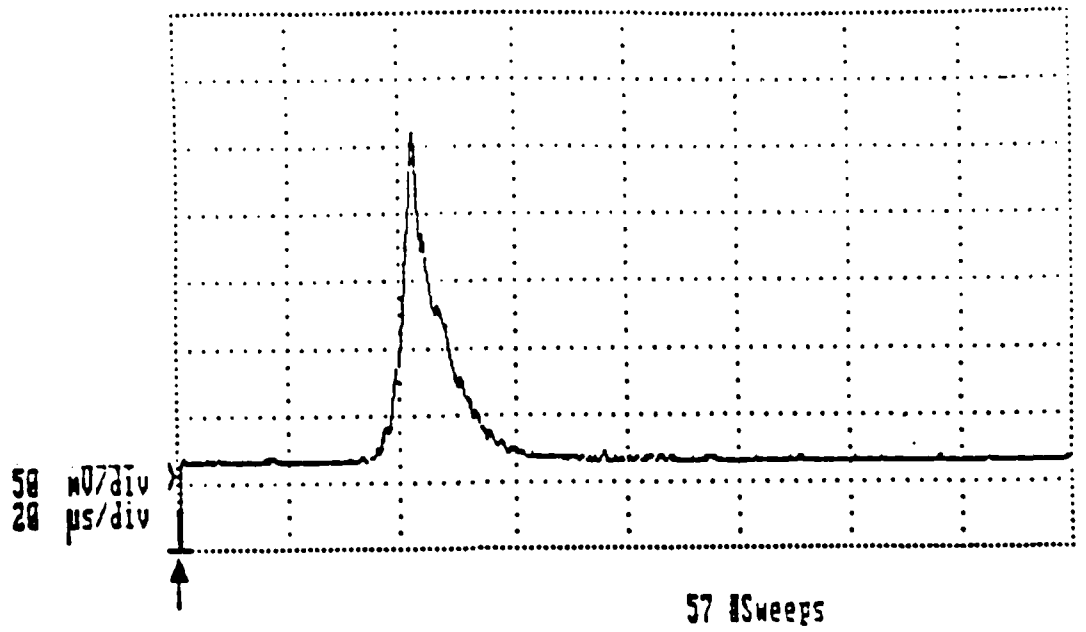

Figure 1: Cu neutral time-of-flight spectrum from Cu surface irradiated by 2 J/cm^2 of 193 nm laser beam. The arrow indicates the onset of the radiation.

nm system is shown in Figure 2a. The excimer laser fluence is 80 mj/cm^2, pulse width is 20 nsec and the laser repetition rate is 1 Hz. The pulsed molecular beam doses Cu surface with chlorine for 8 msec, providing a coverage of 4 L/sec. At the lower mass numbers, ions are observed as well as neutrals (Cl^+, Cu^+, $CuCl^+$). None of the signals shown can be attributed to cracking in the mass spectrometer because each species is observed to possess a different average energy. The mass yields were similar for both single crystal Cu and polycrystalline Cu samples.

Figures 3 and 4 show the raw Time-of-Flight signals for Cu, Cl and CuCl. The Cu^+ ion signal is obtained with the mass spectrometer ionizer turned off (Figure 3a). The laser fluence for this measurement is 66 mj/cm^2 and the Cl_2 coverage is 1 L/sec. Figure 3(b) shows a Cu neutral signal at the same laser intensity but higher Cl_2 dosage (4 L/sec). The fast peak of the signal is attributed to Cu^+. From the difference in the peak energies, it is evident that two different mechanisms are operative in the production of the ions and the neutrals. Figures 3(c), (d) show, similarly, the ion and the neutral Cl signals, obtained at a laser fluence of 70 mj/cm^2.

The CuCl neutral signal (Figure 4a) also shows two peaks which correspond to the faster ions and the slower neutrals. The experimental conditions for obtaining this signal are 70 mj/cm^2 laser fluence and 3.4 L/s Cl_2 dosage. In one set of experiments, performed on a Cu sample which had been extensively used (i.e., extensively dosed with Cl_2) a second, very fast CuCl peak is observed (Figure 4b). The 193 nm laser fluence is 70 mj/cm^2 and the Cl_2 dosage is 3.4 L/s. The occurrence of this very fast ion peak has only been observed with CuCl signals and, at present, is not well understood.

Signal intensity as a function of Cl_2 dosage is summarized in Figure 5. The laser fluence here is kept constant at 70 mj/cm^2. All the neutral species show a near linear increase in yield with increased chlorine coverage. $CuCl^+$ and Cl^+ mass yields peak at about 3.5 L/sec (Figure 5a) while the Cu^+ signal peaks at about 100 L/sec (Figure 5b). At low coverages (< 4 L/s)

Figures 2(a) and 2(b): Mass spectra for the $Cu+Cl_2+$ laser system. Laser fluence is 80 mj/cm^2. Pulsed Cl_2 beam duration is 8 msec, providing 4 L/sec coverage. 0.1% ionizer efficiency assumed to normalize the ion and the neutral intensities.

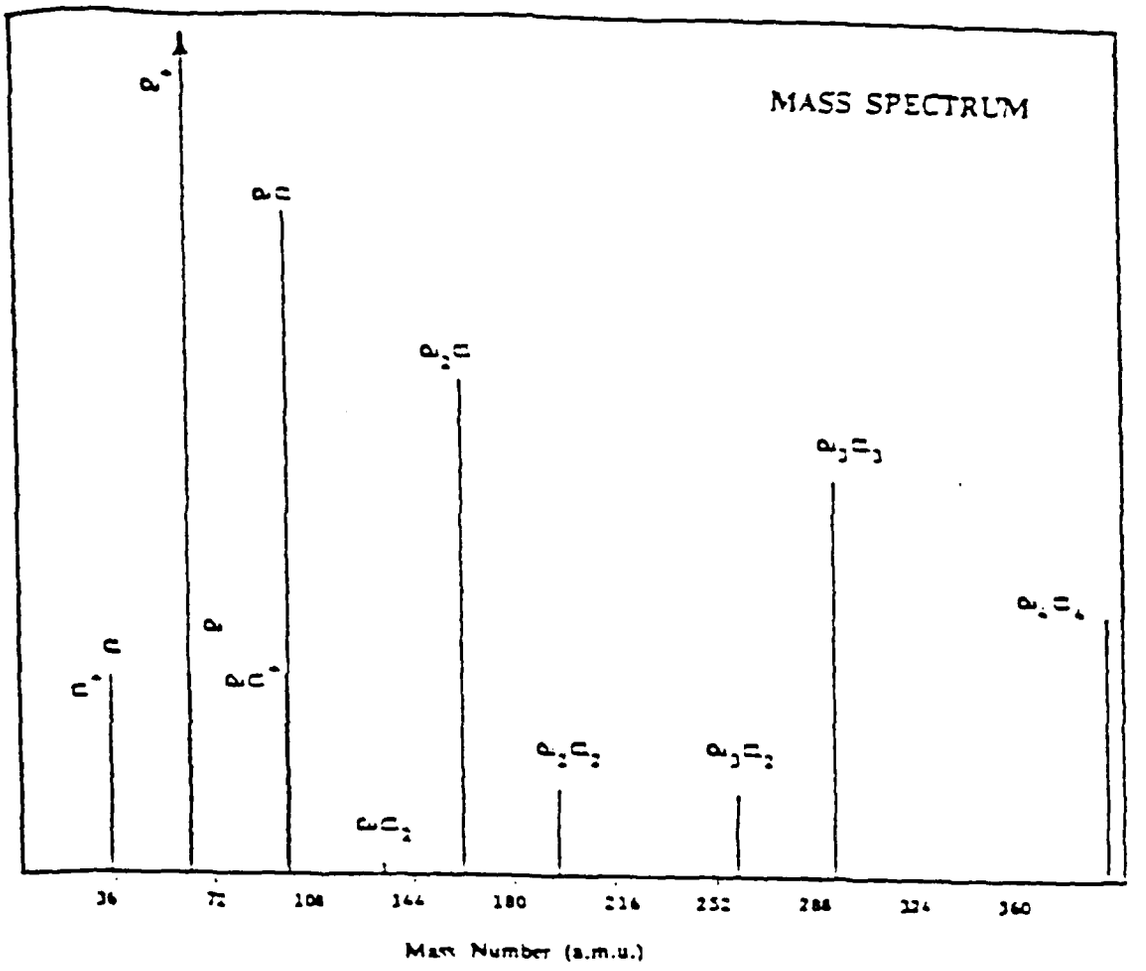

Figure 2(a): 193 nm incident laser wavelength. Cu^+ signal is 4 times greater than that shown.

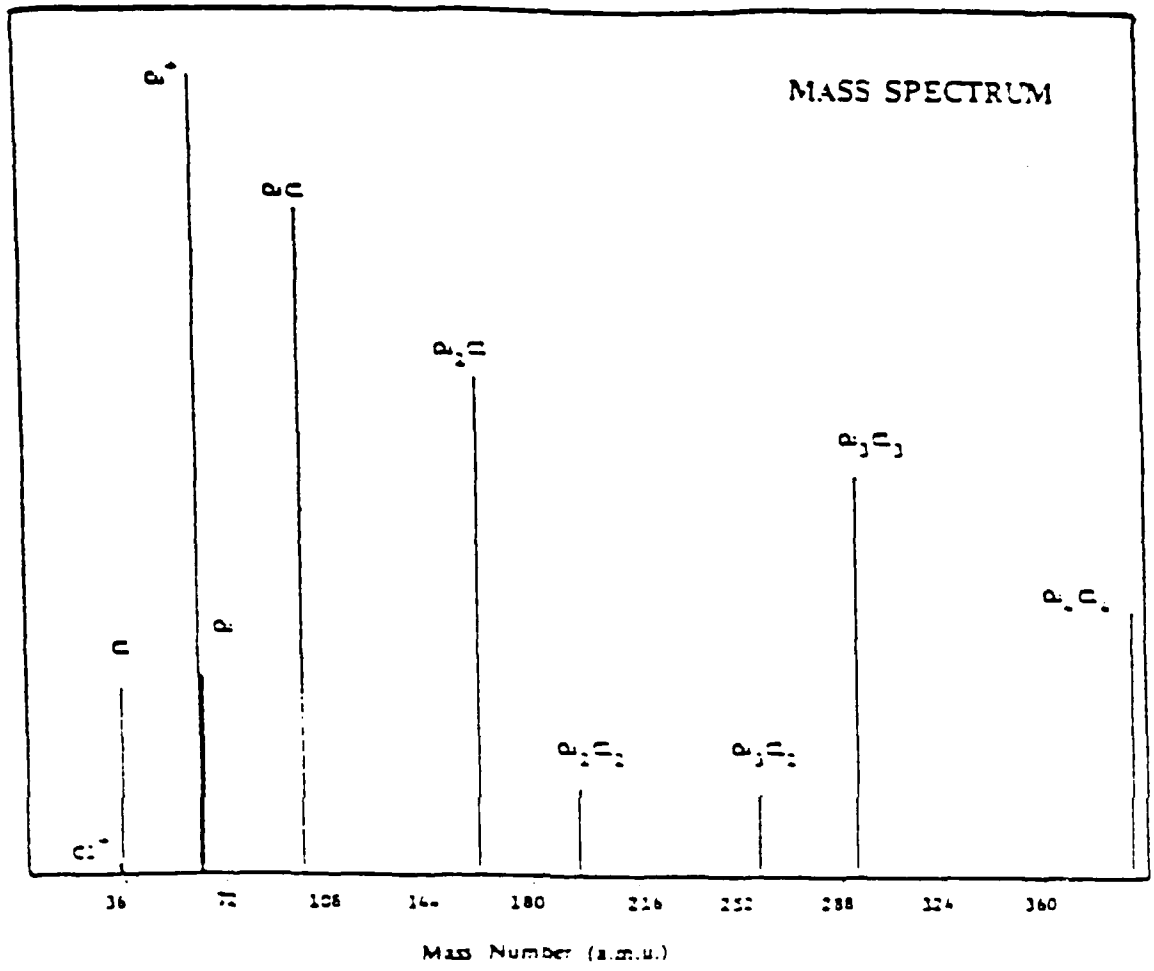

Figure 2 (b) : 248 nm incident laser wavelength.

Figures 3(a)-3(d): Time-of-flight signals for the $Cu+Cl_2$+193 nm system. The arrow indicates the laser onset.

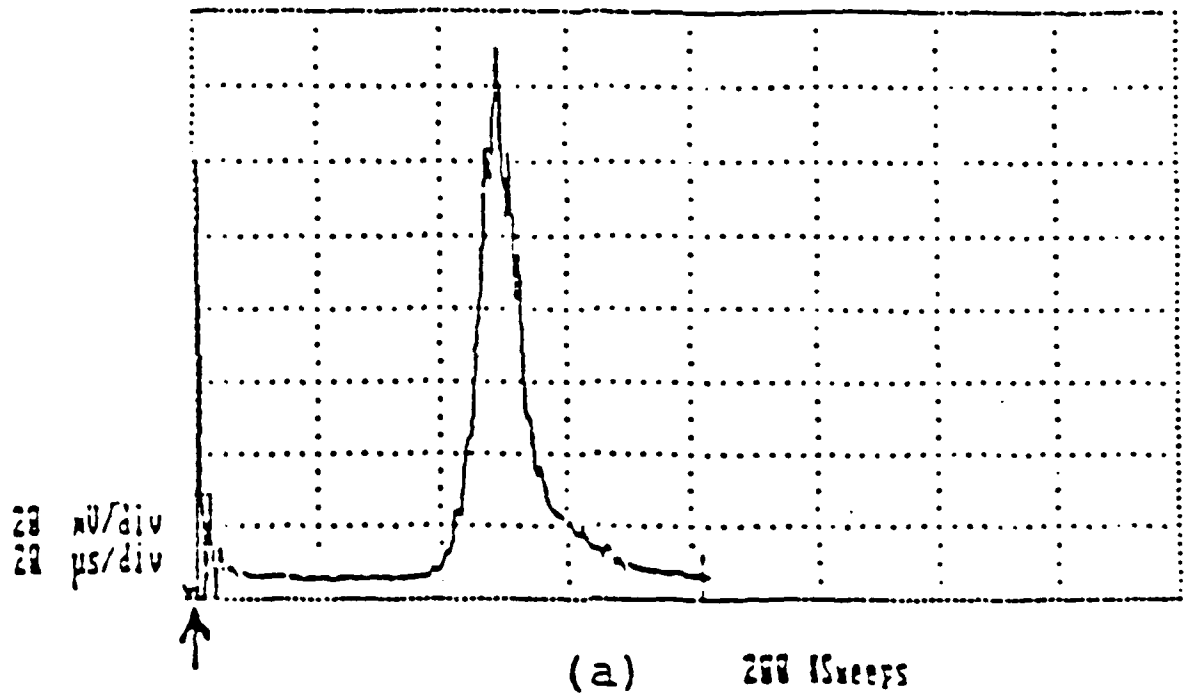

Figure 3(a): Cu^+ signal with the ionizer off.

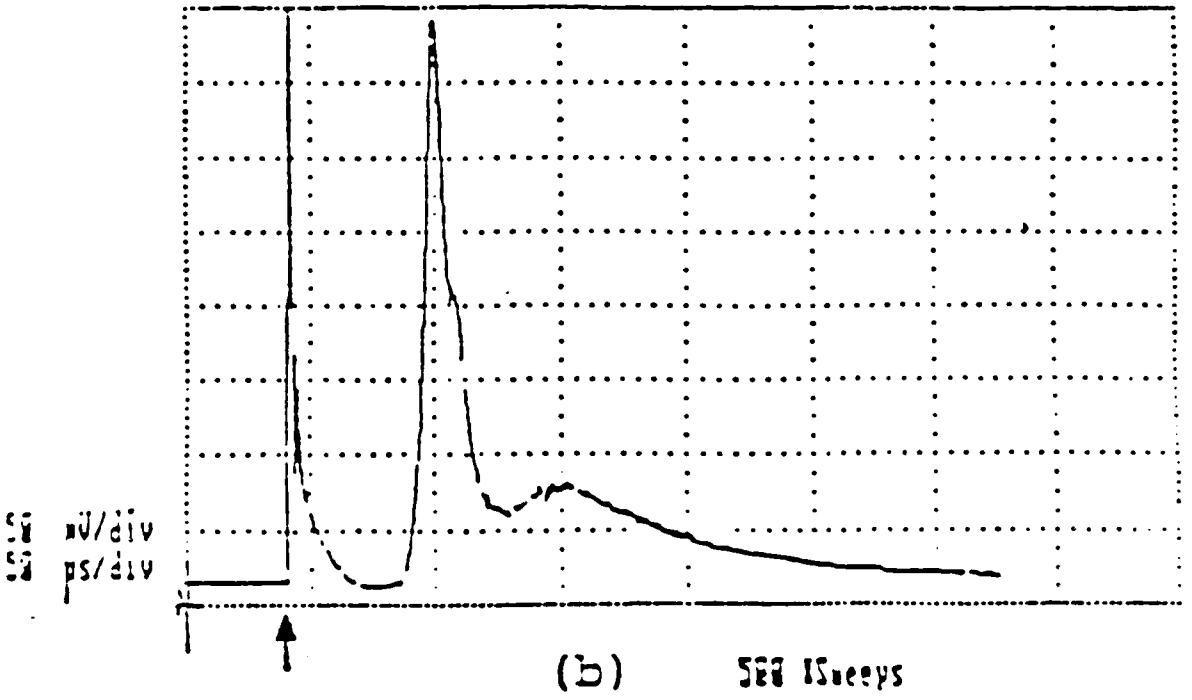

Figure 3(b): Cu signal with the ionizer on. Fast and slow peaks are due to copper ions and neutrals, respectively.

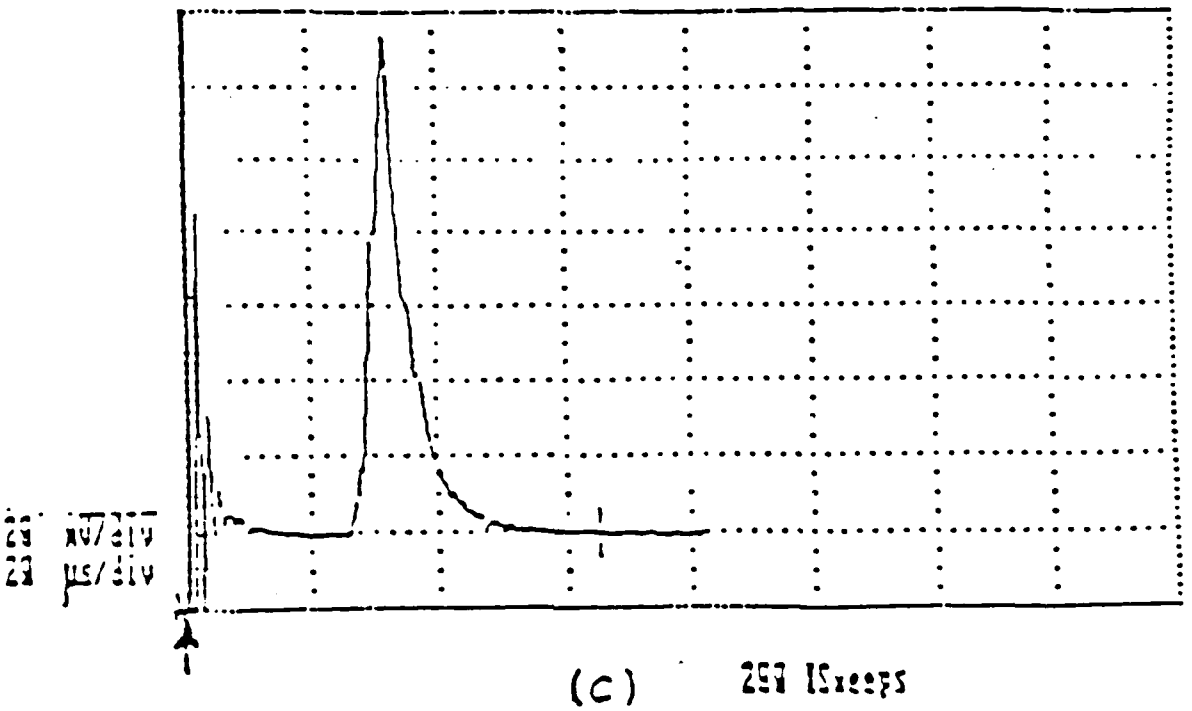

Figure 3(c): Cl^+ signal.

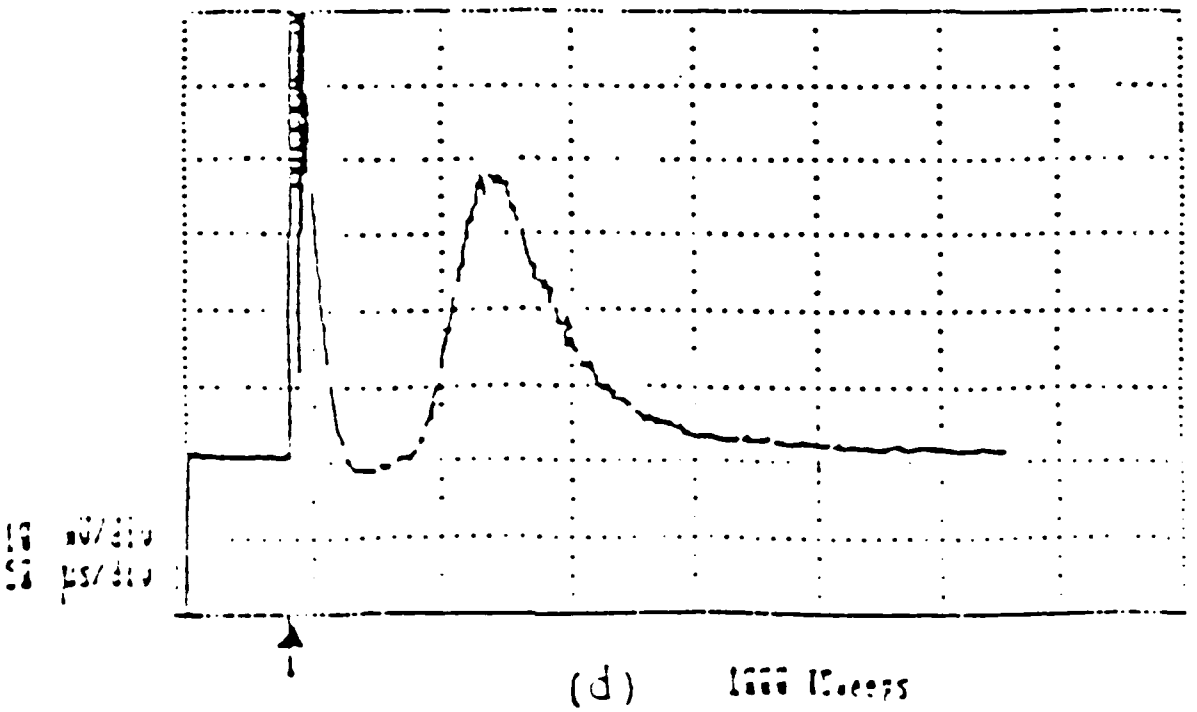

Figure 3(d): Cl neutral signal. Noise near the laser onset is due to scattered photon signal.

Figures 4(a)-4(b): CuCl time-of-flight signals for the $Cu+Cl_2$+193 nm system. The arrow indicates the laser onset. Mass spectrometer ionizer is turned on.

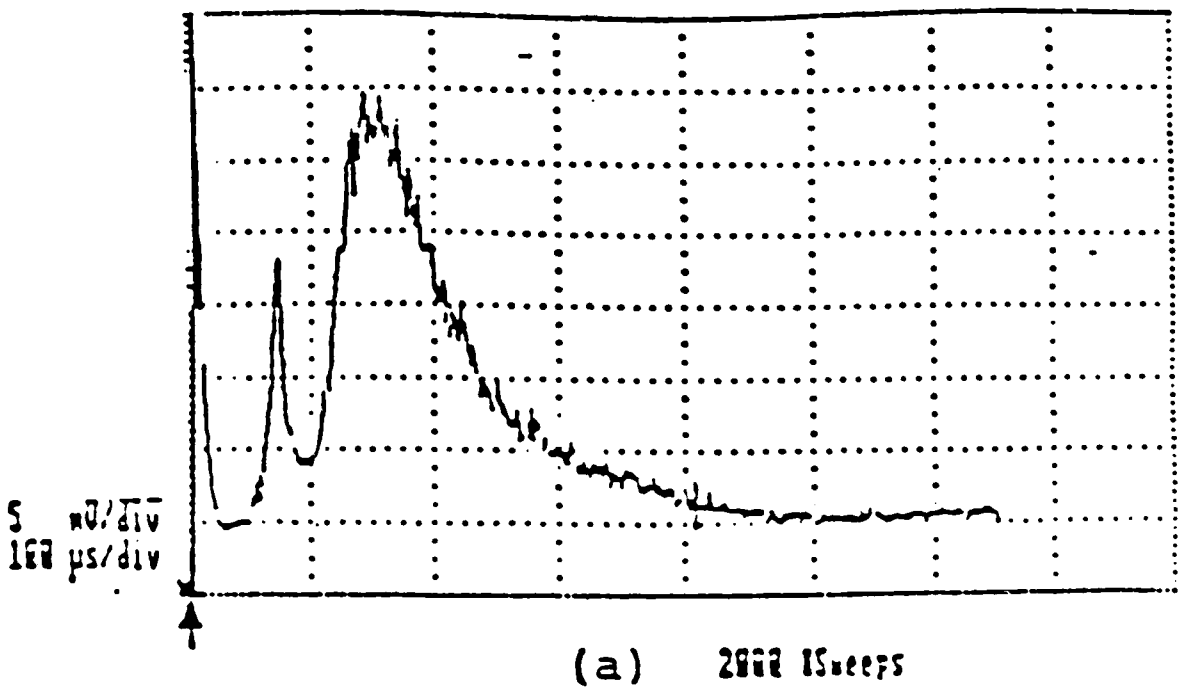

Figure 4(a): Faster $CuCl^+$ ion peak and slower CuCl neutral peak.

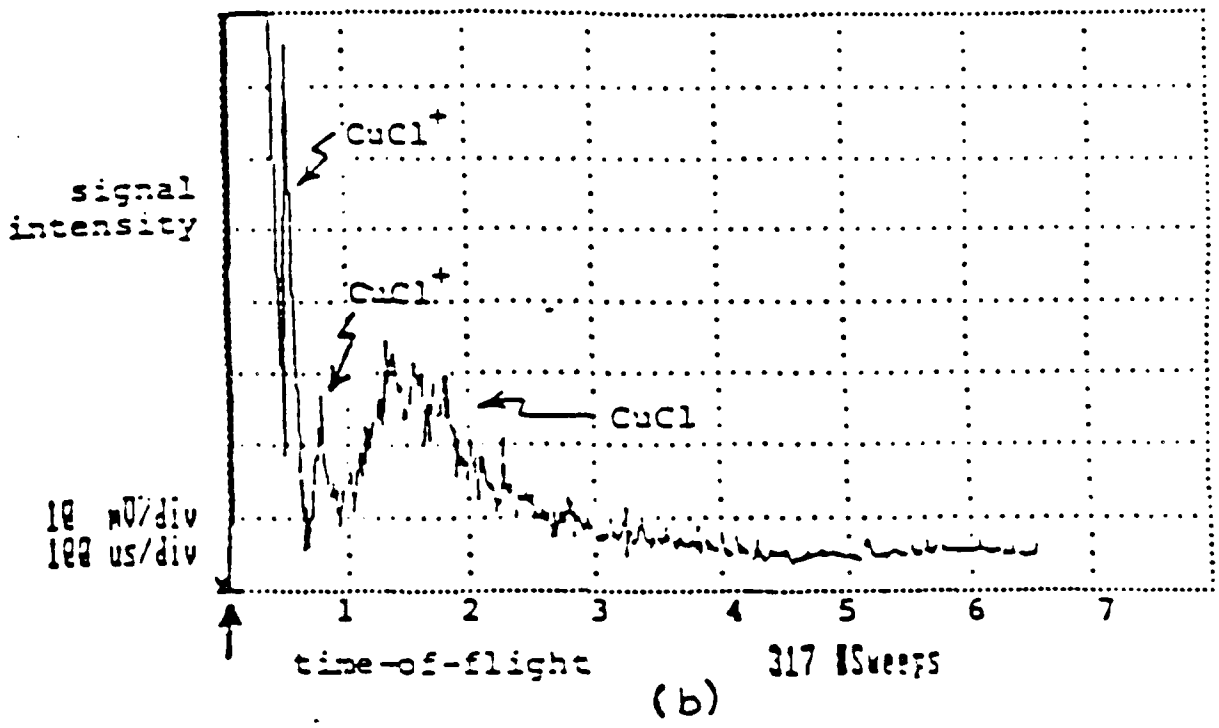

Figure 4(b): Two fast $CuCl^+$ ion peaks are observed for one sample.

Figures 5(a) and 5(b): Typical yield dependences of the lower mass desorbates on the Cl_2 coverage. The laser wavelength is 193 nm and the laser fluence is 70 mj/cm_2.

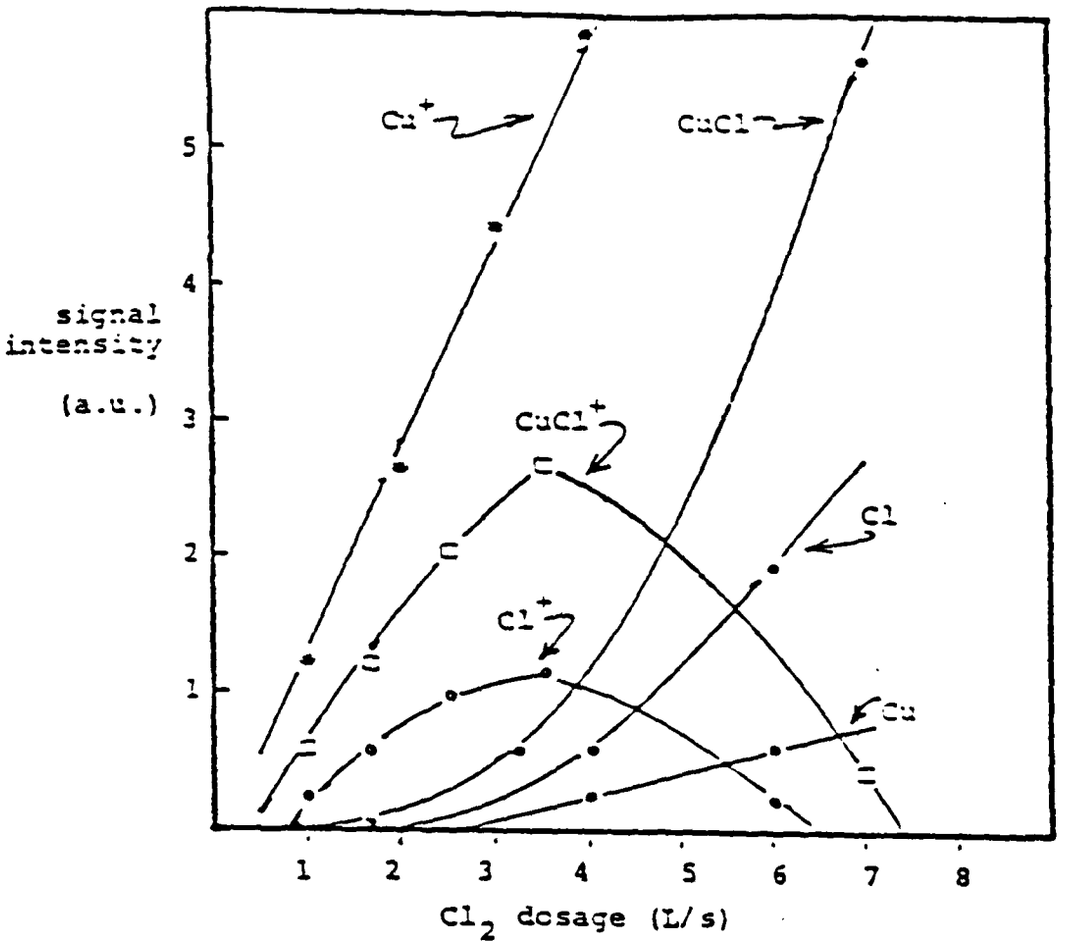

Figure 5(a): Low Cl_2 dosage regime.

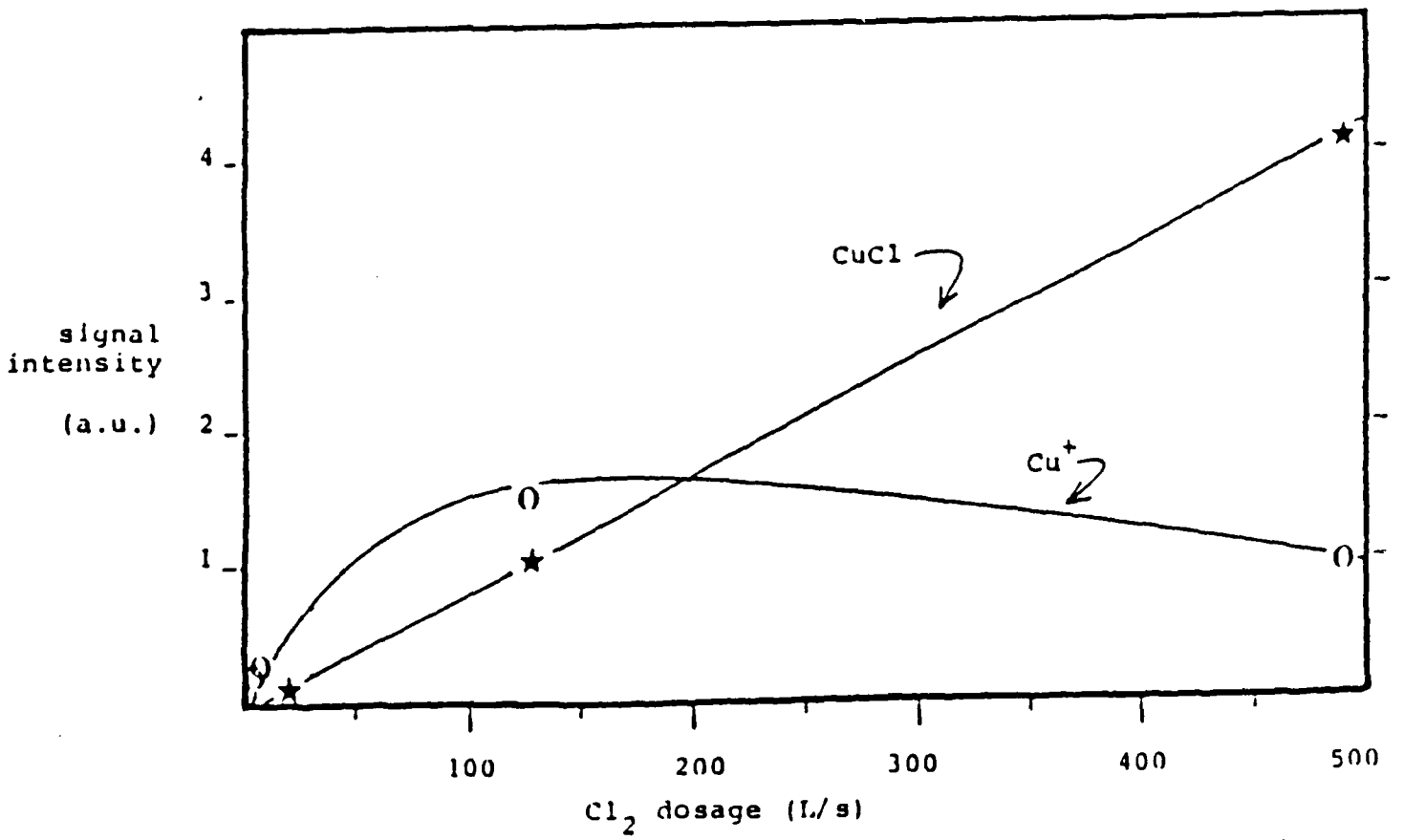

Figure 5(b): Cu^+ and CuCl yields for the high Cl_2 dosage regime.

(Figure 5a), the ion signals rise faster than neutrals, which is especially evident for the Cu signals.

The typical mass yields as a function of 193 nm laser fluence are exemplified by a CuCl neutral signal and a Cu^+ ion signal, as shown in Figure 6. The neutral yield increases linearly with laser fluence while the ions show an $\approx I_{2.5}$ dependence on the laser fluence. The most important feature of these curves is the presence of the laser fluence threshold which is ≈ 45 mj/cm^2 for the Cu^+ and slightly higher for the CuCl neutrals.

b. Cu+Cl_2+248nm -- The mass spectrum is obtained under the similar laser intensity and chlorine coverage conditions as the 193 nm mass spectrum (Figure 2b). Comparing the two mass spectra, we observe that the relative neutral signal intensities are similar for the two mass spectra with the exception of $CuCl_2$ which is not observed for the 248 nm system. The total yield of the neutral desorbates is similar for the two systems. The ion yield, however, is much smaller for the 248 nm system. $CuCl^+$ is no longer observed, and the Cu^+ and Cl^+ yields are reduced to approximately 50% and 1% of the values observed under 193 nm illumination. Typical ion Time-of-Flight mass signals for the 248 system are shown in Figure 7. The dependence of neutral yields and the Cu^+ yield on the Cl_2 dosage and laser fluence for the 248 nm system is similar to the 193 nm system.

Studies of the Cu + Cl_2 + 351 nm system in the laser fluence range of interest (up to 130 mj/cm^2) showed no ion signal, and only a very weak presence of the CuCl neutrals.

4. Conclusion -- In summary, the Cu+Cl_2+ laser system shows interesting results in the low chlorine coverage regime and the low laser fluence regime (<130 mj/cm^2, when the laser induced temperature does not exceed 450 K[3]). Ion removal is most efficient with the 193 nm incident laser radiation, and is not observed at 351 nm in the low laser fluence range studied. The threshold of the incident radiation for the ion emission is,

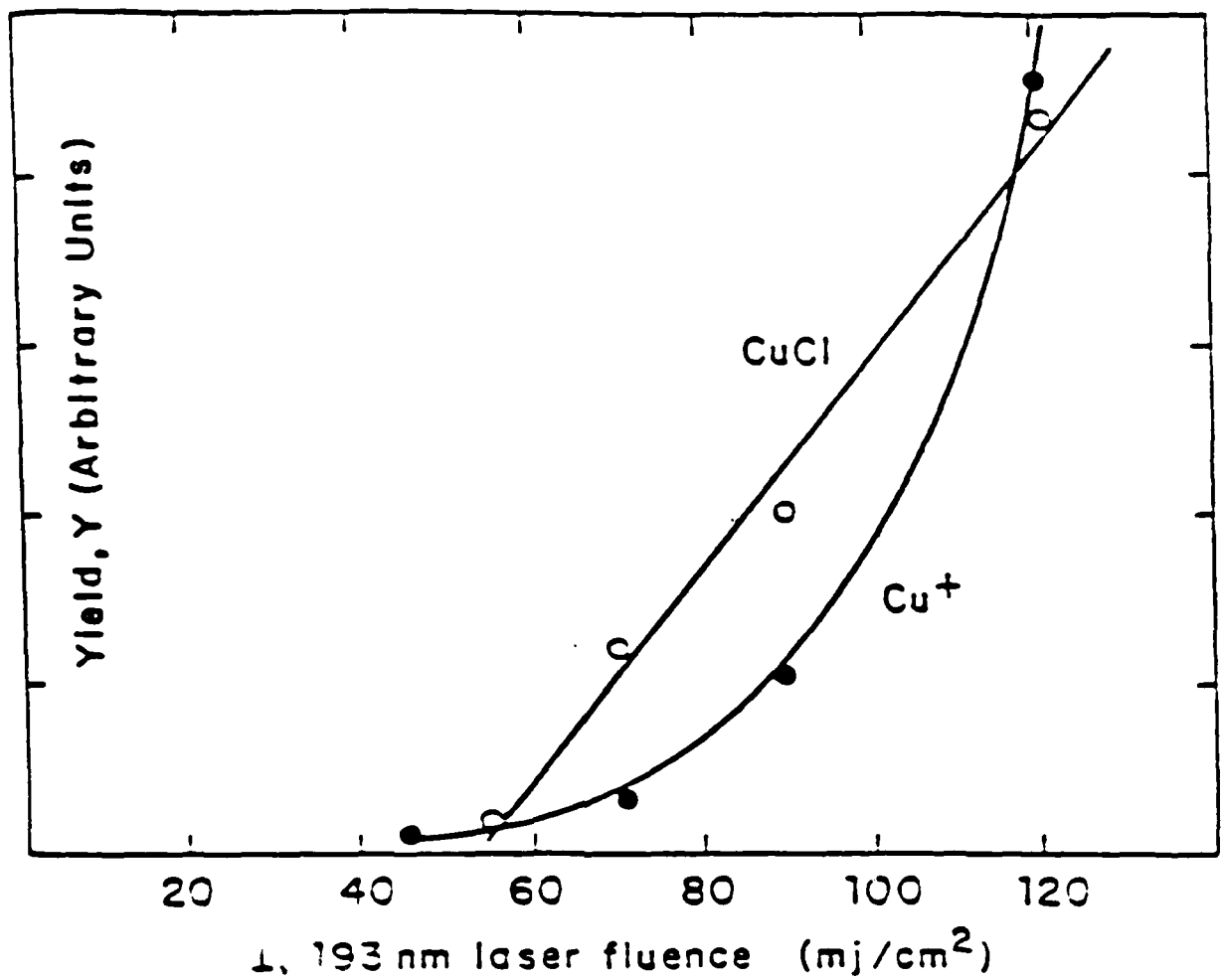

Figure 6: Typical ion (Cu^+) and neutral (CuCl) yields vs. 193 nm laser fluence. The neutral yield dependence is nearly linear while the ion yield shows $\approx I^{2.5}$ dependence on the laser fluence. The laser fluence desorption threshold is ≈ 45 mj/cm^2.

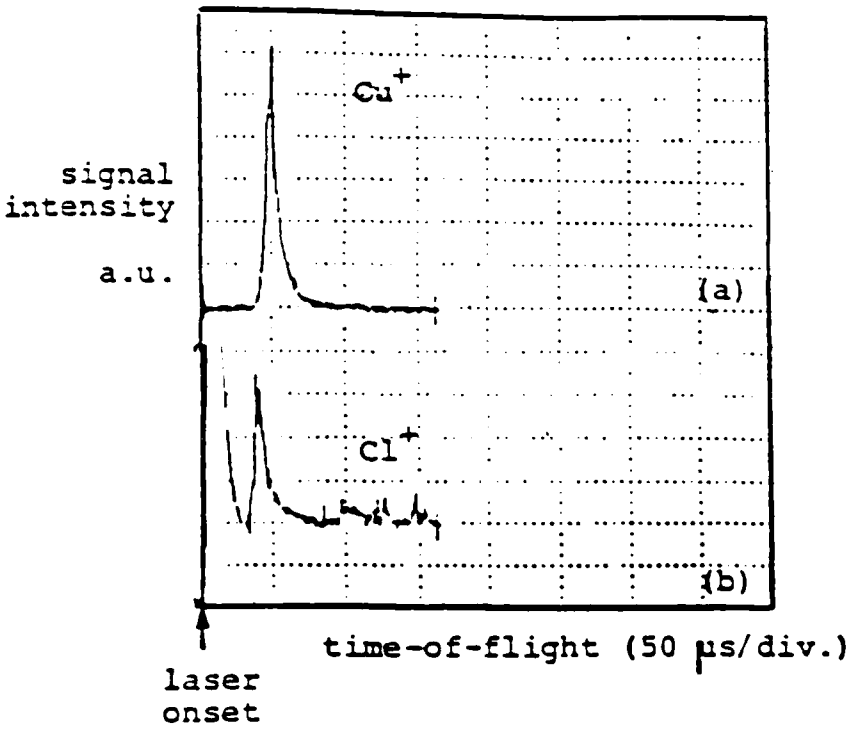

Figure 7: Typical T.O.F. ion signals for the $Cu+Cl_2$+248 nm system. The laser fluence is 66 mj/cm^2, pulse width is 20 nsec. (a) Cu^+ signal. (b) Cl^+ signal. No $CuCl^+$ is observed.

therefore, expected to occur between 351 nm and 248 nm.

Our future studies of the Cu + Cl_2 + laser system include better surface characterization which will be achieved by implementation of ion sputtering and rf annealing procedures in situ. Also, we hope to achieve a better understanding of the ion emission phenomena for the Cu + Cl_2 + 193 nm system in the low laser fluence regime.

This research was also supported by the Semiconductor Research Corporation, Contract SRC-85-02-055; the Office of Naval Research, Contract N00014-86-K-0694; The Air Force Office of Scientific Research, Contract F-49620-85-C-0067; and the Army Research Office, Contract DAAG29-85-K-0210.

References:

1 W. Sesselmann, E. E. Marinero, and T. J. Chuang, Appl. Phys. A 41 (1986) 209.

2 M. F. Winters, J. Vac. Sci. Technol. A 3 (1985) 786.

3 J. F. Ready, Effects of High-Power Laser Radiation, Academic Press, NY, 1971, Chapter 4.

B. ULTRAVIOLET LASER-INDUCED ION EMISSION FROM SILICON

(L. Chen, V. Liberman, J. O'Neill, Z. Wu, R. Osgood, Jr.)
(JSEP work unit 4, 1985-1988)
(Principal Investigator: R. Osgood, Jr. (212) 280-4462)

1. Introduction -- Pulsed UV laser sources have found a variety of semiconductor processing applications in the field of microelectronics ranging from laser induced chemical etching to photolytic metal film deposition processes[1]. A complete understanding of these photoprocesses, however, requires the characterization of the fundamental aspects of the pulsed laser-solid interaction.

This report describes the observation of UV induced photo-ion ejection from semiconductor surfaces, which is shown to be due to nonthermal mechanisms. The effect is observed using a pulsed laser with an energy density far below that required to melt the crystal. The ejection appears to be explicable on the basis of nonlinear optical absorption in the vicinity of surface defects.

2. Experimental -- Polished Si(111) surfaces were chemically cleaned and stripped of their native oxide layer prior to mounting in a UHV sample chamber (10^{-9} torr) equipped with a quadrupole mass spectrometer. The samples were exposed to UV radiation from a pulsed excimer laser operating at 193, 248 or 351 nm at laser fluences from 0-150mJ/cm^2. Positively charged ions corresponding to mass 28 were detected upon irradiation of a Si(111) n-type substrate (10^{+15} cm^{-3}) with 193 and 248 nm light. The contribution of surface contaminants (such as CO, also mass 28) to the observed signals was determined to be negligible since prolonged illumination (up to 10^4 shots) of the substrate caused no attenuation of the observed signal as would be expected if a

surface adlayer were gradually removed by laser desorption. Similarly, irradiation of Ge samples under identical experimental conditions yields no ion signal at mass 28. Also, no neutral or positively charged oxygen species were observed under the present experimental conditions.

3. Results -- At 248 nm under conditions of very high laser fluence (500-600 mJ/cm^2) time-of-flight distributions were measured which correspond to ions with kinetic energies of 30 eV (see Figure 1). This large ion energy gradually decreases with decreasing laser fluence and is attributed to the vaporization of the substrate surface layer and the formation of energetic ions in a dense gas-phase plasma[2].

At laser fluences well below the threshold necessary to cause melting of the bulk silicon, the ion time-of-flight distributions correspond to a kinetic energy of 0.45eV. This value remains constant for irradiation at both 193 and 248 nm for laser intensities in the range of 10-150 mJ/cm^2. The distribution of ion velocities converted from the observed TOF distributions is very narrow and can be fit approximately to a Boltzmann temperature of about 15K. Such a distribution is believed to reflect the efficient collisional cooling of ions above the irradiated semiconductor surface which occurs due to their large coulombic cross-section[3].

The remainder of this report concerns observations made in the low intensity regime (<100 mJ/cm^2). The angular distribution of charged particles emanating from the surface is obtained by rotating the sample rod up to 90^o relative to the mass spectrometer. The observed distribution is found to be sharply peaked in the direction normal to the surface with virtually no ions emitted at angles larger than 20^o from the surface normal. Such an angular variation is consistent with the ion velocity distributions observed in the present experiments where the stream temperature (2900K) is greater than the internal temperature (15K). In such a case, ions reach the detector before significant expansion has occurred away from their

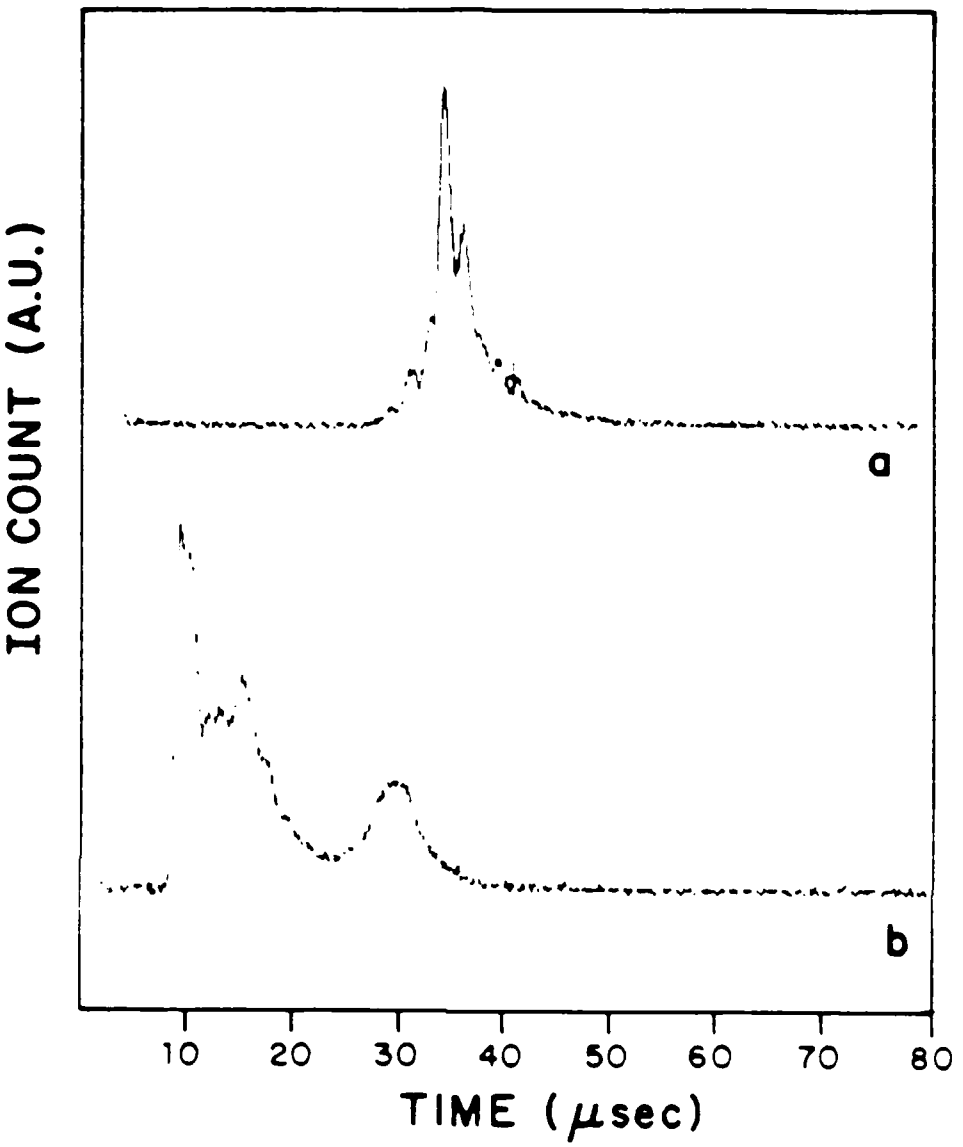

Figure 1: Si+ ion time-of-flight data obtained upon 248 nm excimer laser irradiation of a Si(111) 10^{15} cm^{-3} n-type substrate. These signals were observed with the mass-spectrometer ionizer off. UPPER TRACE: Laser fluence=60mJ/cm^2, E_{tr}=0.45eV. Si^+ ions ejected from irradiated substrate with peak surface temperature of 400K. LOWER TRACE: Laser fluence=600mJ/cm^2, E_{tr}=30eV. Silicon ions resulting from vaporization of the substrate and subsequent formation of an energetic plasma above the surface.

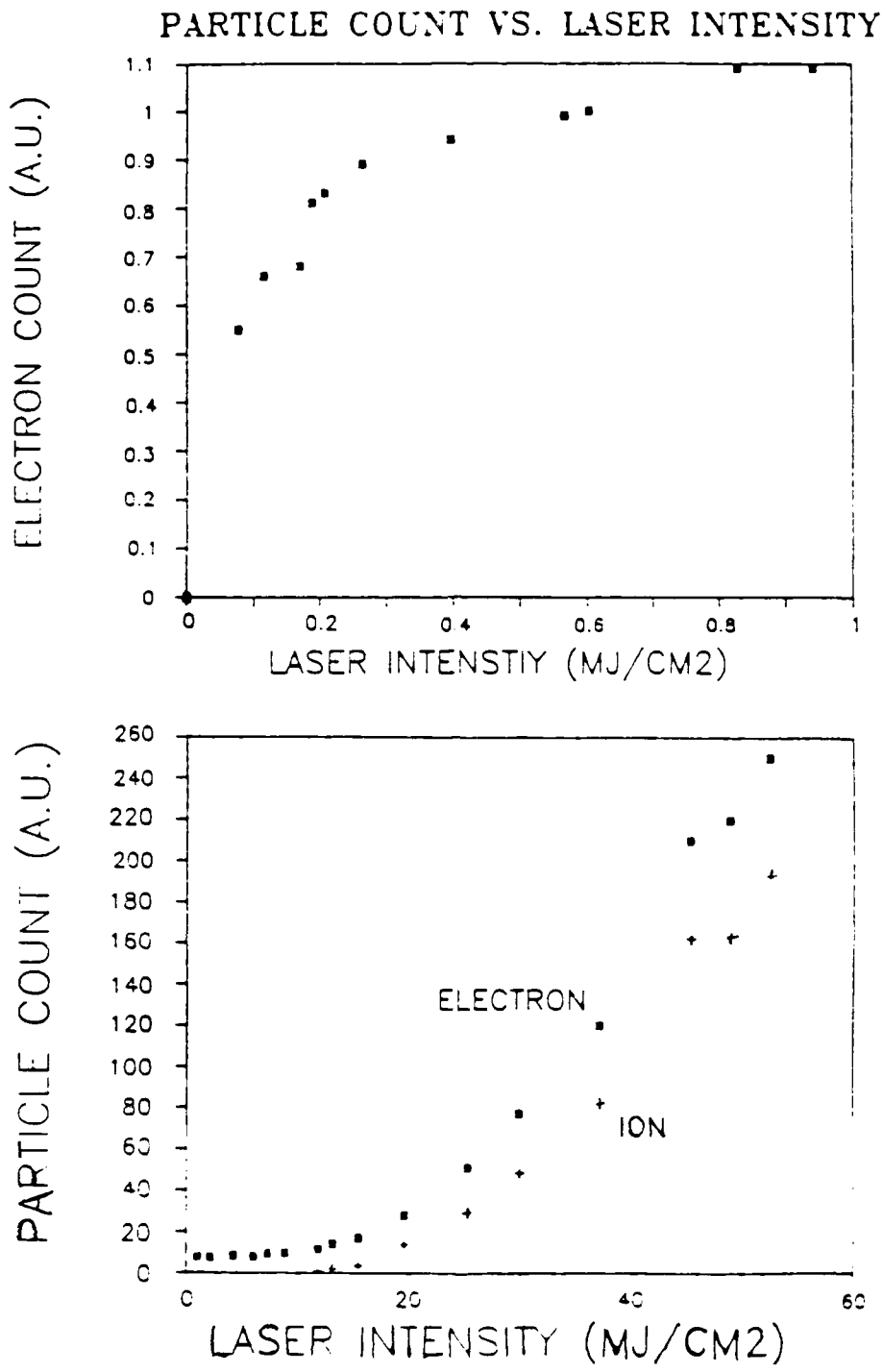

Figure 2: Photoelectron and photoion emission signal as a function of excimer laser intensity at 193 nm for Si(111) 10^{15} cm^{-3} n-type substrate. UPPER TRACE: At very low laser intensity, the electron photoemission increases linearly with laser intensity until space charge effects inhibit electron detection. LOWER TRACE: The photoion emission threshold occurs at 12 mJ/cm^2 for this sample. At this point, the saturation of the electron emission response is relaxed and the electron signal increases.

center-of-mass[4].

Measurements of both electrons and ions are made in an auxiliary sample chamber (10^{-6} torr) equipped with a charged particle collector consisting of a rod biased between $\pm$ 100-500V. Both the electron and the ion yield are found to depend significantly on surface conditions. Both unpolished and mechanically scratched wafers are seen to yield substantially more electrons and ions than smooth, polished samples which have been chemically etched in a buffered HF solution prior to study. Also, the ion yield is observed to be enhanced more by roughening than the electron yield. For a typical n-type Si(111) sample ($10^{15}cm^{-3}$), the dependence of the collected charge on the incident laser fluence is illustrated in Figure 2 under conditions of 193 nm irradiation. For this sample, the photoelectron emission increases linearly with laser intensity at the lowest fluences studied ($<1mJ/cm^2$). As the incident laser fluence increases, however, the observed photoelectric signal saturates as space charge effects significantly inhibit electron collection. As the laser fluence is increased further ($>12mJ/cm^2$), the photoelectric response increases rapidly with a quadratic dependence on the incident laser fluence. At this point, positive Si ions are observed to emanate from the substrate. This ion removal process serves to diminish the space charge field and further enhance the ejection of electrons from the bulk. Irradiation of the same sample at 248 nm shows similar behavior with the ion emission threshold occurring at 36 mJ/cm^2. While the ion threshold observed in these experiments is sensitive to surface roughness, it is consistently lower for 193 nm than for 248 nm illumination, and in all cases it is an order of magnitude below the laser fluence necessary to cause the Si substrate to melt (445 mJ/cm^2). Measurements performed at 351 nm show no emitted electrons or ions for low laser fluences employed in these experiments ($<100mJ/cm^2$).

In order to insure that the ion emission process observed in the present work is truly a low temperature phenomenon, the temperature of the surface during the irradiating laser pulse is

estimated by an experimentally calibrated transient temperature calculation. The numerical calculation is similar to that used previously[5] including temperature dependent optical and thermal coefficients. It predicts that surface melting should occur at laser fluences of approximately 420 mJ/cm^2, which is much higher than the fluences used in the present experiments. Time-resolved reflectivity measurements using a HeNe probe beam show an experimental surface melting threshold of 445 mJ/cm^2, in good agreement with the calculation.

Photoelectric and photoionic emission behaviour similar to that seen in the case of Si is also observed for 193 and 248 nm laser irradiation of a Ge substrate. Neither electrons nor Ge ions are observed upon irradiation at 351 nm except for laser fluences above the threshold for melting.

In the case of silicon, the role of mobile impurity carriers on the observed photo-ion emission process is determined to be minimal since under 193 nm illumination, similar photo-ion signals were obtained over a wide range of n and p-type doping levels (10^{+14}-10^{19}cm-3). The measured photoelectron signal is seen to increase slightly with increased p-type character in keeping with previous observations of Allen and Gobeli.[6]

4. Conclusions -- Recent improvements in our experimental apparatus will enable further study of this ion emission process under carefully characterized surface conditions. Also, the occurrence of this phenomenon in other semiconductor and insulator substrates is presently under investigation in our laboratory.

This work was supported by the Semiconductor Research Corporation, Contract SRC-85-02-055; the Office of Naval Research, Contract N00014-86-K-0694; the Air Force Office of Scientific Research, Contract F-49620-85-C-0067, and the Army Research Office, Contract DAAG29-85-K-0210.

References:

1 P. Brewer, S. Halle, and R. M. Osgood, Jr., Appl. Phys. Lett. 45, 475 (1984); R. M. Osgood, Jr. and T. F. Deutsch, Science 227, 709 (1985); P. Brewer, G. M. Reksten and R. M. Osgood, Jr., Solid State Tech. 273, April 1985; H. H. Gilgen, T. Cacouris, P. S. Shaw, R. R. Krchnavek and R. M. Osgood, Jr., Appl. Phys B 42, 55 (1987); R. Kullmer and D. Bauerle, Appl. Phys A 43, 227 (1987); F. A. Houle, J. Chem. Phys. 87, 1866 (1987).

2 J. F. Ready, Effects of High-Power Laser Radiation, Academic Press, NY, 1971, Chapter 4.

3 J. P. Cowin, D. J. Auerbach, C. Becker and L. W. Wharton, Surf. Sci. 78, 545 (1978).

4 N. G. Utterback, S. P. Tang, J. F. Friichtenicht, The Phys. of Fluids 19, 900 (1976).

5 H. Kurz and N. Bloembergen, Mat. Res. Soc. Symp. Proc. 35, 3 (1985); M. I. Gallant and H. M. van Driel, Phys. Rev. B. 26, 2133 (1982).

6 G. W. Gobeli and F. G. Allen, Phys. Rev. 127, 141 (1962).

C. DIFFERENTIAL VOLTAGE TECHNIQUE FOR CAPACITANCE MEASUREMENT

(E. S. Yang, X. Wu)
(JSEP work unit 3, 1985-1988)
(Principal Investigator, E. S. Yang (212) 280-3103)

1. Technical Report -- One of our major goals in this project is to develop a capacitance spectroscopy for characterization of M-S interface. In order to do so, an accurate measurement of data is very important, particularly in the present situation as the theory of the interface capacitance has not been well established. An inaccurate set of data could easily mislead our interpretation. Therefore, we are not to rely on just one source of data (APCS).[1] It is necessary to have another independent method to exclude any circuit effect and to make sure that the data obtained are true characteristics of the device.

Measurements of diode capacitance in the forward-bias direction are readily subject to error. This is because the capacitance signal of the diode is being overwhelmed by the thermionic emission conductance (G). This conductance is sometimes three or four orders of magnitude larger than the capacitance (ωC). Under this extreme condition, ordinary methods, such as the use of a Boonton capacitance meter, are no longer applicable. Even the Accurate Phase Capacitance Spectroscopy (APCS) method described previously[1] is limited by its instrumentation. First of all, the phase setting in APCS becomes extremely crucial. In practice, for a small phase error, (around 90°), we have

$$\Delta(\omega C) = -G\Delta\phi, \tag{1}$$

where $\Delta(\omega C)$ represents the resultant error of the measured

susceptance and $\Delta\phi$ is in radians. For $G/\omega C$ on the order of 10^4, even a 10^{-4} error in phase would cause a 100% error in the capacitance. Although the APCS method can set the phase in a very high accuracy, it cannot ensure that there will be no phase shift during the measurement. Therefore, no matter how accurately the phase is set initially, a tiny phase drift will nullify the whole measurement. Furthermore, the sensitivity of the instruments, e.g., the lock-in amplifier (LIA), is limited by the conductance signal level. We know that the capacitance signal of a diode is very weak, especially at low frequencies, it is always desirable to use a high sensitivity setting in order to get better noise performance. But the capacitance signal is buried in a huge conductive component, which frequently overloads the preamplifier and drives the LIA into a nonlinear region, making the measurement impossible. For this reason, we have implemented the following differential voltage scheme for measuring the device capacitance when the quality factor ($\omega C/G$) is as low as 0.001.

The basic concept of the Differential Voltage Capacitance Spectroscopy (DVCS) is similar to that of a bridge circuit. Since the main problem arises from the high conductance that is inherently associated with the device, we propose to generate an in-phase signal to cancel out the conductive component of the diode, letting only the capacitive component be retained to pass through the phase sensitive detector. This way, the overload problem is avoided and the influence of the phase drift is also minimized. As a result the accuracy of the measurement is greatly improved.

A schematic description of the differential voltage capacitance spectroscopy technique is shown in Figure 1. A small ac reference signal, V_i, derived from the internal oscillator of a PAR 124 lock-in amplifier, is superimposed on a biasing voltage. This combined voltage is applied between point D and the ground. Two currents are generated. One, i_a, passes through the diode; the other, i_b, through a variable resistor, R. These currents are converted into voltage signals by resistors R', and

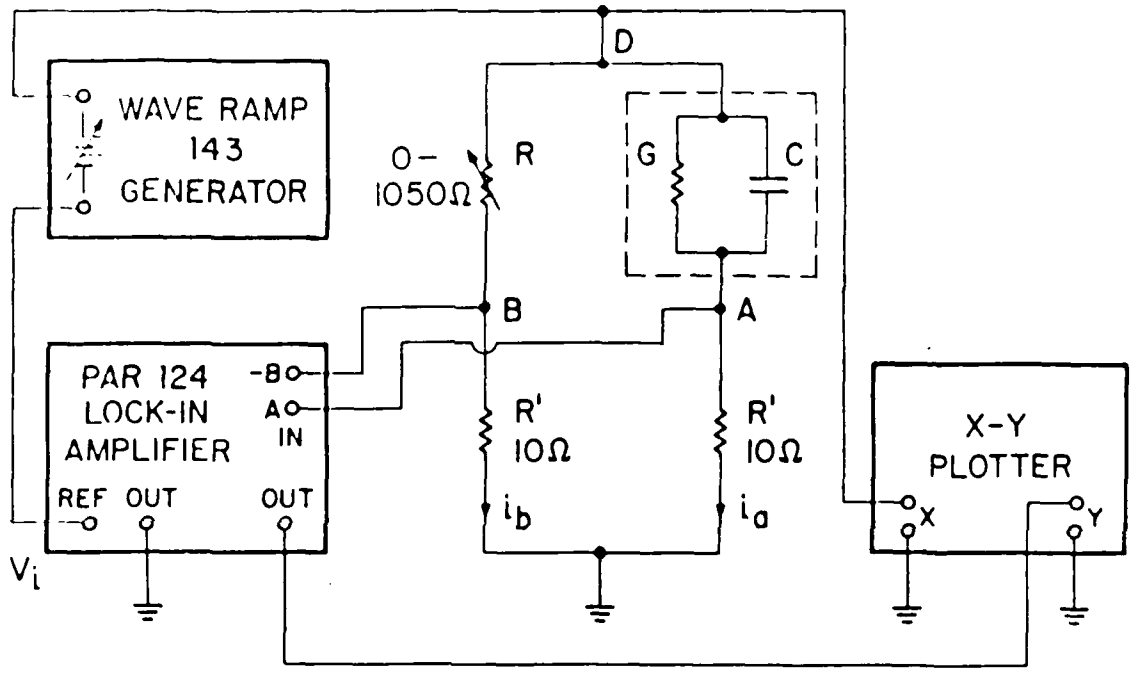

Figure 1: Apparatus of the Differential Voltage Capacitance Spectroscopy.

are then fed into the inputs of the LIA through a differential preamplifier. The output of the differential preamplifier contains only the ac component of $V_a - V_b$; the dc portion is fully rejected. If R' is much smaller compared to 1/G and R, the output of the LIA is

$$V_0(\phi) = V_i R' A[(G - 1/R)\cos\phi + \omega C \sin\phi], \tag{2}$$

where A is the voltage gain of the LIA and ϕ the phase setting of the phase sensitive detector. When the phase is set to 90° with a small error $\Delta\phi$, the output becomes

$$V_0 = (90^\circ + \Delta\phi) = V_i R' A[-(G - 1/R)\Delta\phi + \omega C], \tag{3}$$

and the error is

$$\Delta(\omega C) = -(G - 1/R)\Delta\phi. \tag{4}$$

If the conductive component is nulled out, i.e., $G-1/R \simeq 0$, the error will be very small, even in the presence of a significant $\Delta\phi$. This can be contrasted with Eq. (1) where $\Delta(\omega C)$ is directly proportional to $G\,\Delta\phi$.

The method was used to measure the forward-biased capacitance for a number of diodes. Figure 2 shows a typical result obtained from a Ni-nSi sample.[2,3] In the figure, data obtained from the APCS are also presented as a comparison. It can be seen that the results of the DVCS and the APCS are in good agreement at low bias. At high bias the deviation between the two is caused by a phase error. This was confirmed by a tiny phase readjustment in the APCS measurement, such that a 0.005° phase shift could cause the curve to coincide with the DVCS results. In order to examine the significance of a phase error in the DVCS, we deliberately turned the phase 1° off its correct position. With the real component carefully nulled out, we found the influence on the output reading to be less that 3%, while the phase accuracy in the experiment could be kept to less than 0.1°.

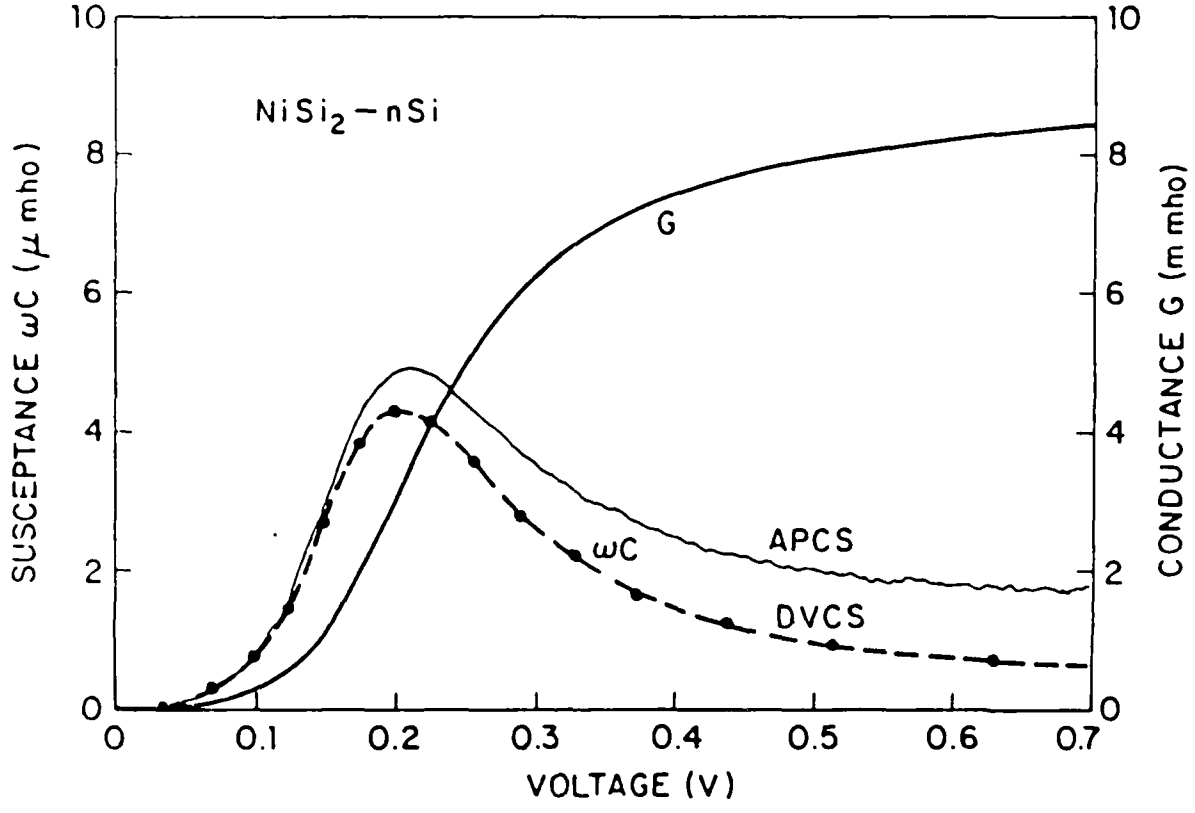

Figure 2: The susceptance (ωC) and conductance (G) curves measured from a Ni-nSi Schottky diode at 108 Hz and 300 K. Note the scale of the conductance is 1000 times that of the capacitance.

Another merit of this new method is clearly seen in the measurements of low resistivity materials, where the conductance is so high that overloading becomes a serious problem in APCS. But with DVCS, the capacitance can be measured without difficulty. It might be worth mentioning that this technique can also be used for $\omega C >> G$. In that case, one merely puts a variable capacitor in place of the variable resistor, where the capacitive component is to be cancelled. This could be useful in the measurement of conductance in MIS devices.

3. Negative Capacitance -- In this section we report a phenomenon, observed for the first time, showing that under forward bias some Schottky diodes manifest a "negative capacitance" in response to an ac signal. It reveals that the Shockley-Read model[4] is inadequate in describing the occupancy probability of interface states at high incidence of hot carriers. Under such circumstance, the impact ionization process must be taken into consideration.

The experimental method used for this study was described in the previous section. Figure 3 shows the data obtained from a $NiSi_2$-nSi Schottky diode. The diode has a barrier height of 0.67 eV and was prepared in a UHV environment. TEM analysis showed that the sample possesses a mixed A/B-type interface.[2] Measurements were made over a range of temperatures from 10 K to 300 K. The data shown here were obtained at 200 K and 108 Hz. It can be seen from the figure that with increasing bias, the diode capacitance rises until it peaks and than decreases rapidly. At sufficiently high bias it goes below the abscissa revealing a "negative capacitance" (NC) tail. It should be pointed out that the "NC" is not unique to the $NiSi_2$-nSi interface. Similar features have been found in Pd-nGaAs and Pd-nSi diodes. The occurrence of the NC depends on the temperature and the frequency of the measurement, and varies from device to device. However, it appears only at high bias, and its magnitude increases with the frequency.

This phenomenon cannot be explained by the usual theory of

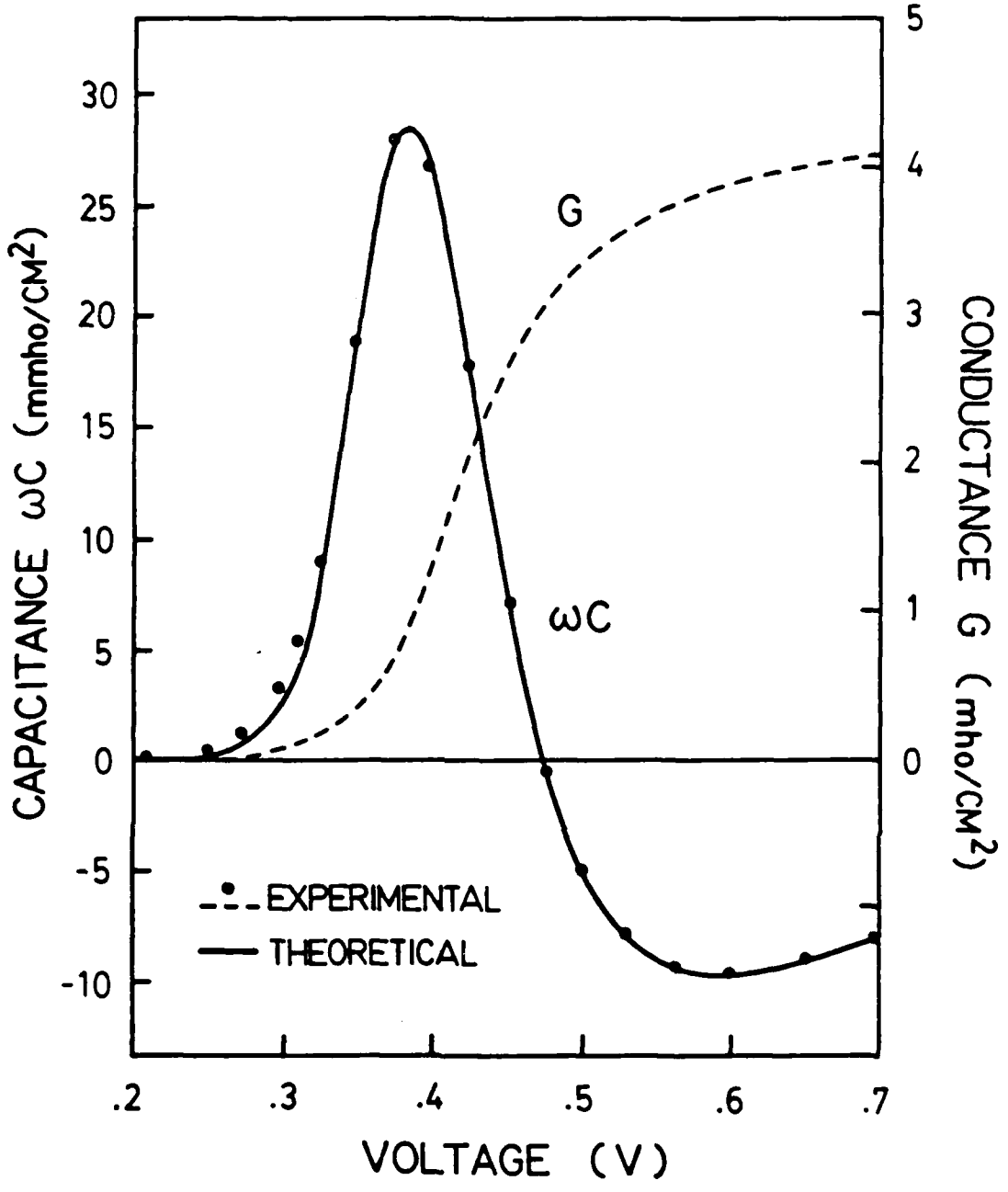

Figure 3: Susceptance and conductance as a function of bias measured at 200 K and 108 Hz from a $NiSi_2$-nSi Schottky diode. The solid line is the calculated susceptance curve according to a two-level model.

interface capacitance, nor by other known bulk effects. We know that any charge accumulation in a device would only give rise to a positive capacitance. A "NC" has, so far, no meaning to us. The regular diode capacitance as we saw in the low bias region can be understood as follows. The existence of localized states at a metal-semiconductor interface results in a charge dipole at the M-S junction, which can be described by its thickness, δ, and the permittivity, ε_i. This dipole produces a potential difference, V_s, on the two sides of the interface. Under forward bias, most of the voltage drops on the depletion layer, while the remainder is shared by the semiconductor bulk and the interfacial dipole. In the presence of an ac influence, V_s varies with ΔV, which alters the diode's barrier height and, hence, modulates the thermionic emission current. The variation of potential V_s arises mainly from carrier capture and emission at interface states. This process requires a certain period of time, which makes ΔV_s lag behind ΔV. If we denote the diode conductance by G, then the susceptance of the diode can be approximated by

$$\omega C = -\mathrm{Im}\left(\frac{\partial V_s}{\partial V}\right) G, \tag{5}$$

where $\mathrm{Im}(\partial V_s/\partial V)$ stands for the imaginary part of the derivative. In most cases, the contribution of the depletion layer charge is negligible; therefore, $\Delta V_s = -\Delta Q_{ss}\,\delta/\varepsilon_i$. ΔQ_{ss} is the variation of interface charge density. It can be calculated from the following integral

$$\Delta Q_{ss} = -q \int N_{ss}(E)\,\delta f(E)\,dE, \tag{6}$$

where $N_{ss}(E)$ is the density of interface states, and $\delta f(E)$ the increment of occupancy probability at the corresponding level. The explicit expression for $\delta f(E)$ is rather complicated.[5] However, it is sufficient to discuss the behavior of $f(E)$, the steady state occupancy under dc bias.

The probability of an interface state being occupied is commonly treated by the Shockley-Read statistics,[4] where the

occupancy probability of a trap state is determined by the charge capture and reemission rates. For an n-type semiconductor, f may be written as[5]

$$f(E) = F_s(E)\frac{c_n n_{s0} + F_m(E)/\tau_T}{c_n n_{s0} + F_s(E)/\tau_T}, \tag{7}$$

Where F_m and F_s are the Fermi functions with the Fermi level equal to that in the metal and the semiconductor bulk, respectively; c_n is the electron capure coefficient, and n_{so} the free electron concentration near the semiconductor surface; the reciprocal of τ_T describes the carrier exchange rate with the metal. At zero bias, f(E) is identical to the Fermi function. Under forward bias, the quasi-Fermi level of the semiconductor, E_f^s, shifts above the metal Fermi level, E_f^m. For any energy level, $F_s \geq F_m$; the properties of Eq. (7) can be summarized as follows:

(1) For states below E_f^m, $F_m=F_s=1$; f(E) is equal to unity.
(2) For those above E_f^s, $F_m=F_s=0$; the states remain empty.
(3) For the states energetically located between E_f^m and E_f^s, $F_m=0$ but $F_s=1$; the states become partially occupied, and their occupancy probability increases monotonically with the current ($\sim n_{so}$) through the interface.

The analysis presented above tells us that the charge at the interface always increases with an increment of bias. In other words, from the Shockley-Read model we may expect only a positive capacitance.

Then where does the NC come from? Phenomenologically, a "NC" indicates that the current variation in the device lags behind the voltage agitation. This somehow resembles an inductance. One possibility is that the alignment of electron spin or orbital magnetic momentum at the interface makes the device act like an inductor under ac influence. This hypothesis, however, was quickly ruled out by an electron spin resonance

measurement, where no appreciable enhancement of the NC signal was observed. Other potential causes, such as carrier recombination and minority carrier effects, have also been examined. None can reasonably account for this phenomenon.

Is there any possibility that the charge at the interface decreases under current injection instead of accumulating? If this happens, the diode current will gradually increase along with the decreasing of interface charge. The NC could then be explained. Based on the behavior of temperature and frequency data, we conclude that this is the right answer. The theory is established using the following arguments.

Electrons that are able to overcome the Schottky barrier do fill up the empty states at the interface. But because they possess excess energy, when colliding with the electrons trapped at the interface states, they are also capable of striking electrons out of the traps, provided that the ionization energy of these traps is smaller than the Schottky barrier energy. This mechanism is similar to the impact ionization process[6] and electron multiplication in a superlattice[7] or, perhaps more precisely, to the Auger effect. However, to move an electron out of the interface trap into the metal requires much less energy than to create an electron-hole pair in the bulk. The strong coupling of the trap states to the metal conduction band makes the ionization energy very different on the two sides of the interface. On the semiconductor side, the minimum energy is $E_c - E_t$, where E_t represents the trap level being considered. However, this energy will be much lower if the excitation is made towards the metal. The thermionic electrons in the conduction band, on the other hand, experience a drastic potential change at the interface. They gain a kinetic energy of $q\phi_b$ (where ϕ_b is the barrier height) when falling off the Schottky barrier. This energy is large enough to ionize an interface trap state in the band gap. To describe this process, we modified the Shockley-Read model by adding an impact-loss term in the expression of df/dt, which is proportional to the incident current density. The resultant occupancy function now becomes

$$f(E) = F_s(E)\frac{c_n n_{s0} + F_m(E)/\tau_T}{(c_n + a_n/4)n_{s0} + F_s(E)/\tau_T}, \qquad (8)$$

where a_n is the impact-loss coefficient. The factor 1/4 comes from the relation $J=q\bar{v}n_{so}/4$, where $\bar{v}$ is the electron mean thermal velocity. This modification has a significant influence on f. Compared to Eq. (7), Eq.(8) shows that the states a few kT below E_f (where $F_m=F_s=1$) are now partially empty. Their occupancy probability, in fact, decreases with the increasing n_{so}. Here, two points need to be noted. One is τ_T. This parameter can be regarded as the lifetime of a nonequilibrium state, either empty or occupied. For $f>F_m$, it represents the lifetime of an electron that occupies a normally empty state. For $f<F_m$, it describes how long a normally occupied state may stay empty below the Fermi level. These empty states below E_f can be looked upon as "holes." Obviously, τ_T in these two cases could be very different. Because of the large number of electrons in the metal, the lifetime of the "hole" will be much shorter than the "electron" state (the state above E_f). The other point is that the modification will not substantially affect the occupancy of the deep level states. For those states, a_n as well as τ_T decreases quickly with the energy level. A qualitative plot of Eq.(8) under forward bias is sketched in Figure 4 for illustrative purpose. The result of this distribution can be interpreted from another point of view. The electrons injected into the interface region carry an energy that is higher than the average of other electrons. They are so called "hot electrons." The local temperature of electrons at the interface is, therefore, effectively higher than the lattice temperature. This strongly alters the energy distribution of electrons, making f bear some resemblance to a high temperature situation.

The decrease of electron occupancy at the states below E_f^m allows us an understanding of why the NC is often observed at low temperatures and high frequencies. If the states below E_f^m have a much higher density than the states above,[8] the integral of Eq.(6) will reverse its sign; namely, the overall charge at the interface will decrease for an increase of bias. Thus, from

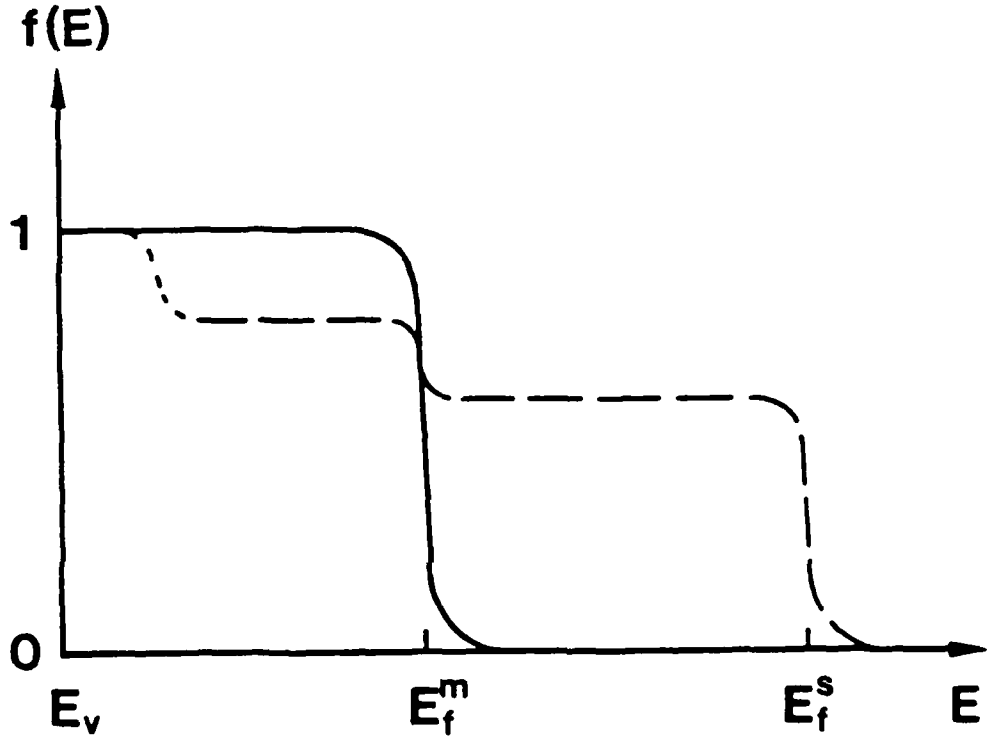

Figure 4: Variation of interface state occupancy, f(E), under the influence of forward bias.

Eq.(5), the device equivalent capacitance is expected to be negative in this region. At high temperatures, the carrier interaction between the metal and traps is relatively strong. The empty states created by electron impact are quickly refilled by the electrons from the metal. In such a case, the occupancy below E_r^m is virtually unaffected by the ionization process. Hence, no NC is observed. The frequency property of data can be understood in the same manner. With increasing frequency, the contributions from the "holes" will become [illegible] significant in determining the diode characteristics [illegible] a shorter τ_r. That explains why the NC appears [illegible] high frequencies.

Quantitative analysis of the capacitance [illegible] a two-energy-level simplified model, where [illegible] 0.25 eV above E_r^m and the other is assumed [illegible]. The parameters [illegible] and [illegible] are taken to be [illegible] A and [illegible] respectively. It is known that the electron capture cross [illegible] independent of the trap level.[4] Indeed, the [illegible] section, σ_i, varies with the [illegible] state, but they are basically in the same order [illegible] dealing with the states far below E_r^m [illegible] [illegible] and [illegible] upper and lower levels. The [illegible] value was obtained [illegible] device capacitance [illegible] experimental data [illegible] were estimated [illegible] upper level, and [illegible] level, respectively [illegible] from measurement [illegible] therefore, [illegible] characteristic [illegible]

[illegible]

(2) At 0.25 V, G starts to rise, indicating an increasing current flow. At this stage the electron injection is still low; the capture process prevails, so that the capacitance rises with the conductance.

(3) With increasing bias, the occupancy of the states above E_f^m approaches its asymptotic value, while the impact-loss process continues to be strengthened. The charge accumulation at the interface slows down considerably, which causes the capacitance curve to fall (0.38-0.47V).

(4) As the current gets high enough, the loss of electrons at the lower level eventually exceeds the electron trapping at the upper level; whereupon the variation of the interface charge, ΔQ_{ss}, changes its direction. As a consequence, a NC appears.

The two-level model should be regarded as merely a first order approximation. Nevertheless, it elucidated the nature of the NC. In reality, the interface states are continuously distributed. Using the peak region of the C-V curve (where the impact loss is negligible) the spectrum of the states above E_f^m was deduced.[9] The parameters used here for the upper level were initially taken from those measurements. Unfortunately, in the NC region the contributions from the states above and below E_f^m overlap. No attempt has been made to resolve the details of the state distribution below E_f^m. It should be pointed out that a rigorous justification of our theory has not yet been found. However, there is certain evidence that correlates to our conclusions. For instance, the high density of interface states below E_f^m has been observed experimentally by the electron emission spectroscopy in some other devices.[8] Those states may be responsible for the Fermi level pinning.[10]

This research was also supported by the Air Force Office of Scientific Research under Contract [illegible].

References

1. [illegible] and P. S. Ho, Appl. Phys.

Lett., 46(5), 486 (1985).

2 M. Liehr, P. E. Schmid, F. K. LeGoues and P. S. Ho, Phys. Rev. Lett., 54(19), 2139(1985).

3 P. S. Ho, E. S. Yang, X. Wu and H. L. Evans, Phys. Rev. Lett., 56(2), 177 (1986).

4 W. Shockley and W. T. Read, Phys. Rev., 87, 835(1952).

5 X. Wu, Ph.D. Thesis, Columbia University 1987.

6 G. E. Bulman, V. M. Robbins and G. E. Stillman, IEEE Trans. on Elec. Device, 32, 2454 (1985).

7 K. Brennan, T. Wang, and K. Hess, IEEE Elec. Device Lett. 6, 199 (1985).

8 R. Ludeke, D. Straub, F. J. Himpsel and G. Landgren, J. Vac. Sci. Technol. A, 4, 874 (1986).

9 E. H. Nicollian and A. Goetzberger, Bell Sys. Tech. J., 46 1055 (1967).

10 J. Bardeen, Phys. Rev., 71, 717 (1947).

D. LOW ENERGY ION BEAM OXIDATION OF SILICON

(E.R. Fossum, S. Todorov)
(JSEP work unit 4, 1985 - 1988)
(Principal Investigator: E.R. Fossum (212) 280-3107)

1. Low Energy Ion Beam Oxidation of Silicon -- The low energy ion beam oxidation of silicon, which has been demonstrated to produce very thin oxide films (40-70 Å) at room temperature which are suitable for MOSFET devices, has been extensively studied experimentally and theoretically.

The growth process is governed by the competing processes of implantation and sputtering. Low energy (60 eV) oxygen ions are implanted in silicon with a range of approximately 5 Å. However, the straggle of the implant distribution is large, and appreciable oxygen deposition occurs at depths of 20 Å. When the concentration of oxygen becomes comparable to the silicon density, the material becomes silicon dioxide. Oxygen implanted above this concentration does not react and outdiffuses to the surface. The measured thickness of the film grows logarithmically under constant flux conditions, in accordance with the exponentially decaying straggle. The film reaches an apparent saturating thickness which is of the order of 50 Å.

The beam, which contains argon, also results in the sputtering of the silicon/silicon dioxide surface. Such erosion competes with the growing film, and leads to truly saturating film thicknesses.

Simulation of the growth process requires knowledge of the sputtering rate and implantation range. The sputtering rate of silicon dioxide at low energy was measured separately and has been submitted for publication. The measurement technique is more accurate than previously reported methods. In this case, thin oxide films were grown thermally and their thickness

determined by ellisometry. Following bombardment by inert argon ions, the film thickness was remeasured. This procedure was repeated several times and the sputtering yield per unit dose for various energies was determined.

The sputtering yield is easily predicted using previously reported data for silicon. If the assumption is made that the sputtering is limited by the silicon component of the target (which appears to be valid for low energies) then excellent agreement between theory and experiment is observed provided the silicon density difference between silicon and silicon dioxide is accounted for.

With computer simulation of the model, agreement between the predicted energy dependence and dose dependence and experiment is excellent.

This work is reported as the Ph.D. thesis of Dr. Stan Todorov.

2. Nitridization of Germanium by a Low Energy Ion Beam -- Germanium wafers (p-type) provided by Ford Aerospace were exposed to a low energy ion beam of nitrogen. Typical process parameters were energy 60 eV, beam current 70 uA, and exposure time 6 minutes. Metal contacts were evaporated and the test structures analyzed by current-voltage and capacitance-voltage measurements. The samples had an insulator thickness of approximately 60 Å which was stable over at least several weeks. Further investigation is needed to pinpoint optimal process parameters and to perform compositional analysis on the thin films.

3. Gallium Arsenide Schottky Diode Leakage Current -- Photochemical means were used to deposit excess arsenic on the surface of gallium arsenide substrates. Such deposition was verified by subsequent surface analysis. The deposition took place prior to gate electrode metallization and patterning. The effect of the treatment of gate leakage current was investigated. It appears that the excess arsenic does indeed reduce gate

leakage current by over a factor of three even for fine geometries.

This research was also supported by the National Science Foundation under Grant NSF-PYI ECS-85-52572.

III. GENERATION AND DYNAMIC PROPERTIES OF METASTABLE SPECIES FOR QUANTUM ELECTRONICS AND LASER MICROPROCESSING

A. ROTATIONALLY RESOLVED ISOTOPE EFFECT IN THE HOT ATOM COLLISIONAL EXCITATION OF CO_2 $(00^0 1)$ BY TIME-DEPENDENT DIODE LASER SPECTROSCOPY

(S. A. Hewitt, J. F. Hershberger, G. W. Flynn, R. E. Weston, Jr.)
(JSEP work unit 5, 1985 - 1988)
(Principal Investigator: G. W. Flynn (212) 280-4162)

The study of collisional energy transfer between translational and internal degrees of freedom has received increased attention in recent years.[1-8] An efficient source of translational energy is the excimer laser photolysis of small molecules to produce hot atoms with energies of several eV. In the present work, hot deuterium atoms have been produced by photolysis of D_2S:

$$D_2S + h\nu(193\ nm) \longrightarrow D^* (E_{tr}=2.16\ eV) + DS \qquad (1)$$

Inelastic scattering then produces excited CO_2:

$$D^* + CO_2(00^00, J) \longrightarrow D + CO_2\ (00^01, J') \qquad (2)$$

High resolution diode laser spectroscopy is then used to probe the rotational level of the CO_2 (00^01) state:

$$CO_2(00^01, J') + h\nu(4.3\ \mu m) \longrightarrow CO_2\ (00^02, J'-1) \qquad (3)$$

In this report we describe the observation of a preference for excitation of high J relative to low J levels of $CO_2(00^01)$ by hot D atoms compared to hot H atoms.

This experiment is based on an earlier study of the

rotational distribution of CO_2 (00^01,J) due to collisions with hot H atoms at 2.30 eV produced by the photolysis of H_2S.[9] In that study the rotational distribution was found to be peaked at J=33, substantially higher than the room temperature Boltzmann distribution peak of J=15. In work completed prior to that study[7,8], the total number of quanta in the CO_2 asymmetric stretch and bend vibrations was measured, and the data indicated a substantial isotope effect with the heavier D^* atom exciting the lower frequency bend preferentially.

In the present experiments, 193 nm pulses from an ArF excimer laser with unstable resonator optics (Lambda-Physik EMG 201) are propagated down a 9 foot sample cell through which flows a 1/1 mixture of D_2S/CO_2 or H_2S/CO_2. Tunable cw radiation from a diode laser (Laser Analytics) at 4.3 μm is propagated through the cell collinearly with the excimer beam. The diode laser is tuned to specific rotational lines of the 00^01--->00^02 vibrational band of CO_2. Time resolved changes in the transmitted IR intensity are measured with an InSb detector. The signals are digitized, summed, and sent to a computer for storage and later analysis.

Transient absorption signals of the 00^01--->00^02 P(13), P(19), P(29), P(35), P(39), P(41), P(51), P(59), and P(65) transitions in CO_2 were obtained at sample pressures of 25 mTorr. The low pressures used assure that rotational relaxation of the CO_2 (~4 μs) is substantially slower than the rise time of the detection system (~0.5 μs), permitting direct measurement of nascent rotational populations. The observed signals for high rotational levels of 00^01 CO_2 have an initial fast rise due to direct formation of excited CO_2 by hot H or D atoms (see inset of Figure 1), followed by a slower decay which is attributed to rotational relaxation. For low rotational levels of 00^01 CO_2 the fast rise is small or nonexistent, and the signals have a slow rise due to rotational relaxation which fills the lower J states.

To obtain the rotational distribution directly, the fast rise amplitudes must be normalized for excimer and diode laser intensities and absorption line strengths; this was done in the earlier H^* atom experiment.[9] In the present experiments, to

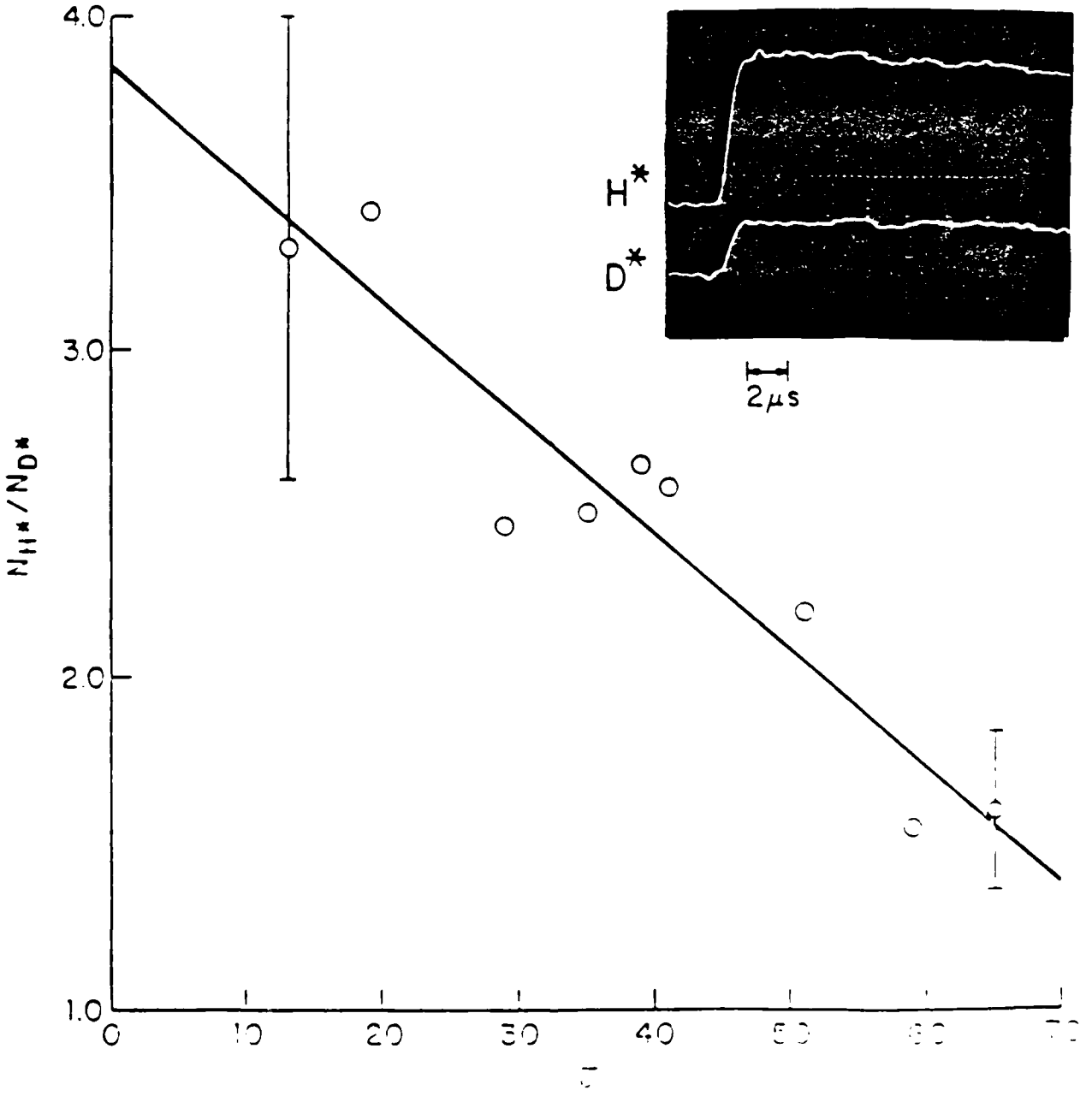

Figure 1: Experimental values for N_{H*}/N_{D*} vs. CO_2 rotational level (J) for 1/1 mixtures of H_2S/CO_2 and D_2S/CO_2 at 25 mtorr. $N_{H*}(N_{D*})$ is the population increase in a given 00^01 rotational state after the $H*(D*)/CO_2$ collisional interaction. The solid curve is a linear least squares fit of the data. The inset scope trace shows the change in absorption of the diode probe beam for the $00^01 \rightarrow 00^02$ P(39) transition after 193 nm photolysis of H_2S in CO_2 and D_2S in CO_2 in a 9 foot cell.

avoid the errors involved with such normalizations, ratios of H^* and D^* atom fast rise amplitudes were measured by locking the diode laser on a given $00^0 1,J'--->00^0 2,J'-1$ transition and flowing through the gas cell an H_2S/CO_2 sample and then a D_2S/CO_2 sample. When plotted as a function of rotational level, these ratios show a significant negative slope (see Figure 1). From the ratios and the previously measured H^* atom distribution,[9] the D^* atom distribution can be obtained. While the overall vibrational excitation of CO_2 $(00^0 1,J)$ by H^* atoms is about twice as efficient as excitation by D^* atoms, Figure 1 shows a clear preference for higher J by deuterium as compared to hydrogen.

The available angular momentum in a hot H or D collision is $L=\mu bg$ where μ is the reduced mass, b the impact parameter, and g the relative speed. For fixed b, D^*/CO_2 collisions have a square root of 2 larger L than H^*/CO_2 collisions. This probably accounts for the increasing excitation probability of high J $00^0 1$ levels by D^* atoms compared to H^* atoms.

This research was also supported by the Department of Energy, Contract DE-AC02-78-ER-04940 and the National Science Foundation, Grants NSF-CHE 85-17460 and NSF-CHE 80-23747.

References:

1 C. R. Quick, Jr., R. E. Weston, and G. W. Flynn, Chem. Phys. Lett. 83, 15 (1981).

2 F. Magnotta, D. J. Nesbitt, and S. R. Leone, Chem. Phys. Lett. 83, 21 (1981).

3 C. F. Wood, G. W. Flynn, and R. E. Weston, Jr., J. Chem. Phys. 77, 4776 (1982).

4 C. A. Wight and S. R. Leone, J. Chem. Phys. 78, 4875 (1983).

5 J. O. Chu, G. W. Flynn, and R. E. Weston, Jr., J. Chem. Phys. 78, 2990 (1983).

6 C. A. Wight and S. R. Leone, J. Chem. Phys. 79, 4823 (1983).

7 J. O. Chu, C. F. Wood, G. W. Flynn, and R. E. Weston, Jr., J. Chem. Phys. 81, 5533 (1984).

8 J. A. O'Neill, J. Y. Cai, G. W. Flynn, and R. E. Weston, Jr., J. Chem. Phys. 84, 50 (1986).

9 J. A. O'Neill, C. X. Wang, J. Y. Cai, G. W. Flynn, and R. E. Weston, Jr., J. Chem. Phys. 85, 4195 (1986).

B. ROTATIONALLY RESOLVED HOT ATOM COLLISIONAL EXCITATION OF $CO_2(10^00)$ TIME-DEPENDENT DIODE LASER SPECTROSCOPY

(S. A. Hewitt, J. F. Hershberger, J. Z. Chou, G. W. Flynn, and R. E. Weston, Jr.)
(JSEP work unit 5, 1985 - 1988)
(Principal Investigator: G. W. Flynn (212) 280-4102)

Studies of energy transfer between translational and internal degrees of freedom provide detailed information about inelastic collisional scattering in small molecules. Recently, translationally "hot" atoms (1-3 eV), produced by excimer laser photolysis, have been employed to investigate translational to vibrational/rotational (T-V/R) energy transfer.[1-10] In the present study, hot hydrogen (or deuterium) atoms have been produced by UV photolysis of H_2S (or D_2S):

$$H_2S + h\nu(193\ nm) \rightarrow H^*(E_{tr} = 2.30\ eV) + HS \qquad (1)$$

Vibrationally and rotationally excited CO_2 molecules are then produced by inelastic scattering:

$$H^* + CO_2(00^00,J) \rightarrow H + CO_2(mn^1p,J') \qquad (2)$$

High resolution time-resolved diode laser spectroscopy is then used to probe the nascent rotational distribution of CO_2 molecules scattered into the [illegible] excited symmetric stretch vibrational state:

$$CO_2(10^00,J') + h\nu(\sim 4.3\ \mu m) \rightarrow CO_2(\ldots)$$

Previous work in this lab on the $H^* + CO_2$ system has determined that 1) hot D atoms preferentially excite [illegible]

frequency CO_2 bend state compared to hot H atoms which preferentially excite the higher frequency CO_2 asymmetric stretch state[5], 2) the nascent rotational distribution of $CO_2(00^01,J')$, after H^* or D^* atom collision, is broadly peaked at J~33, substantially higher than the room temperature Boltzmann distribution peak at J=15[9], and 3) there is a preference for excitation of high J relative to low J levels of $CO_2(00^01,J')$ by hot D atoms compared to hot H atoms[10]. The present work has been conducted to determine how symmetric stretch excitation compares with these results for the bend and antisymmetric stretch states of CO_2.

In this experiment, the pulsed output of an ArF excimer laser with unstable resonator optics (193 nm) and the cw output of a tunable diode laser (~4.3 μm) are collinearly propagated down a 9 ft. sample cell through which flows a 1/1 mixture of H_2S CO_2 or D_2S CO_2. The diode laser is tuned to specific rotational lines in the 10^00 --> 10^01 vibrational band of CO_2. Time-resolved changes in the transmitted intensity of the IR probe beam following the UV photolysis pulse are monitored with an InSb detector. The signals are digitized, averaged, and sent to a computer for storage and analysis. A CO_2 reference cell, lock-in detector, and feedback loop are used to lock the diode laser to a specific frequency.

Transient absorption signals of the 10^00 --> 10^01 P(6), P(12), P(16), P(22), P(26), P(34), P(36), P(46), and P(56) transitions in CO_2 were measured at total sample pressures of 25 mTorr. The nascent rotational populations can be determined directly at these low pressures because the CO_2 rotational relaxation time (~4 μs) is much slower than the risetime of the detection system (~0.5 μs).

The observed rotational distribution of $CO_2(10^00)$ is much broader (see Figure 1) than that for $CO_2(00^01)$[9] and other vibrational states currently being studied in this lab. This very broad rotational distribution may be due to the fact that the symmetric stretching state is actually a linear combination of the [illegible] symmetric stretch state and the 02^00 bend state (~50%

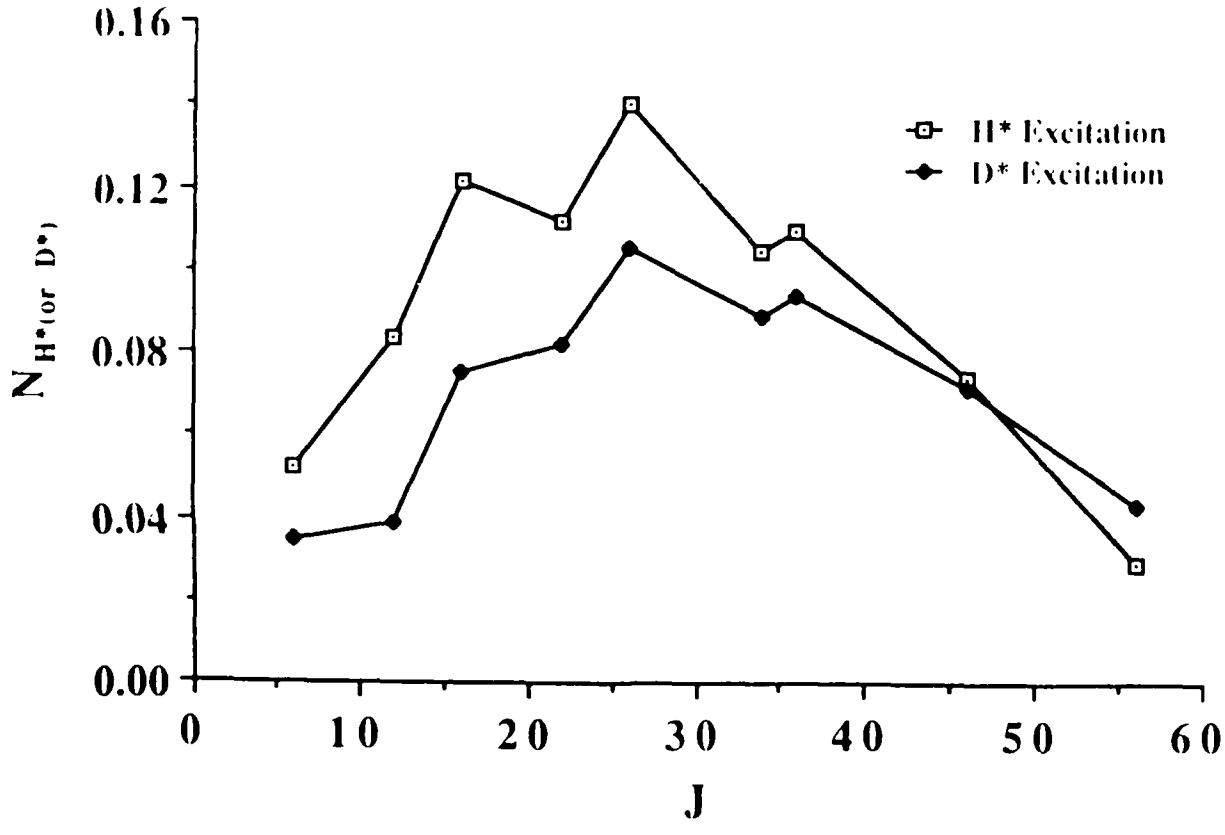
CO_2 (10^{0}0) Rotational Distribution
0.16
0.12
0.08
0.04
0.00
$N_{H^*(or\ D^*)}$
H* Excitation
D* Excitation
0
10
20
30
40
50
60
J

Figure 1

[illegible] are required [illegible] rotational distribution [illegible] vibrational state.

By measuring [illegible] versus b^* (see Figure [illegible]) systematic [illegible] differences between [illegible] observable. [illegible] greater for H^* atoms than I^* atoms [illegible] agreement with a simple argument based [illegible] of the force acting during the [illegible] there is a preference for higher [illegible] hydrogen, as seen for [illegible] increased available angular momentum [illegible] compared to a hot H atom collision.

This research was also supported by the Department of Energy, Contract DE-AC02-78-ER-[illegible] and the National Science Foundation, Grants NSF-CHE 85-[illegible] and NSF CHE [illegible].

References:

1 C. R. Quick, Jr., R. E. Weston, Jr., and G. W. Flynn, Chem. Phys. Lett. 83, 15 (1981).

2 F. Magnotta, D. J. Nesbitt, and S. R. Leone, Chem. Phys. Lett. 83, 21 (1981).

3 C. F. Wood, G. W. Flynn, and R. E. Weston, Jr., J. Chem. Phys. 77, 4776 (1982).

4 C. A. Wight and S. R. Leone, J. Chem. Phys. 78, 4875 (1983).

5 J. O. Chu, G. W. Flynn, and R. E. Weston, Jr., J. Chem. Phys. 78, 2990 (1983).

6 C. A. Wight and S. R. Leone, J. Chem. Phys. 79, 4823 (1983).

7 J. O. Chu, C. F. Wood, G. W. Flynn, and R. E. Weston, Jr., J. Chem. Phys. 81, 5533 (1984).

8 J. A. O'Neill, J. Y. Cai, G. W. Flynn, and R. E. Weston, Jr., J. Chem. Phys. 84, 50 (1986).

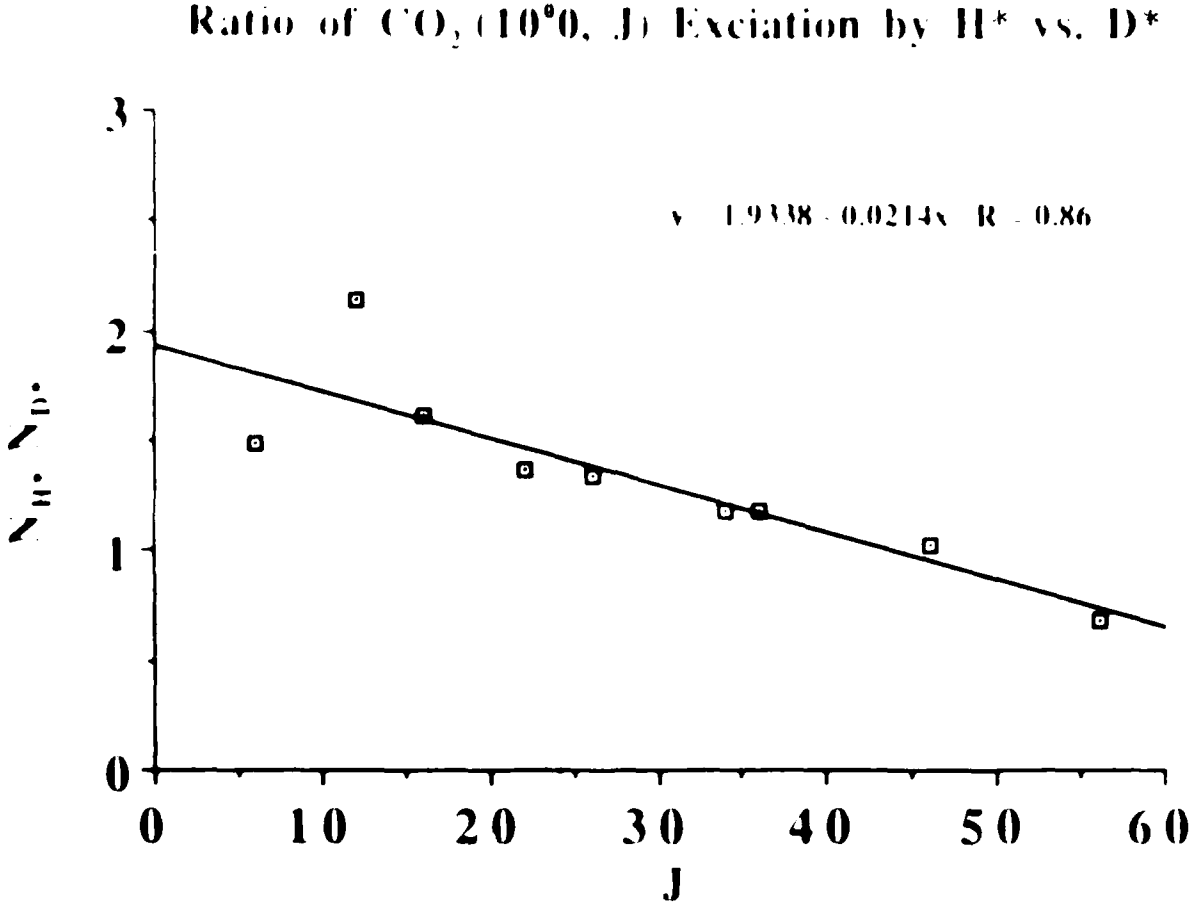
Ratio of CO_2 ($10^0$0, J) Excitation by H* vs. D*
y = 1.9338 - 0.0214x R = 0.86
3
2
1
0
0
10
20
30
40
50
60
J

Figure 2

9 J. A. O'Neill, C. X. Wang, J. Y. Cai, G. W. Flynn, and R. E. Weston, Jr., J. Chem. Phys. 85, 4195 (1986).

10 S. A. Hewitt, J. F. Hershberger, G. W. Flynn, and R. E. Weston, Jr., J. Chem. Phys. 87, 1894 (1987).

C. TRANSIENT LINEWIDTHS OF CO_2 AFTER HOT ATOM COLLISIONS

(J. F. Hershberger, J. Z. Chou, R. E. Weston, Jr., and G. W. Flynn)
(JSEP work unit 5, 1985 - 1988)
(Principal Investigator: G. W. Flynn (212) 280-4162)

Substantial progress has been made in recent years in measuring the internal state distributions of CO_2 after collisions with hot atoms.[1-5] Initial results of classical trajectory studies provide encouraging agreement with experiment.[6] It is of interest to measure the translational recoil of the CO_2 immediately after the collision. Doppler broadened linewidth measurements give the distribution of CO_2 velocities after the collision.

Hot hydrogen or deuterium atoms were created by excimer laser photolysis of H_2S or D_2S:

$$H_2S + h\nu\ (193\ nm) \text{ ---> } H^* + HS \qquad (E_{trans}=2.30\ eV) \qquad (1)$$

The hot atoms collisionally excite carbon dioxide:

$$H^* + CO_2 \text{ ---> } H + CO_2\ (mn^1p;J;v) \qquad (2)$$

A tunable diode laser probes the CO_2 quantum state:

$$CO_2\ (mn^1p;J;v) + h\nu\ (4.3\ \mu m) \text{ ---> } CO_2\ (mn^1p+1;J-1;v) \qquad (3)$$

The experiment was performed by passing collinear diode and excimer beams through a 9-ft. sample cell containing 25 mTorr of a 1:1 mixture of H_2S and CO_2 or D_2S and CO_2. Time resolved changes in infrared absorption were detected by an InSb detector, amplified, and signal averaged on a digital oscilloscope. During the experiment the diode was modulated at 1 KHz over a frequency

range of about .01 to .015 cm^{-1} while locked onto the line of interest by a feedback loop. Different positions within the Doppler profile were sampled by firing the excimer at different delay times with respect to the start of the modulation cycle. This method works because the transient signals are on a microsecond timescale, much faster than the diode modulation. The wavenumber axis was calibrated with a Fabry-Perot etalon.

The experiment was performed on three rotational levels of the $00^0 1$ vibrational state: P(13), P(35), and P(59). In all cases the data were well fit by Gaussian profiles. All of the linewidths measured were significantly broader than the room temperature Doppler width of CO_2 (FWHM=.0042 cm^{-1}). Deuterium atoms gave broader linewidths than hydrogen atoms, as expected because of the greater momentum. In addition, the linewidth increased with higher rotational quantum number, as shown in Figure 1. The estimated error bars on these numbers are about 15%, primarily due to inaccuracies in the frequency calibration.

By measuring signal amplitudes at times later than the detector response time, the translational relaxation of the line back to a room temperature Doppler profile can be seen. Figure 2 shows the lineshape profile of $00^0 1$ P(35) at three different times. Figure 3 shows the fitted linewidth for $00^0 1$ P(35) as a function of time after the excimer laser pulse. Given a collision time of about 4 microseconds at these pressures, it can be seen that relaxation back to the room temperature Doppler width is roughly gas kinetic.

Experiments have also been performed on $01^1 0$ P(49) and P(59). The error bars are larger for these states because of smaller signals and the required additional correction of diode power versus wavenumber due to the absorption by cold gas. Preliminary results indicate somewhat broader linewidths than for the $00^0 1$ lines.

This research was also made possible by the Department of Energy, Contract DE-AC02-78-ER-04940 and the National Science Foundation, Grants NSF-CHE 85-17460 and NSF-CHE 80-23747.

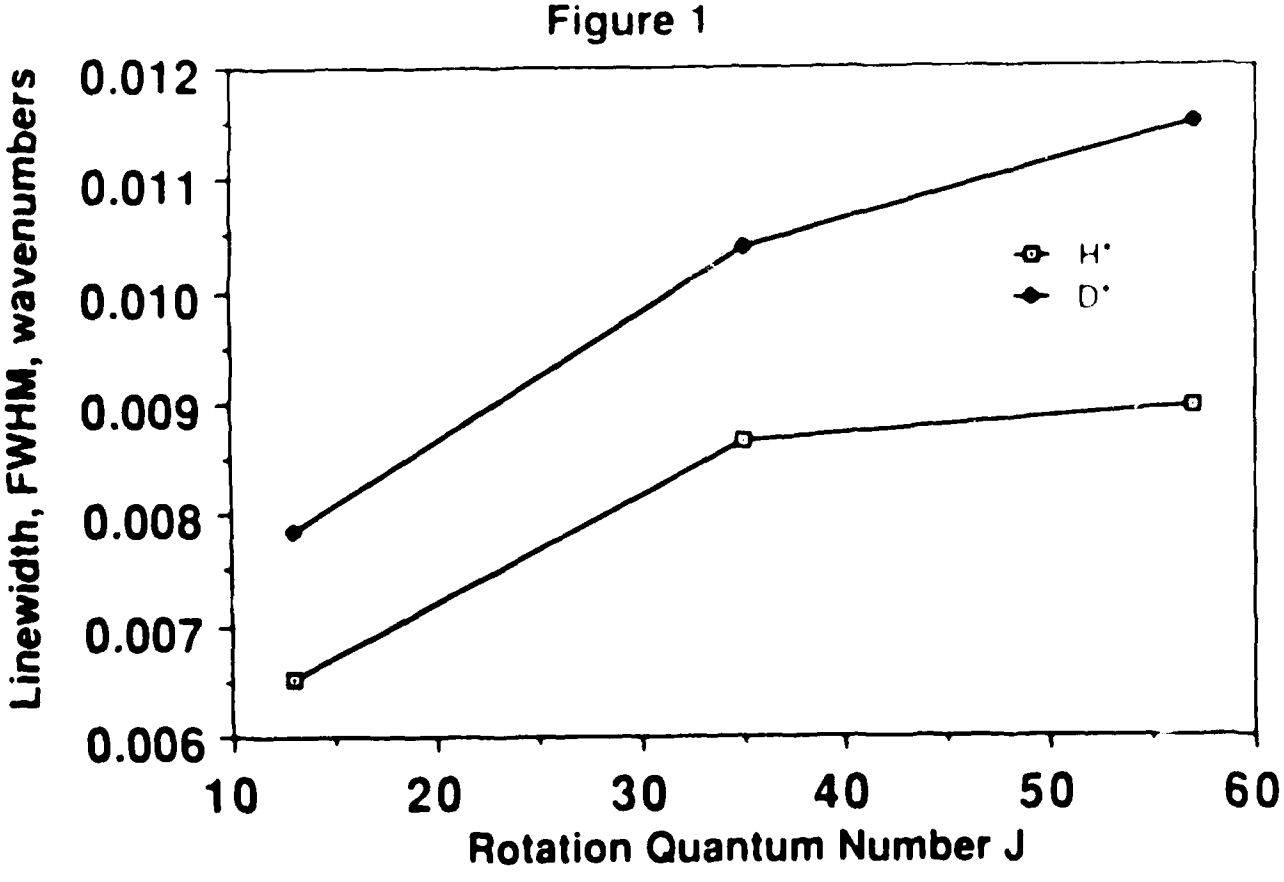

Figure 1: Transient linewidths of CO_2 in $00^0 1$ states after collision with hot atoms.

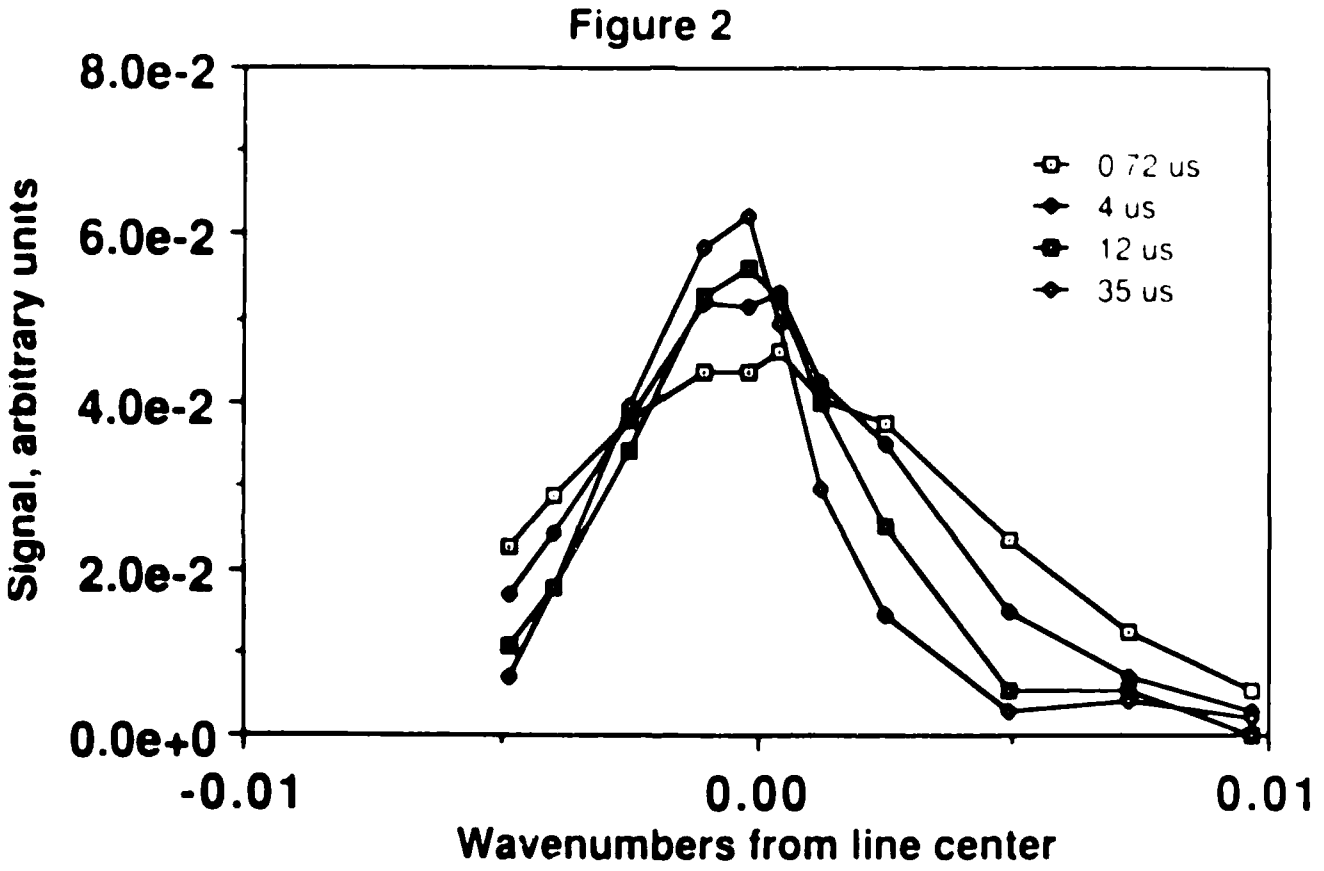

Figure 2: Lineshape profile of CO_2 in $00^0 1$ P(35) state.

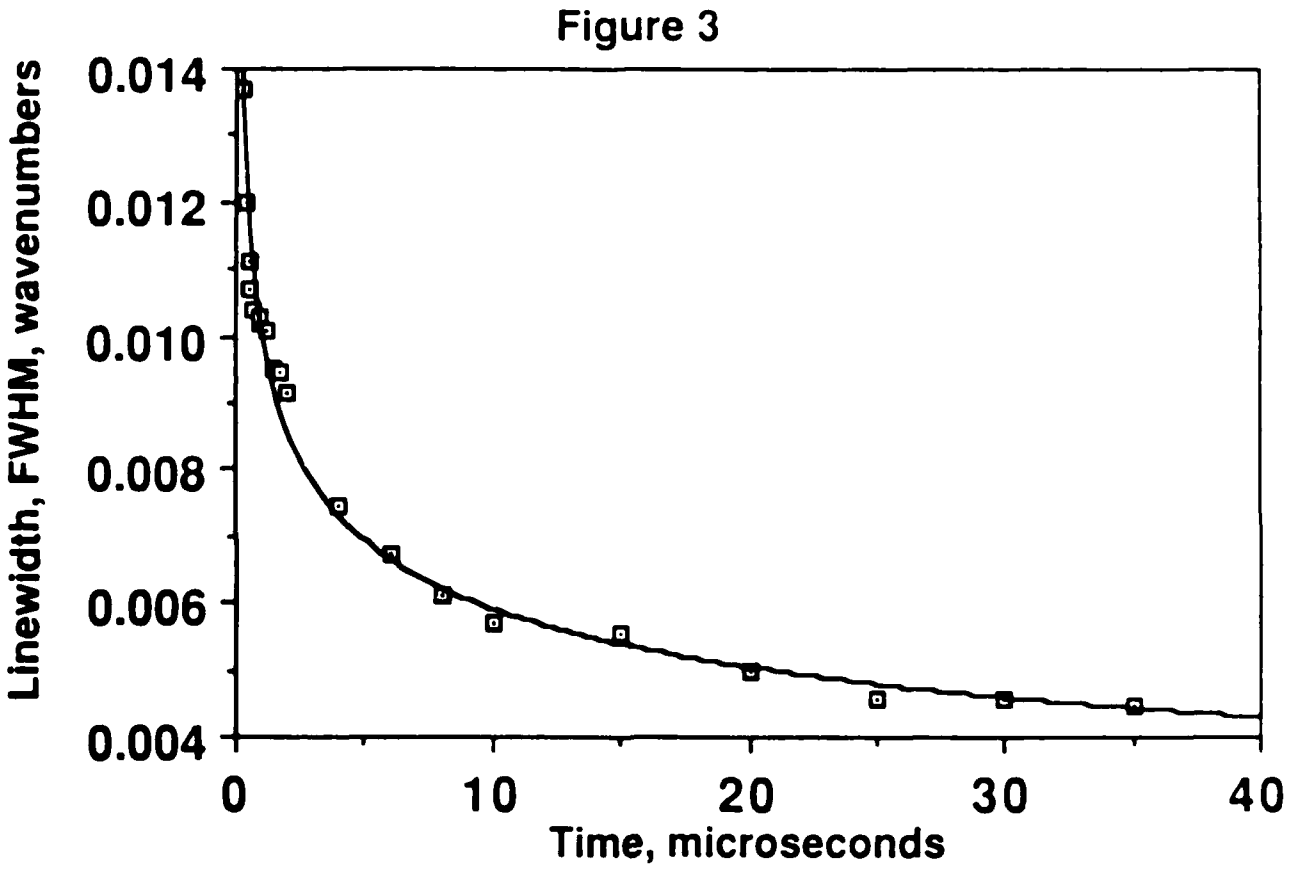

Figure 3: Linewidth of CO_2 in $00^0 1$ P(35) state as a function of time after excimer laser pulse.

References:

1 C. R. Quick, Jr., R. E. Weston, Jr., and G. W. Flynn, Chem. Phys. Lett. 83, 15 (1981).

2 F. Magnotta, D. J. Nesbitt, and S. R. Leone, Chem. Phys. Lett. 83, 21 (1981).

3 J. A. O'Neill, J. Y. Cai, G. W. Flynn, and R. E. Weston, Jr., J. Chem. Phys., 84, 50 (1986).

4 J. A. O'Neill, C. X. Wang, J. Y. Cai, G. W. Flynn, and R. E. Weston, Jr., J. Chem. Phys., 85, 4195 (1986).

5 S. A. Hewitt, J. F. Hershberger, G. W. Flynn, and R. E. Weston, Jr., J. Chem. Phys., 87, 1894 (1987).

6 G. C. Schatz, M. S. Fitzcharles, and L. B. Harding, private communication.

D. OBSERVATION OF A DELTA-J PROPENSITY IN HOT ATOM INELASTIC SCATTERING OF CO_2

(J. F. Hershberger, S. A. Hewitt, R. E. Weston, Jr., and G. W. Flynn)
(JSEP work unit 5, 1985 - 1988)
(Principal Investigator: G. W. Flynn (212) 280-4162)

Quantum state resolved studies of the inelastic scattering of CO_2 by hot atoms is of considerable interest.[1-6] VCC-IOS calculations by Alexander and Clary[7,8] on He-CO_2 collisions showed interesting oscillations in cross sections as a function of rotational quantum number for excitation into states involving non-zero vibrational angular momentum. This effect was attributed to symmetries in the 6-j coefficients. We report here the first experimental observation of such oscillations in the ro-vibrational excitation of $CO_2(01^10)$ by hot atoms.

The diode absorption probe technique has been described previously.[6] Briefly, hot hydrogen or deuterium atoms are produced by the excimer laser photolysis of H_2S or D_2S at 193 nm:

$$D_2S+h\upsilon(193\ nm) \text{ ----}>DS+D^* \qquad (E_{trans}=2.1_6\ eV) \qquad (1)$$

Collisions with CO_2 cause rotational and vibrational excitation:

$$D^*+CO_2(00^00;J) \text{ ----}>D+CO_2(mn^1p;J') \qquad (2)$$

A tunable diode laser probes absorption in the ν_3 band of CO_2:

$$CO_2(mn^1p;J)+h\upsilon(\sim4.3\ \mu m) \text{ ----}> CO_2(mn^1p+1;J-1) \qquad (3)$$

Tunable diode radiation was passed through a 9-ft sample cell, collinearly with 193 nm excimer radiation. The diode was tuned to various rotational lines in the P-branch of the ν_3 vibrational band of CO_2. A 1:1 mixture of D_2S and CO_2 at 2

mtorr flowed through the cell. Time-resolved changes in infrared absorption were detected by an InSb detector, amplified, and signal averaged on a digital oscilloscope.

A typical time-resolved signal displays a detector-limited fast rise (~700 ns) followed by a slow rise or decay. The collision time at 25 mTorr is ~4 μs, much slower than the detector response time, so the fast rise amplitude represents the nascent population produced by the hot atom collision. The slow component of the signal is due to subsequent collisional relaxation. The fast rise amplitudes were normalized by excimer and diode laser powers to obtain the rotational distribution of the $01^{1}0$ state, shown in the figure. The most obvious feature in the distribution is that odd J levels have much more population than even J levels. When the same experiment is performed with the absorption cell cooled to -50 degrees Celsius, the population of the even J levels are reduced, and the odd J levels are increased; thus the odd/even ratio increases at lower temperatures. This effect is at least partly due to the reduction in the ambient Boltzmann population of CO_2 in the v_2 state. For such molecules, both even and odd initial states exist, so averaging over the initial Boltzmann distribution would tend to obscure any delta-J propensity. For the dominant v_2 molecules, however, only even J can exist, so a delta-J odd propensity is not averaged out. This implies that pure rotational scattering within the 01^{1} manifold is only a rather minor contribution to the observed distribution. Since 5% of the CO_2 molecules are in the $01^{1}0$ state at room temperature, the cross section for ro-vibrational excitation must be at least ~0.1 that of the cross section for pure rotational excitation.

A similar rotational distribution is observed for hydrogen atom scattering, although the total excitation probability into the v_2 manifold is smaller by a factor of about 2.5. The v_1+v_3 combination state, however, shows the opposite propensity in that the scattering probability into even J states is greater than into odd J states. This is due to the factor of -1 put into the wavefunction symmetry by the v_3 vibration.

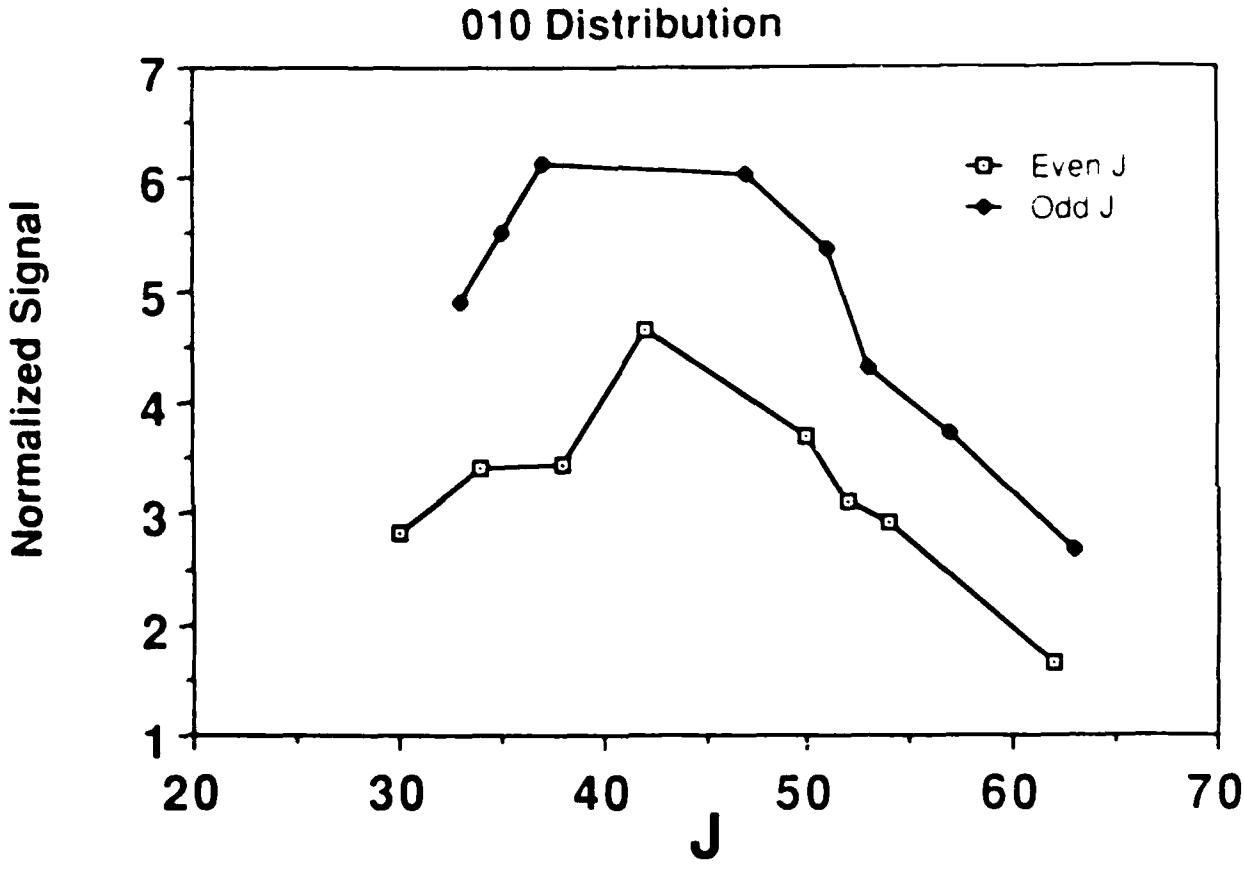

Rotational distribution of CO_2 in 01^10 state after collision with hot deuterium atoms.

Another feature of the distribution is that it is sharply peaked at about J=43, significantly greater than the J=33 peak for the v_3=1 distribution.[4,5] This is likely an effect of different trajectories for the different vibrational modes. Quasiclassical calculations[9] indicate that the v_3 stretch is excited primarily by end-on collisions, while broadside collisions play a more significant role in exciting the v_2 bend. A broadside collision has greater orbital angular momentum available, so one would expect greater rotational excitation.

This research was also made possible by the Department of Energy, Contract DE-AC02-78-ER-04940 and the National Science Foundation, Grants NSF-CHE 85-17460 and NSF-CHE 80-23747.

References:

1 C. R. Quick, Jr., R. E. Weston, Jr., and G. W. Flynn, Chem. Phys. Lett. 83, 15 (1981).

2 F. Magnotta, D. J. Nesbitt, and S. R. Leone, Chem. Phys. Lett. 83, 21 (1981).

3 J. A. O'Neill, J. Y. Cai, G. W. Flynn, and R. E. Weston, Jr., J. Chem. Phys., 84, 50 (1986).

4 J. A. O'Neill, C. X. Wang, J. Y. Cai, G. W. Flynn, and R. E. Weston, Jr., J. Chem. Phys., 85, 4195 (1986).

5 S. A. Hewitt, J. F. Hershberger, G. W. Flynn, and R. E. Weston, Jr., J. Chem. Phys., 87, 1894 (1987).

6 J. O. Chu, C. F. Wood, G. W. Flynn and R. E. Weston, Jr., J. Chem. Phys., 81, 5533 (1984).

7 M. H. Alexander and D. C. Clary, Chem. Phys. Lett., 98, 319 (1983).

8 D. C. Clary, J. Chem. Phys., 78, 4915 (1983).

9 G. C. Schatz, M. S. Fitzcharles, and L. B. Harding, private communication.

AD-A190 198 RESEARCH INVESTIGATION DIRECTED TOWARD EXTENDING THE USEFUL RANGE OF THE ELECTROMAGNETIC SPECTRUM(U) COLUMBIA RADIATION LAB NEW YORK G W FLYNN ET AL 2/2

UNCLASSIFIED 31 DEC 87 DAAG29-85-K-0049 F/G 17/5 NL

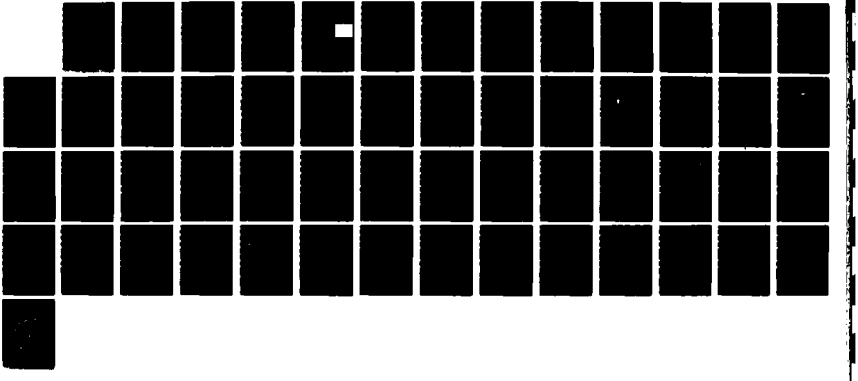

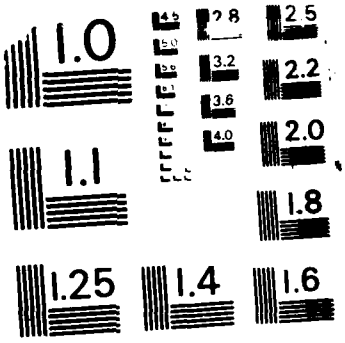

E. DETECTION OF THE CHLORINE ATOM USING INFRARED DIODE LASER TECHNIQUE

(S. Sarkar, G. W. Flynn)
(JSEPT work unit 5, 1985 - 1988)
(Principal Investigator: G. W. Flynn (212) 280-4162)

1. Introduction -- The production and chemistry of atomic species are important in a wide variety of applications. Chlorine atoms, one such important species, have many useful chemical reactions in the gas phase as well as on metal/semiconductor surfaces. These studies can provide insight into the fundamental dynamical properties such as spin-orbit effects on reaction rates and energy transfer processes. They are also expected to have practical impact in areas of chemical laser development, laser direct writing/microelectronics and atmospheric modeling. Therefore, a suitable optical method, preferably in-situ and real-time, is essential for its detection and quantitative measurement in a chemically reacting system.

Our detection scheme utilises the $^2P_{3/2}$ --> $^2P_{1/2}$ spin-orbit transition of halogen atoms in the infrared.[1,2] The powerful infrared diode laser absorption technique which has already been developed in our laboratory is therefore well-suited for Chlorine atom studies. The cw-diode laser with low single mode power ($\sim$0.1 mw) and low photon energy ($\sim$0.1 ev) is a non-perturbing probe and is capable of real time diagnostics with resolution ranging from 100 ns to 1 sec depending on the experimental requirement. The objective of the present work is the development of a diode laser spectrometer to detect the Cl $^2P_{3/2}$ --> $^2P_{1/2}$ transition near 882.36 cm^{-1}(11.33 μm). Measurements locating the line position and line strength provide the information needed to implement quantitative measurements of Cl concentrations using this high resolution technique and allow

for an assessment of the ultimate sensitivity of such an apparatus in real time experiments.

2. Experimental Set-up -- The experimental apparatus is as follows: The laser diode (880-895 cm^{-1}) is contained in a Laser Analytics helium-cooled, closed-cycle refrigerator. The diode laser beam, after collimation (f/2 ZnSe lens), passes through a 270 cm long cell containing Cl_2(<1 Torr). The laser light is detected after passing through a 0.5 m monochromator (to select a single laser mode and coarse wavelength setting) with a liquid-nitrogen cooled HgCdTe detector/preamplifier (1 s response time). The diode probe and photolysing dye laser (330-380 nm, 10 mJ pulse) beams are made collinear in the cell by passing the diode beam through a ZnSe flat which is coated for high reflectivity at dye laser wavelengths.

Diode laser frequency is coarse set by the temperature of the diode, and the frequency scan is accomplished by ramping the diode current. The absorption lines are measured in the second derivative mode where the laser frequency is modulated by applying a low-amplitude saw-tooth wave function to the diode current and the absorption signal is recorded with the lock-in amplifier set for detection at twice the modulation frequency.

3. Calibration Procedure -- The frequency scale is determined using Carbonyl Sulphide (OCS) absorption lines with the OCS line positions taken from the work of Maki.[3] In its ν_1 band, OCS (band centre 859 cm^{-1}) has a useful spectrum for the purpose of diode laser calibration. Although the spectrum is quite rich in the 859 cm^{-1} region, the frequency range needed for our work (higher J-transitions in the R-branch) suffers some limitations owing to the simplicity and regularity of the spectrum (Figure 1). Fortunately, however, the hot band transition (010-->110) and isotopic species (like $^{16}O^{13}C^{32}S$) transitions still make it possible to use OCS for calibration, nonetheless with more cautious effort.

A computer program LINESEAR, designed in our lab to aid in

assigning diode modes by fitting observed line positions to tabulated spectra of various gases, was used. To assign a diode mode, the observed diode spectra under full modulation amplitude is recorded in single mode condition. A Ge etalon (one inch thick, FSR=0.0475 cm^{-1}) is used to measure the relative frequency spacings between several lines within a mode (usually 3-5 lines are sufficient). With the help of a set of etalon fringe counts, the approximate frequency range set by the monochromator, and the absorption coefficients, the program searches the database for a specific pattern of lines and plots them on a plotter. With the help of this program, we are able to characterize several modes of our present diode by employing a few Torr of OCS in a 270 cm long cell (Figure 1).

4. Estimate of Chlorine Atom Concentration -- A preliminary estimate has been made for the working Cl-atom concentration in the present apparatus. The precursor Cl_2 molecule produces two $^2P_{3/2}$ chlorine atoms upon laser photolysis in its absorption band (280-420 nm). With typical dye laser pulse energy of 10 mJ at 330nm (absorption peak with measured cross-section of 0.0083 cm^{-1} $torr^{-1}$) we can produce $3X10^{16}$ atoms by photolysing 1 torr Cl_2 in a 2.7 meter path. These atoms are produced in a typical laser beam volume of $20cm^3$ giving a working density of $1.5X10^{15}$ cm^{-3}, which is well within the sensitivity limit of the apparatus.

5. Estimate of the Apparatus Sensitivity -- The magnetic dipole allowed transitions between the ^2P_j levels have hyperfine structures which give rise to six possible transitions (882.3149 - 882.3907 cm^{-1}) each for ^{35}Cl and ^{37}Cl isotopes. The strongest is the F"=3-->F'=2 transition at 882.3626 cm^{-1}. At room temperature, the Doppler width (FWHM = 55 MHz) is larger than the isotope shift (28 MHz), and the strongest transition is due to both isotopes. From the predicted ratios of the line intensities, the fraction of ground state population in the hyperfine level associated with the strongest transition is

CALIBRATION SPECTRUM FOR CHLORINE ATOMS

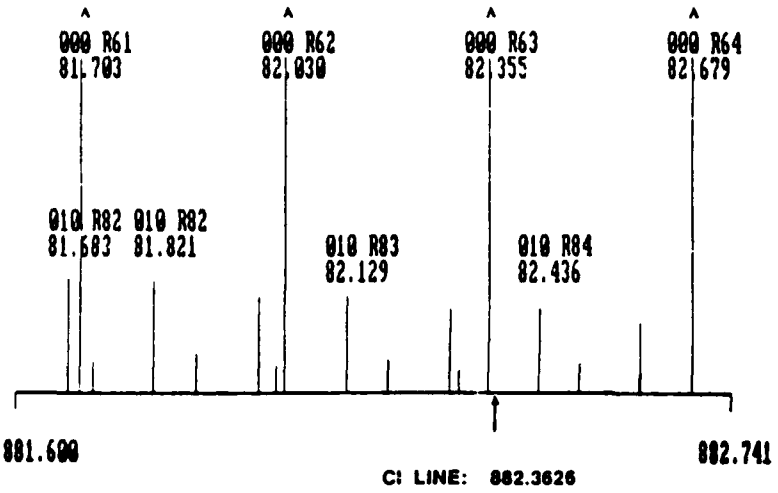

Cl LINE: 882.3626

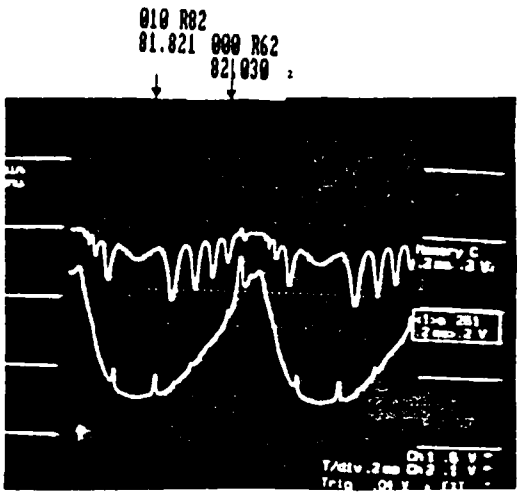

TYPICAL SINGLE MODE OF THE DIODE

FIGURE 1

calculated to be 0.44. Assuming a modest estimate of detecting 0.1% diode laser absorption (with S/N of 10) in the apparatus, the minimum detectable concentration, n_{min}, for a Doppler-broadened line is given by:

$$[S(nj/n) \times n_{min} XL]/[2.13 \times \nu_{dop} \times N_0] = 10^{-3} \qquad (1)$$

where S is the line strength (0.1 cm^{-2} atm^{-1}), ν_{dop} is the Doppler HWHM (0.9 $X10^{-3}$ cm^{-1}), L is the path length (270 cm) and N_o is the number density at 1 atm and 300 K. For the present set-up, a conservative estimate of n_{min} is 4-5 X 10^{12} cm^{-3} although an order of magnitude improvement can be achieved.

This research was also made possible by the Department of Energy, Contract DE-AC02-ER-04940 and the National Science Foundation, Grants NSF-CHE 85-17460 and NSF-CHE 80-23747.

References:

1 H. K. Haugen E. Weitz and S. R. Leone, J. Chem. Phys. 83, 3402 (1985).

2 J. Wormhoudt, A. C. Stanton, A. D. Richards and H. H. Sawin, J. Appl. Phys. 61, 142 (1987).

3 A. Maki, National Bureau of Standards (Private Communication).

F. TEMPERATURE DEPENDENCE OF ROTATIONALLY RESOLVED EXCITATION OF $CO_2(00^01)$ COLLISIONS WITH HOT HYDROGEN ATOMS

(T. G. Kreutz, F. A. Khan, G. W. Flynn, R. E. Weston, Jr.)
(JSEP work unit 5, 1985 - 1988)
(Principal Investigator: G. W. Flynn (212) 280-4162)

Workers in our laboratory have recently measured the rotationally resolved excitation of $CO_2(00^01)$ by collisions with hot hydrogen atoms:[1]

$$H_2S + h\nu(193nm) \rightarrow H^* + HS \qquad (1)$$

$$H^* + CO_2(00^00) + CO_2(01^10) \rightarrow H + CO_2(00^01;J) + CO_2(n,m^\lambda,p;J). \qquad (2)$$
$$(92\%) \qquad (8\%)$$

While the majority of CO_2 molecules are in the vibrational ground state at room temperature, the 8% fraction in the (01^10) level admits the possibility of a second significant scattering channel into (00^01). The effects of these two channels may, in principle, be isolated by lowering the temperature of the CO_2, such that the (01^10) population is made negligibly small. Such an approach is valid, however, only if the vibrationally inelastic cross sections do not vary significantly with the gas temperature. In these experiments, the extremely high velocity ($\sim$2eV) of the hydrogen atoms far outweighs small variations in the CO_2 velocity due to changes in the gas temperature. Thus, the relative efficiency of the two inelastic channels may be investigated by comparing the low temperature (00^01) rotational distribution with that measured at room temperature.

The apparatus used for excimer laser photolysis/diode laser probing has been described in detail elsewhere;[1,2] briefly it is as follows. The pulsed output of an excimer laser at 193 nm is collinearly propagated with the 4.3μm cw diode laser radiation

through a 3 m cell containing a flowing 1:1 mixture of H_2S and CO_2. The diode laser is tuned to a given absorption line of the type:

$$CO_2(00^01;J) + h\nu(4.3\ \mu m) \rightarrow CO_2(00^02;J\pm1), \qquad (3)$$

and time resolved changes in the IR probe beam (following each excimer laser photolysis pulse) are monitored with a cooled InSb detector and acquired on a signal averager.

In the low temperature experiments, the gas mixture is cooled by first flowing it through an insulated "pre-cooler" consisting of a 50 cm long glass coil surrounded by a jacket in which chilled ethanol is circulated. The gas then flows through the similarly jacketed and cooled 3 m pyrex sample cell. The temperature of the wall of the sample cell is maintained at -50 ± 2C, as monitored by an iron-constantan thermocouple. The temperature of the gas mixture was experimentally verified by measuring the absorption coefficients of various rotational lines in the $CO_2(02^20)$ R-branch. This data was fit to a rotational Boltzman distribution and yielded a temperature within ±2C of the value given by the thermocouple. The pressure of the gas mixture was maintained at 25 mTorr at room temperature and 19 mTorr at -50 C, thus ensuring a common gas density at both temperatures.

In order to minimize systematic errors, the apparatus was calibrated repeatedly throughout the course of the experiment by means of frequent (~45 minute intervals) measurements of a single 'indicator' absorption line, e.g. $(00^01)R(17)$. The measured rotational populations were then normalized by the amplitude of this transition, which slowly decreased with time due to slow degradation of the apparatus via fogging of the windows on the cell, gradual beam misalgnment, etc. Error bars (~15%) were determined primarily by repeated measurements of each transition.

We have measured the rotationally resolved scattering into $(00^01;J)$ at both room temperature and at 223 K. The ratios of these populations are shown in Figure 1 as a function of J. Note that the dependence on J is roughly linear over the measured

region; recent data (not shown) indicates that the ratios rise more quickly beyond J=50 and equal unity at J~60. In the limit of rotationally elastic scattering J=60, the ratios are given trivially by the ratios of the initial hot/cold Boltzman distributions, a result which is graphed for comparison in Figure 1. While the true dynamics are far from rotationally elastic, this simple result suggests that at least part of the J dependence of the ratios is due to the small shift of the initial rotational distributions to smaller J values as the temperature is lowered. Other contributions to the J dependence arise from the details of the scattering cross sections. In this regard, we are presently engaged in a data analysis based upon the infinite order sudden (IOS) approximation, from which state-to-state inelastic cross sections for this process may be obtained.

By integrating the measured $(00^0 1)$ rotational distributions, we obtain total cross sections for $(00^0 1)$ excitation. The ratio of the hot/cold <u>total</u> excitation cross sections, $R = \sigma_{001}(T_{HOT})/\sigma_{001}(T_{COLD})$, is found experimentally to be 0.9 ± 0.1. In order to see what light this result sheds upon the relative efficiencies of two scattering channels, we turn to Figure 2, where the calculated value of R is graphed as a function of $F = \sigma_{010 \rightarrow 001}/\sigma_{00^0 0 \rightarrow 001}$, the ratio of the scattering efficiencies out of $(01^1 0)$ versus $(00^0 0)$. Note that when $F<1$, the $(01^1 0) \rightarrow (00^0 1)$ channel has little significance, and as a result, R is rather insensitive to variations in F. At higher values of F, however, scattering out of $(01^1 0)$ becomes increasingly important and the temperature effect is more dramatic. Our measured value of $R \sim 0.9$, which is also graphed in Figure 2, indicates that the efficiency of scattering from $(01^1 0)$ does not exceed the efficiency from $(00^0 0)$. This appears to be a plausible result; while the $(00^0 0) \rightarrow (00^0 1)$ transition has a somewhat larger energy gap than $(01^1 0) \rightarrow (00^0 1)$, the latter transition requires an exchange of two vibrational quanta. Unfortunately, the uncertainty in our measurement and the relative insensitivity of R with respect to F do not permit a more precise determination of F. This situation can be improved

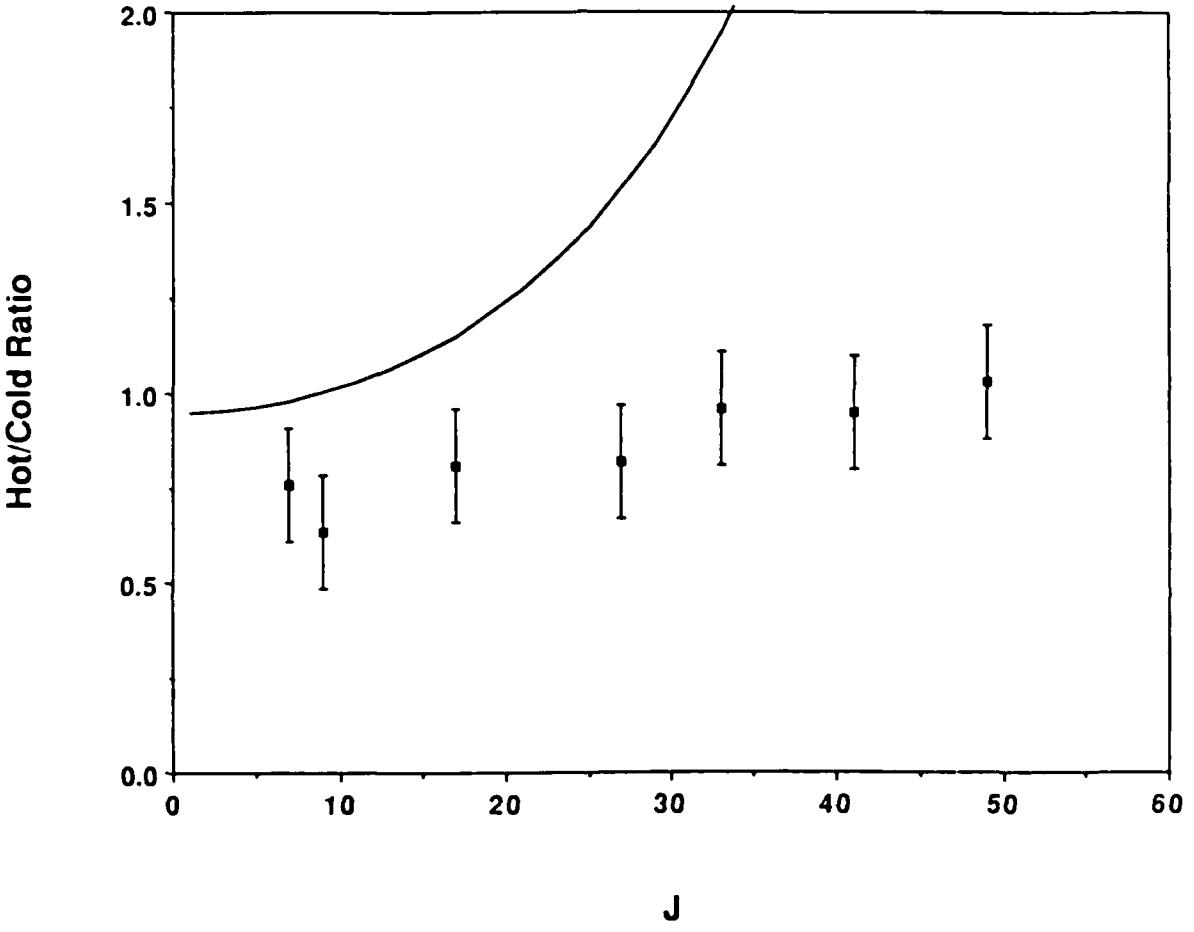

Figure 1: The rotationally resolved ratio of inelastic scattering into $CO2(00^0l)$ at 298 K versus 223 K. The solid line depicts this quantity calculated in the rotationally elastic (i.e.$\Delta J=0$) limit.

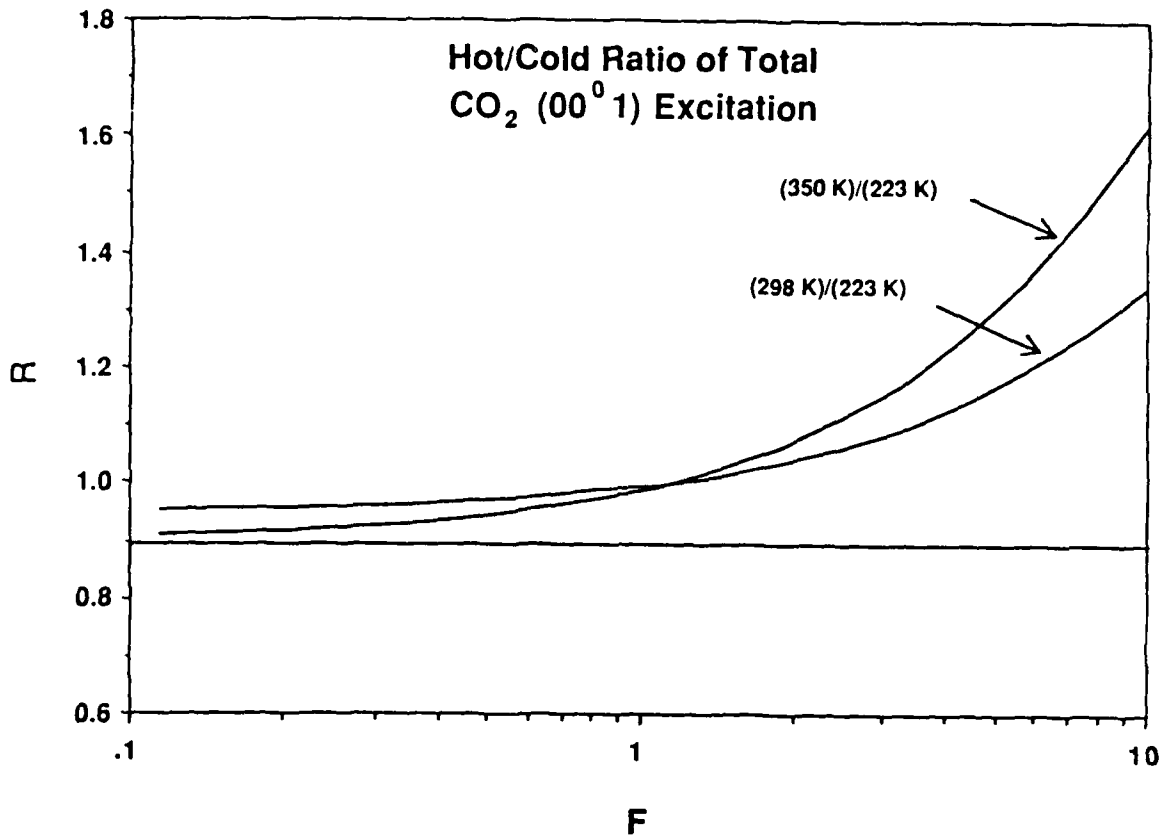

Figure 2: The calculated ratio of the <u>total</u> inelastic cross sections into $CO_2(00^0 1)$: $R=\sigma_{001}(T_{HOT})/\sigma_{001}(T_{COLD})$, as a function of $F=\sigma_{010-->001}/\sigma_{00^0 0-->001}$, the efficiency ratio of the two major scattering channels. Note that R is given for both 298 K/223 K and for 350 K/223 K. The experimental value of 0.9 ± 0.1 for R is shown by a horizontal line and a shaded band representing the uncertainty in the measurement.

somewhat by measuring the ($00^0 1$) rotational distribution at an elevated temperature (see Figure 2). Experiments such as these should provide a better understanding of this important scattering system.

This research was made possible by the Department of Energy, Contract DE-AC02-78-ER-04940 and the National Science Foundation, Grants NSF-CHE 85-17460 and NSF-Che 80-23747.

References:

1 J. A. O'Neill, C. X. Wang, J. Y. Cai, G. W. Flynn, and R. E. Weston, Jr., "Rotationally Resolved Hot Atom Collisional Excitation of $CO_2 00^0 1$ and $00^0 2$ Stretching Vibrations by Time-Resolved Diode Laser Spectroscopy," submitted: J. Chem. Phys.; J. A. O'Neill, C. X. Wang, J. Y. Cai, G. W. Flynn, and R. E. Weston, Jr., J. Chem. Phys. 85, 4195 (1986).

2 J. A. O'Neill, J. Y. Cai, G. W. Flynn, and R. E. Weston, Jr., J. Chem. Phys. 84, 50 (1986); J. O. Chu, C. F. Wood, G. W. Flynn, and R. E. Weston, Jr., J. Chem. Phys. 80, 1703 (1984); 81, 5533 (1984).

G. ROTATIONALLY AND TRANSLATIONALLY RESOLVED PRODUCT STATE DISTRIBUTIONS IN CO_2 BENDING STATES PRODUCED BY THE 193 nm PHOTOLYSIS OF PYRUVIC ACID

(T. G. Kreutz, G. W. Flynn)
(JSEP work unit 5, 1985 - 1988)
(Principle Investigator: G. W. Flynn (212) 280-4162)

Laser photolysis is a convenient method of initiating a "half-collision" or "half-reaction" between excited photoproducts, and state resolved energy deposition within the photofragments provides an extremely detailed picture of the dynamics of photodissociation. In this report, we describe preliminary results in a continuing study of the 193 nm photolysis of pyruvic acid,[1] in which we have measured the extent of rotational and translational excitation in the CO_2 photofragment.

The experimental apparatus, which has been described previously in detail,[1,2] can be summarized as follows. Pulsed excimer laser radiation at 193 nm is collinearly propagated with a cw diode laser beam through a 2 m sample cell containing flowing pyruvic acid vapor at ~25 mTorr. Pyruvic acid is photolyzed by the excimer pulse and produces excited CO_2 fragments:

$$CH_3COCOOH + h\nu(193\ nm) \rightarrow CH_3CHO^* + CO_2(n,m^{\lambda},p;J) \qquad (1)$$

whose relative rotational and vibrational populations are probed via diode laser transitions of the type:

$$CO_2(n,m^{\lambda},p;J) + h\nu(4.3\ \mu m) \rightarrow CO_2(n,m^{\lambda},p+1;J\pm1). \qquad (2)$$

The frequency of the diode is fixed at the frequency of a particular CO_2 absorption line by means of an ancillary CO_2 reference cell and a feedback loop to the diode laser. Time

domain changes in the diode laser light which occur immediately after the excimer laser pulse (due to the appearance of CO_2 photofragments in the sample cell) are detected with a cooled InSb detector and acquired on a signal averager.

In the rotationally state resolved experiments, the change in absorption is measured after a delay of 600 ns following the excimer pulse, corresponding to the response time of the IR detector. With a pyruvic acid pressure of 25 mTorr, this time delay represents only $\sim 1/7$ of the characteristic time for a single gas kinetic collision. The measurement is thus made on a timescale which is short compared to that required for rotational relaxation of the CO_2 photofragments,[3] and so is representative of the relative nascent population of CO_2 formed in the probed rovibrational state.

Rotationally state resolved populations of the CO_2 photofragment have been measured in the R-branches of the (00^00), (01^10), and (02^20) vibrational levels. The (02^20) distribution, graphed in Figure 1, shows a substantial degree of rotational excitation in the nascent molecules; note that the distribution can be roughly fit to a Boltzman distribution having a temperature of 1300 K. These results might possibly be explained by the presence of an internal hydrogen bond in the gas phase pyruvic acid.[4] As the C-C bond breaks, the residual hydrogen bond may impart substantial rotational motion to the departing CO_2 fragment, as shown schematically in Figure 2. The high efficiency of such a process may reconcile the rather high degree of rotational excitation observed in the CO_2 fragment with the more moderate translational excitation ($\sim$300 K) observed below.

The extremely high resolution of the diode laser ($\sim$0.0003 cm^{-1}) was exploited in a second set of experiments measuring the absorption lineshapes of the nascent CO_2 molecules. In these experiments, the diode current is modulated with a 1 kHz sawtooth waveform which repetitively ramps the frequency of the diode over a range of $\sim$1 cm^{-1}. At this rate, the diode light sweeps through the frequency range of a single CO_2 absorption line in $\sim$1 us, a time which is fast compared to the timescale for collisional

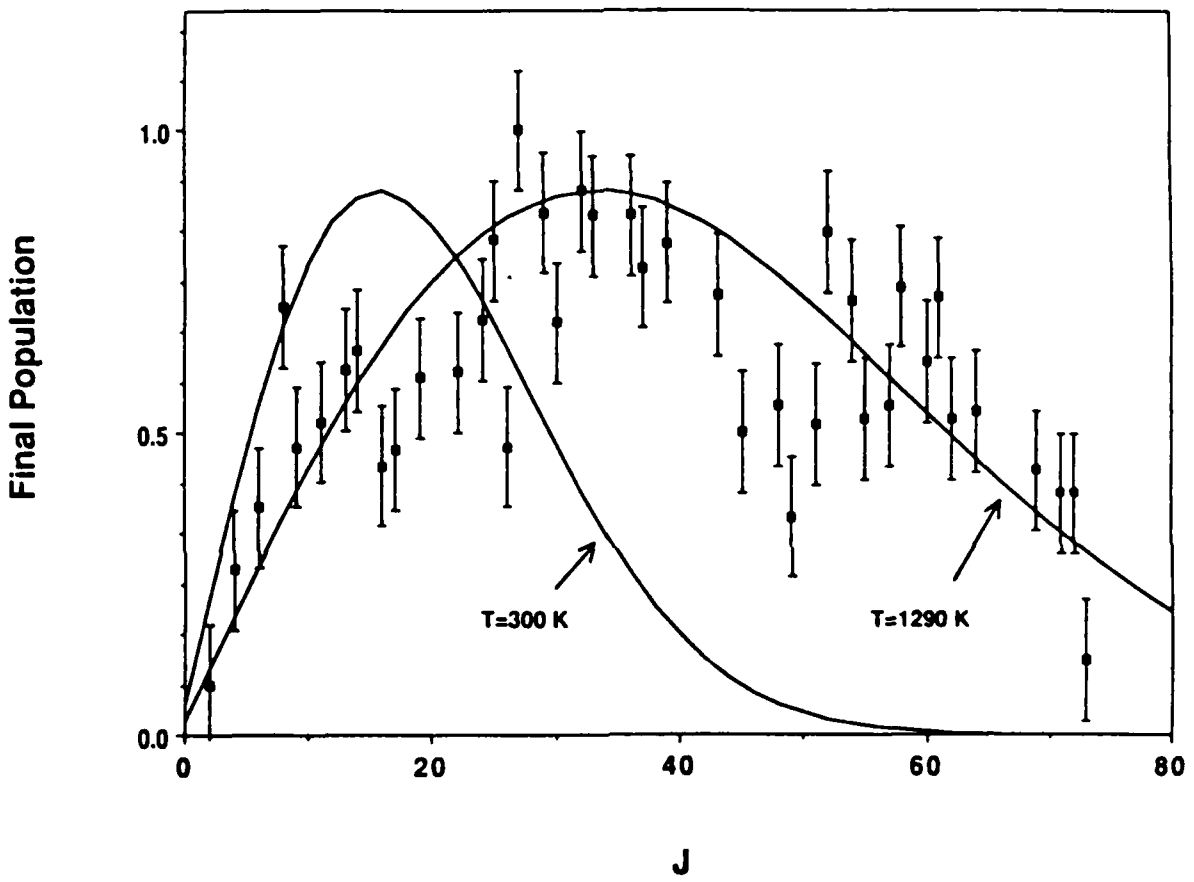

Figure 1: Nascent distribution of CO_2 population among the rotational levels of (02^20). Rotational Boltzman distributions at 298 K and 1300 K are plotted for comparison.

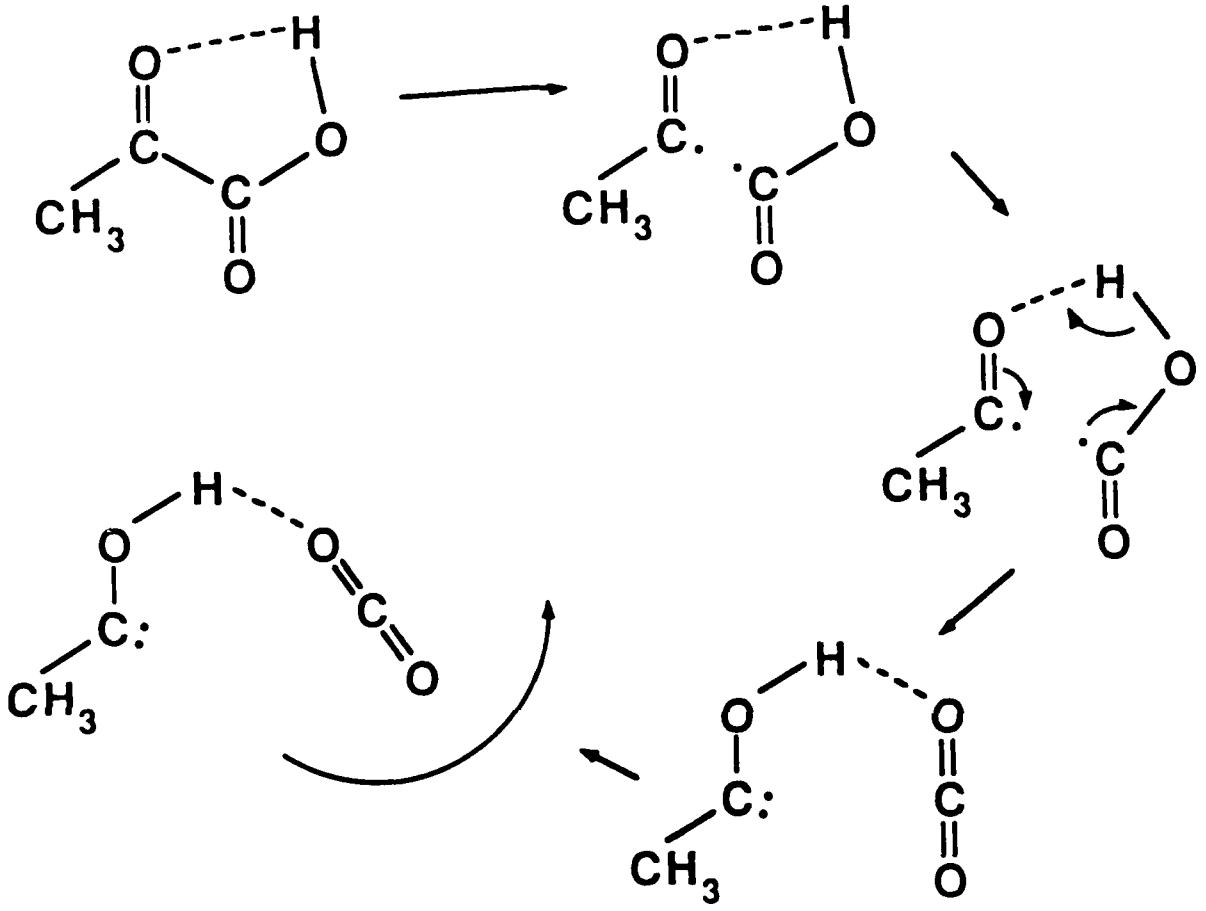

Figure 2: A schematic depiction of one possible cause of the high degree of rotational excitation in the CO_2 photofragment. 'Memory' of the internal hydrogen bond in the parent pyruvic acid converts the translational energy of the separating fragments into rotational excitation.

reorientation at a gas pressure of 25 mTorr. The excimer laser is fired synchronously with the diode laser modulation--but at only 1 Hz--such that the excimer pulse occurs immediately prior to the diode laser sweep through the transition of interest. The transient line profile is captured on a signal averager and is calibrated with both Fabry-Perot etalon fringes and static CO_2 absorption lines.

Lineshapes were measured for numerous transitions throughout the CO_2 (01^10) and (02^20) Q and R branches. All of the measured line profiles were symmetric, gaussian in shape, and had widths which, within the 20-30% accuracy of the measurements, were equal to the room temperature CO_2 doppler linewidth. To a first approximation then, these experiments suggest that the CO_2 fragment leaves the parent molecule with rather low velocity. This translational energy may be further moderated by substantial rotational excitation which occurs in the exit channel. Such slow fragment velocities, coupled with the 300 K rotational distribution of the parent pyruvic acid molecules would explain the isotropic distribution of CO_2 fragment velocities (responsible for gaussian lineshapes) found in these experiments.

These results would appear to be in agreement with our recent measurements of nascent vibrational excitation in the CO_2 photofragment, in which 97% of the molecules were observed to be in the vibrational ground state. Both studies suggest a photodissociation mechanism which occurs primarily on an electronically excited surface, and involves rather low "velocity" along the reaction coordinate(s). In this model, the vast majority of the 6.4 eV photon energy is left behind in an electronically excited acetaldehyde fragment. Moreover, the assumed inability of acetaldehyde to absorb this much energy has prompted us to look for further fragmentation products, and indeed, recent diode laser probes indicate substantial evolution of both excited CO and CH_4 upon photodissociation. Further study of vibrational, rotational, and translational excitation in these fragments is presently underway.

This research was also supported by the Department of Energy, Contract DE-AC02-78-ER-04940 and the National Science Foundation, Grants NSF-CHE 85-17460 and NSF-CHE 80-23747.

References:

1 J. A. O'Neill, T. G. Kreutz, and G. W. Flynn, J. Chem. Phys. 87, 4598 (1987); C. F. Wood, J. A. O'Neill, and G. W. Flynn, Chem. Phys. Lett. 109, 317 (1984).

2 J. A. O'Neill, C. X. Wang, J. Y. Cai, G. W. Flynn, and R. E. Weston, Jr., "Rotationally Resolved Hot Atom Collisional Excitation of $CO_2 00^0 1$ and $00^0 2$ Stretching Vibrations by Time-Resolved Diode Laser Spectroscopy," submitted: J. Chem. Phys.; J. A. O'Neill, J. Y. Cai, G. W. Flynn, and R. E. Weston, Jr., J. Chem. Phys. 84, 50 (1986); J. O. Chu, C. F. Wood, G. W. Flynn, and R. E. Weston, Jr., J. Chem. Phys. 80, 1703 (1984); 81 5533 (1984).

3 T. A. Temple, D. R. Suhre, and P. D. Coleman, Appl. Phys. Lett. 22, 349 (1973); E. E. Stark, Jr., Appl. Phys. Lett. 23, 335 (1973); R. R. Jacobs, K. J. Pettipiece, and S. J. Thomas, Phys. Rev. A11, 54 (1975).

4 W. J. Ray, J. E. Katon, and D. B. Phillips, J. Mol. Struct. 74, 75 (1981).

IV. PICOSECOND ENERGY TRANSFER DYNAMICS AND LIQUID SURFACE STRUCTURE

(J. Pinto, C. Goh, A. Castro, B. Bowman, H. Lu, E. Sitzman, and K. B. Eisenthal)
(JSEP work unit 6, 1985 - 1988)
(Principal Investigator: K. B. Eisenthal (212) 280-3175)

A. SURFACE STRUCTURE AND ENERGETICS OF LIQUID WATER

We are exploiting the surface-sensitive property of second harmonic generation in an attempt to elucidate the surface structure of liquid water. The orientational nature of the interface is of intrinsic importance in a diverse array of chemical and biophysical systems. Through temperature-dependent studies, we are probing the energetics of dipole orientation. Other polarization measurements of the second harmonic signal allow us to deduce the net orientation which is of immediate concern in the formation of a more exact structural picture of hydrogen bonding and associated geometry in the first few layers of liquid water.

B. FREE ENERGY OF ADSORPTION AT THE AIR-WATER INTERFACE

Surface second harmonic generation is a useful technique for studying adsorption at interfaces. We are investigating the adsorption of a number of alkylphenols and anilines and their ions at the air-water interface. These species are found to obey the Langmuir adsorption isotherm over all ranges of concentrations. Thus, free energies of adsorption can be calculated. Varying the size of the alkylchain, the competition between hydrophobic and solvation forces at the surface are investigated.

C. FEMTOSECOND LASER STUDIES OF ISOMERIZATION DYNAMICS

We have recently finished construction of an amplified femtosecond laser. This laser is capable of producing pulses as short as 75 femtoseconds with powers up to 0.5 mJ. The experiments in progress are now concerned with understanding the role of the solvent in barrier crossing. We are presently in the process of measuring the barrier height of the activated isomerization of 1, 1'-binaphthyl in alcohol and alkanes. These results will allow us to make meaningful comparisons to barrier crossing theories. In the near future we will be investigating the influence of high pressure on the isomerization of 1,1'-binaphthyl.

D. PICOSECOND DYNAMICS OF ELECTRONIC RELAXATION AT THE AIR-LIQUID INTERFACE

The manifestation of second harmonic generation at the air-liquid interface has led to new activity in studies of molecules at liquid surfaces. Of specific interest was the recent work that showed that there can be a dramatic change in simple chemical equilibria due to the asymmetry of forces encountered by a molecule at the surface.1 With this in mind it was recognized that steric restrictions imposed by the interfacial region and specific electronic interactions between a molecule and the surface may often yield new photochemical phenomena.

We have addressed this issue by considering how the photophysical properties of a molecule can be affected when it is placed at the air-liquid interface. Specifically, we chose to examine the excited state relaxation of organic dye molecules. We optically pump the ground state molecules and then probe for changes in the nonlinear susceptibility of the surface molecules, using the second-harmonic generation technique, as a function of time delay between the pump and probe pulse. The key point to the experiment is that the different electronic states of the

surface molecules often have significantly different nonlinear susceptibilities, and thus will affect the resulting second harmonic field that is produced. For example, it was found that excitation at 532nm of a solution of erythrosin in water/methanol (9:1, v/v) yielded a dramatic increase in the second harmonic field (at 266nm). The rise time of this enhancement in the second harmonic field was less than 40 psec. Furthermore, it was found that the signal persists on the order of several hundred picoseconds. These results are accounted for by a reversible photobleaching of the ground state erythrosin molecule at the surface. The increase in signal is due to population of an excited state or states. In summary, we have directly observed the excited state relaxation of molecules at an air-liquid interface. Further work is in progress.

These reports were also supported by the Air Force Office of Scientific Research, Grant AFOSR-88-0014 and the National Science Foundation, Grant NSF-CNE 85-13553.

Reference:

1 K. Bhattacharyya, E. V. Sitzmann and K. B. Eisenthal, J. Chem. Phys. 87, 1442 (1987).

V. OPTICIAL COHERENT TRANSIENT SPECTROSCOPY

A. FEMTOSECOND RELAXATION TIME MEASUREMENT WITH INCOHERENT LIGHT

(F. Moshary and S. R. Hartmann)
(JSEP work unit 2, 1985-1988)
(Principal Investigator: S. R. Hartmann (212) 280-3272)

1. Introduction -- Photon echoes with incoherent light were first performed by our laboratory in late 1983 by R. Beach and S. Hartmann.[5] They carried out an echo experiment using incoherent light in Na. In 1984, Morita and Yajima carried out a theoretial analysis demonstrating the potential of such an experiment in time resolved coherent transient spectroscopy.[6] This method has been used to make time resolved measurements in Nd:Glass[1], and Cresyl Violet in cellulose.[2] The latter work is essentially very similar to the work of Ippen at al[7] in Cresyl Violet in PMMA performed using short pulses. For phase relaxation measurement, the two methods are in principal identical. Incoherent four wave mixing has also been used for time resolved study of relaxation times of the third order susceptibility in CS_2 and Nitobenzene.[3] The results obtained are in agreement with experimental results using short pulses. The use of this method has recently been extended to T_1 measurements using three beams in a noncopalar geometry.[4]

Our recent work has been the study of excitation phase relaxation in color glass filters. These materials consist of a host glass doped with small (100Å) semiconductor (CdS_xSe_{1-x}) crystallites possessing large and fast third order nonlinearities (10^{-8} esu) which is of interest in optical signal processing applications.[8-11] Finite size affects have been observed in these systems making them an alternative to quantum well heterostructures for the study of electron confinement effects.[10] Population relaxation time measurements in these materials have

given values for T_1 in the range of 16-30 psec.[11]

2. Experiment -- Amplified spontaneous emission is used as the broadband source in our experiment (Figure 1). One pass amplification of the spontaneous emission in a transversely pumped (Nd:YAG@532nm) flow through dye cell containing a mixture of SR640 and DCM dies will yield a spectrum 300 to 400 Å wide. Figure 2 shows the spectrum of an incoherent source used in a recent experiment. The output pulses are 7nsec long. The basic experimental set up is illustrated in Figure 3. The four wave mixing signal may be detected in one or both of the phase matched directions as illustrated in Figure 4.

The electric field of an incoherent pulse may be modeled in the form:

$$E = \mathcal{E}(t-n.r/v)\exp(-i\omega t+ik.r)+CC$$
$$\mathcal{E} = \varepsilon(t)R(t)$$

Where:
$$\langle R(t)\rangle=\langle R^*(t)\rangle=0$$
$$\langle R(t)R(t+\tau)\rangle=\langle R^*(t)R^*(t+\tau)\rangle=0$$
$$\langle R^*(t)R(t+\tau)\rangle=f(\tau)$$

$f(\tau)$ is a correlation function with width τ_c, the correlation time, ($\tau c << \tau_p$, the pulse duration).

Assuming a two level system with phenomenological relaxation times T_1 and T_2, where $T_1 >> T_2, \tau_c, T_2^*$, the observed signal as a function of pulse separation τ will have the form:

$$I(\tau)\approx\int_0^\infty dy \int_0^\infty dy' \int_0^\infty dx \int_0^\infty dx' f(y-y')[f(x'-\tau)g(y'-x')+f(x'+\tau)g(y'+x')]$$
$$[f(x-\tau)g(y-x)+f(x+\tau)g(y+x)]\exp(-(y+x+y'+x')/T_2)$$

where
$$g(t)=\int d\omega \exp(-i\omega t)G(\omega)$$

$G(\omega)$ is the inhomogeneous line shape function with the width $\approx 1/T_2^*$. Also $f(t)$ in the above formula is assumed to be real for simplicity. As seen from the above, the time resolution of such

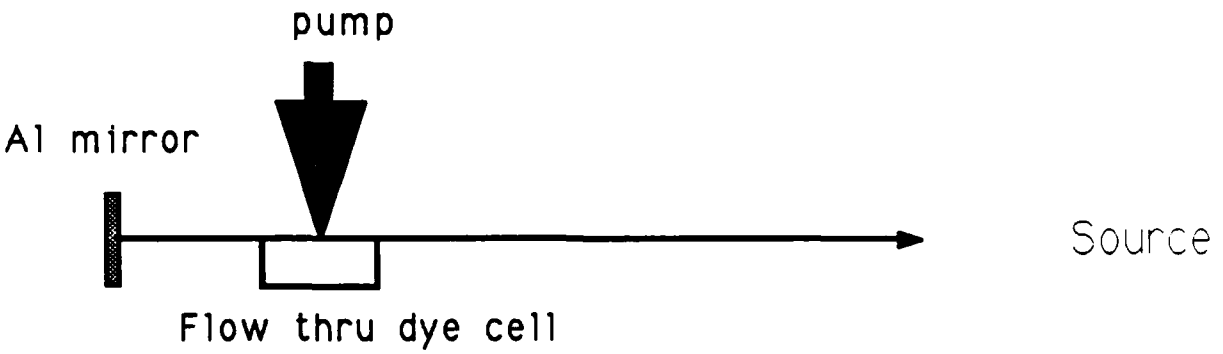

FIG 1. INCOHERENT SOURCE USED IN THE TIME-DELAYED FOUR WAVE MIXING EXPERIMENT

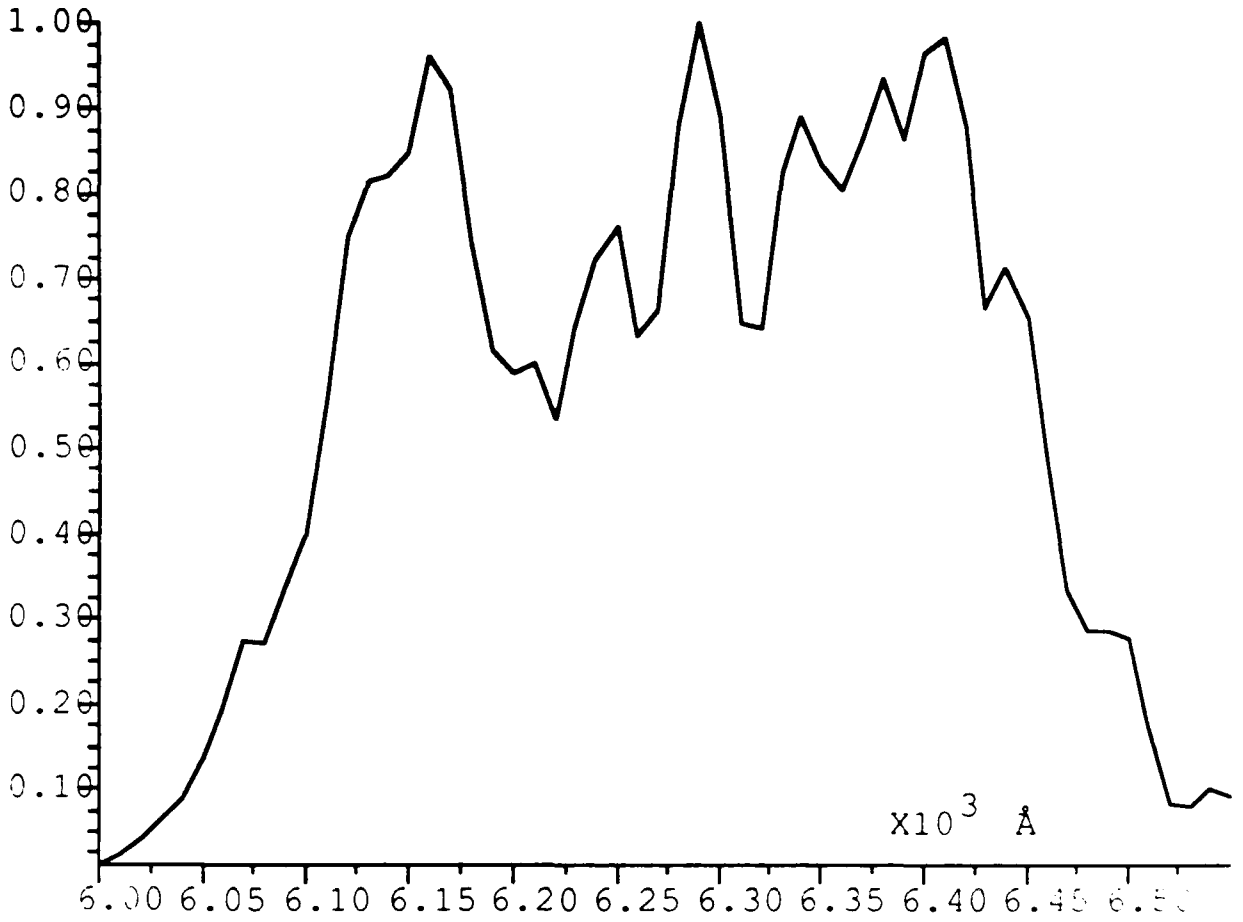

FIG 2. Power spectrum of the incoherent source.

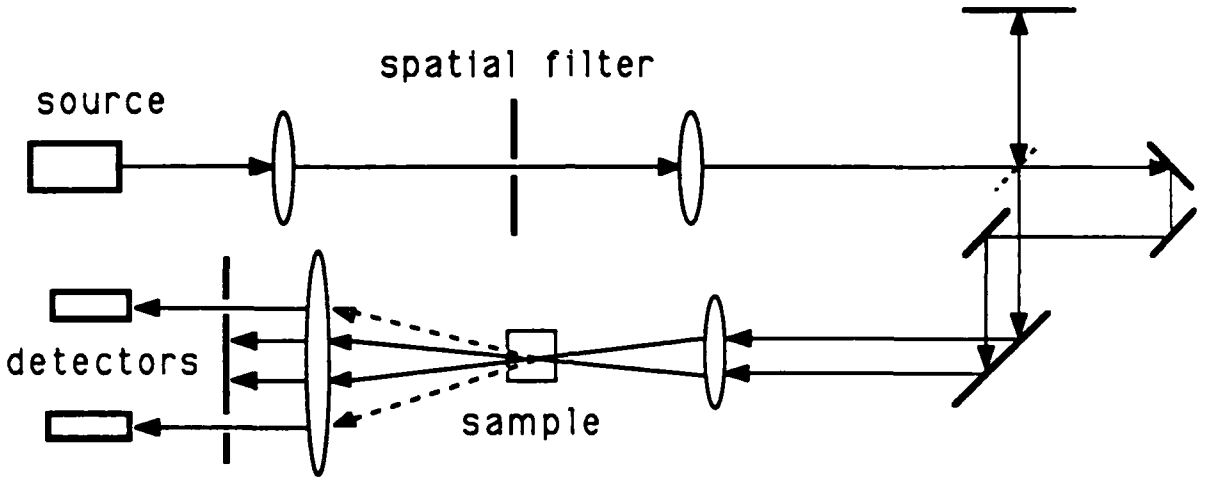

FIG 3. EXPERIMENTAL SET UP.

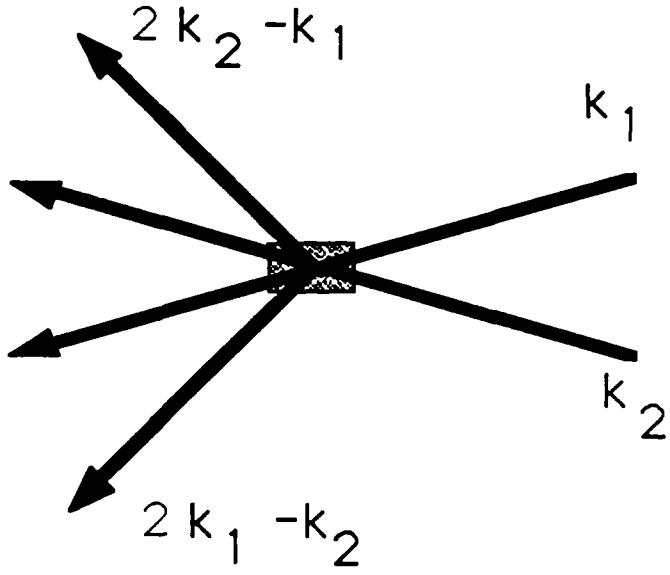

FIG 4. DIRECTIONS OF RADIATION DUE TO FOUR WAVE MIXING

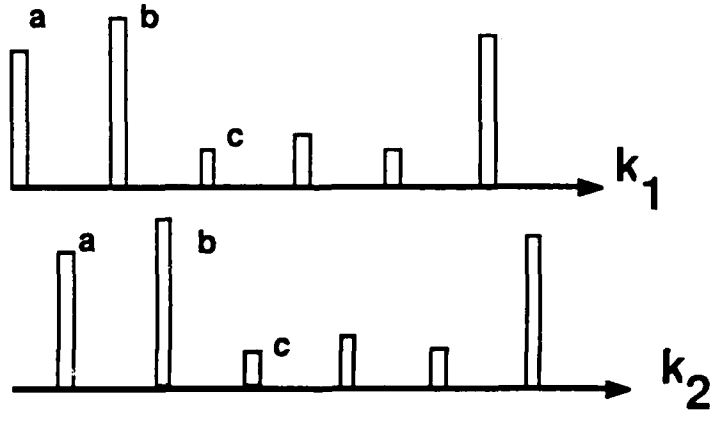

FIG 5. PULSE TRAIN VIEW OF THE INCOHERENT LIGHT BEAMS

an experiment is on the order of τ_c the correlation time, not the pulse width. If we have the functional form of f(t) and g(t), we can fit the experimental data to obtain a value for T_2.

These results can be interpreted in terms of the random pulse train model of the incoherent light as follows:

When the light is divided into two beams and incident on the material, the sample senses two pulse trains, one with wave vector k_2 delayed by τ with respect to the other, with wave vector k_1. At this same time there occurs a number of three pulse process with various combinations of incident pulses belonging to one or the other pulse trains (see Figure 5).

There are in general two groups of such processes; the first group has pulses 1 and 2 separated by τ and from the same original pulse. Therefore these two pulses are correlated and their phase relation is always constant. A pair of incident pulses generates a population grating in the sample and each of the above pairs contributes to the same population grating. As a result, for a given third pulse, the fields from all such three pulse processes add coherently and the output intensity depends on τ. The second group consists of three pulse processes in which the three incident pulses have no correlation among them. The output fields do not add coherently and the output intensity is independent of τ. These processes lead to an incoherent background term.

To get information on τ_c, one can perform a fourier transform on the power spectrum. The result is the autocorrelation function f(t). This is also verified by a time domain measurement utilizing the property of the large thermal grating effect in a dye solution such as Nile Blue in Methanol. A time delayed four-wave-mixing experiment with parallel polarization in the dye yields the square of the autocorrelation of the source (Figure 6).

The results of the time delayed four-wave-mixing experiment in the Corning color glass filter 2-59 is in qualitative agreement with the theory and yields a T_2 in the range of 30 to 40 fsec. However, different results have been obtained in low

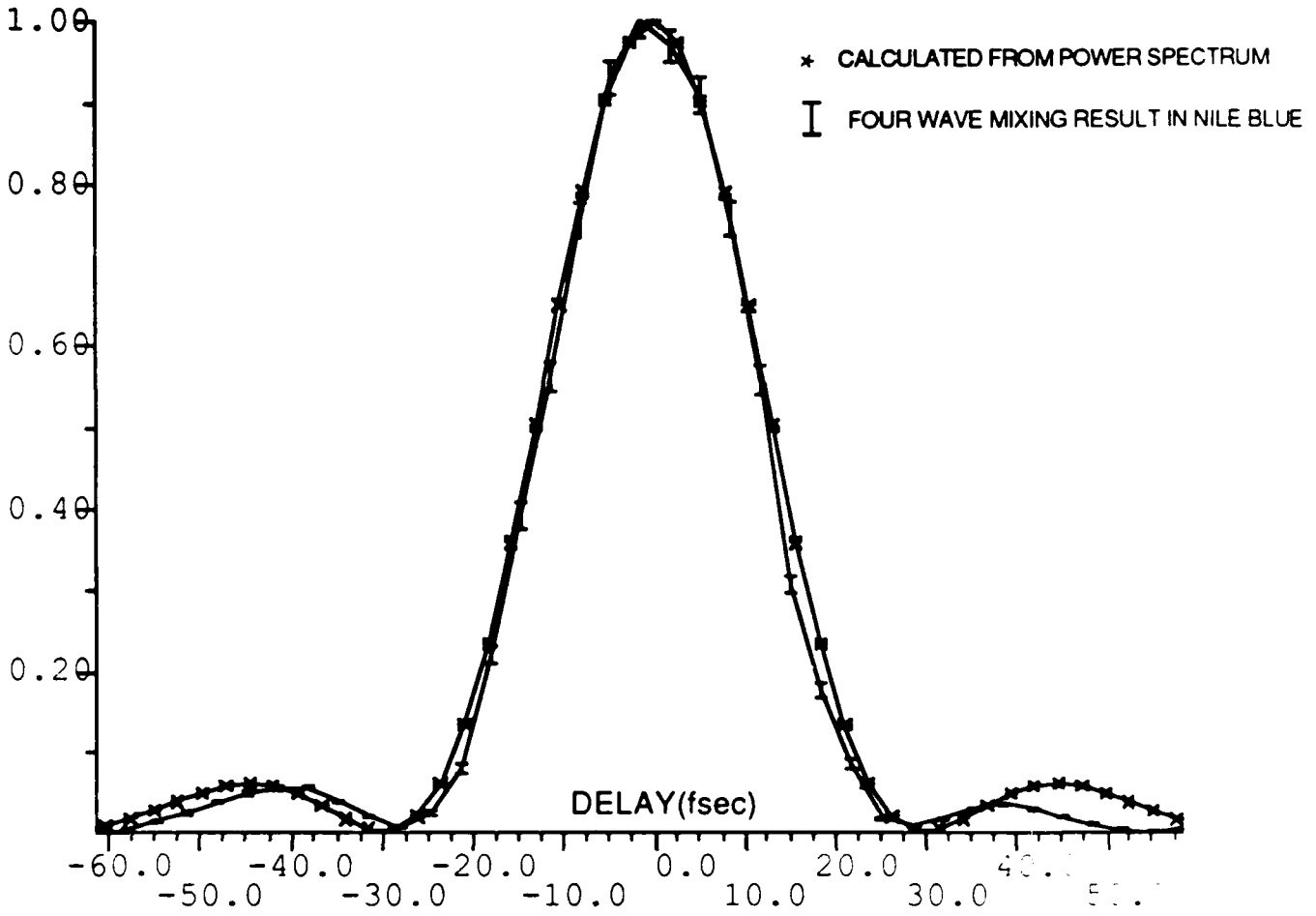

FIG 6. INTENSITY AUTOCORRELATION OF THE SOURCE

and high optical density samples. The optical density (OD) is varied by using samples of various thickness. At low OD, the experimental results indicate a homogeneously broadened linewidth (Figure 7) while at high OD, the transition seems to be inhomogeneously broadened as indicated by the antisymmetry of the signal intensity of the two phase-matched directions as a function of the delay time (see Figure 7). We believe that this may be due to the fact that the experiments in the two different conditions give information on different parts of the absorption band and the sample itself plays the role of a tuning element.

In the near future, we plan to continue the above experiment studying the effects of OD and excitation pulse intensity on the system. A measurement of $X^3(\omega)$ will also be undertaken. Temperature dependent experiments are also planned to be carried out measuring the relaxation rate and the linehape as a function of temperature. We also plan to perform Modulation Photoreflectance Spectroscopy on our samples to get information on their energy level structure.

Future experiments will apply this technique to dye molecules in solutions (e.g. Nile blue in Methanol) and Multi-Quantum Well structures.

This research was also supported by the Office of Naval Research, Contracts N00014-78-C-0517 and N00014-86-G-0154.

References:

1 H. Nakatsuka, M. Tomita, M. Fujiwara and S. Asaka, Optics Comm. 52, 150 (1984).

2 M. Fujiwara, R. Kurdo and H. Nakatsuka, JOSA B 2, 1634 (1985).

3 K. Kurokawa, T. Hattori and T. Kobayashi, (to be published).

4 N. Morita, T. Tokizaki and T. Yajima, JOSA B 4, 1269 (1987).

5 R. Beach and S. R. Hartmann, Phys. Rev. Lett. 53, 662 (1984).

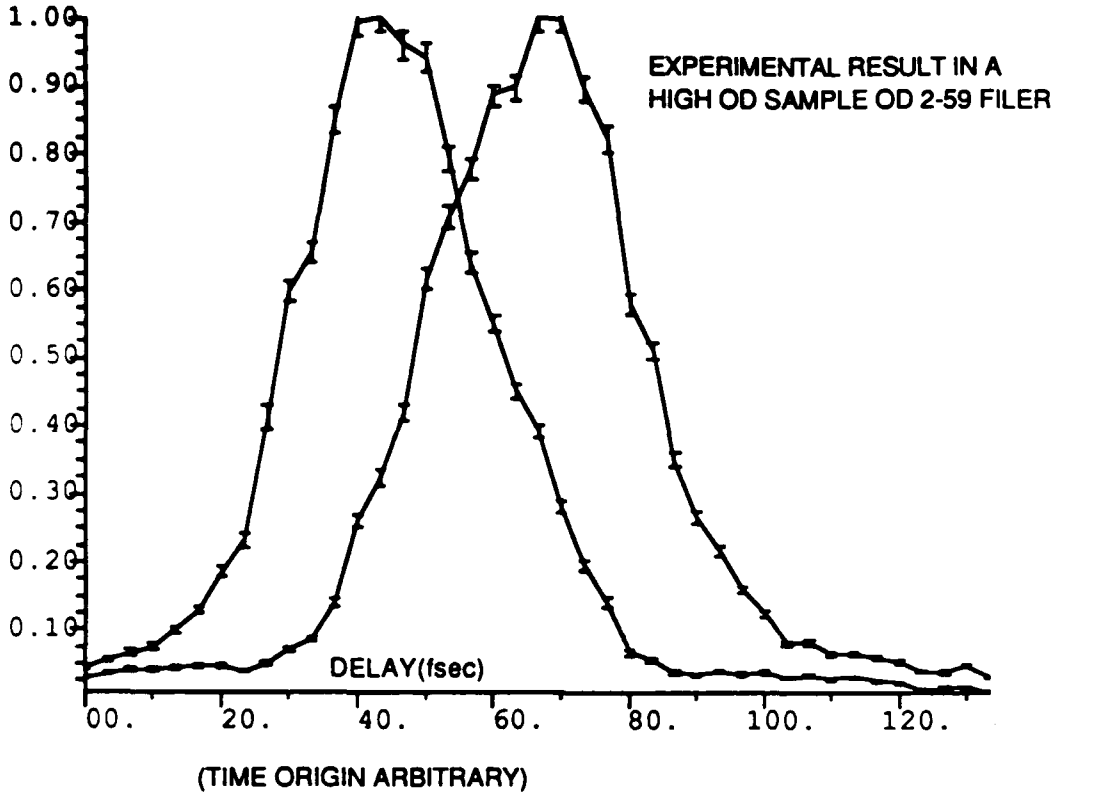

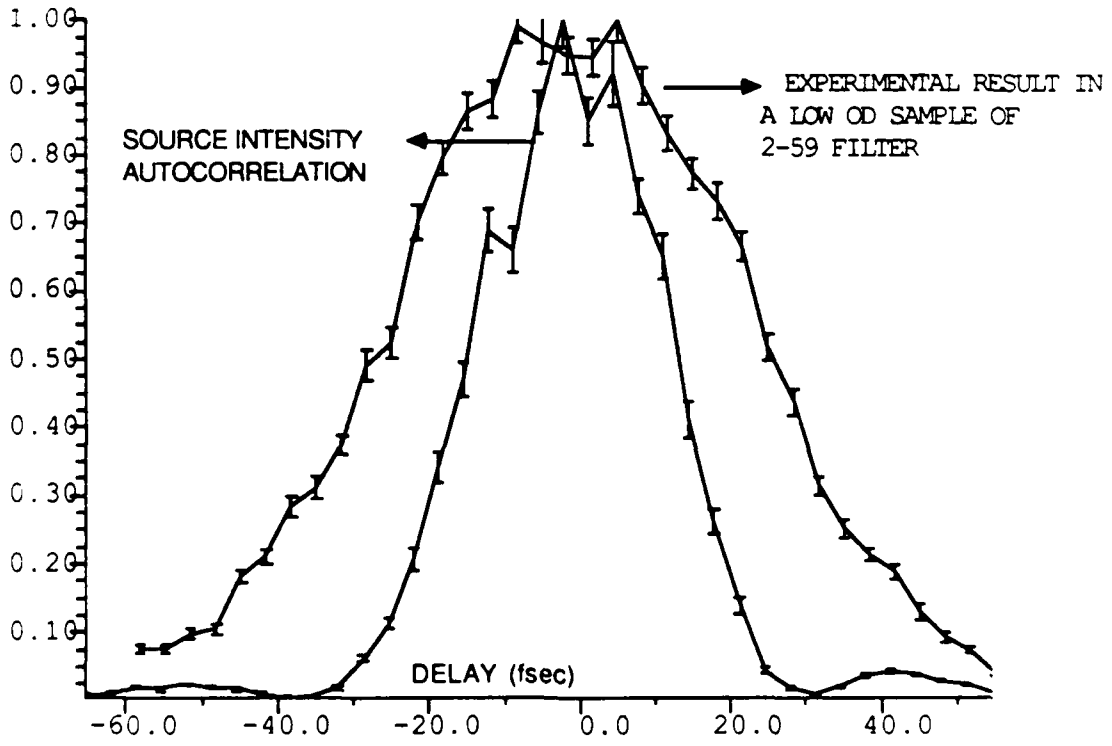

FIG 7. EXPERIMENTAL RESULTS IN THE CORNING 2-59 SAMPLE

6 N. Morita and T. Yajima, Phys. Rev. A 30, 2525 (1984).

7 A. M. Weiner, S. DeSilvestri, and E. P. Ippen, JOSA B 2, 654 (1985).

8 M. Dagenais and F. Sharfin, JOSA B 2, 1179 (1985).

9 A. Ekimov, Al. Efros and A. Onushchenko, Solid State Comm. 56, 921 (1985).

10 J. Warnock and D. Awshalom, Phys. Rev. B 32, 5529 (1985).

11 S Yao, C. Karagleff, R. Fortenberry, C. Seaton and G. Stegeman, Appl. Phys. Lett. 46, 801 (1985).

B. PHOTON ECHO EXPERIMENTS WITH INTENSE INCOHERENT LIGHT

(L. Van Wagenen, S. R. Hartmann)
(JSEP work unit 4, 1985 - 1988)
(Principal Investigator: S. R. Hartmann (212) 280-3272)

Incoherent light as an innovative approach to studying a wide variety of phenomena on very short time scales has become a topic of intense interest, but before the advantages of incoherent light as a spectroscopic tool can be realized it is necessary to understand the physics involved in the interaction of incoherent light with matter more completely. Professor Hartmann in collaboration with Professor R. Friedberg has produced a new, non perturbative analysis of the interaction of incoherent light with matter.[1] The theory places no restrictions on the intensity of the pulses involved, and is exact for the case of non overlapping excitation pulses (see references 2 and 3 for comparison with existing theories). We now have a way to predict analytically the relative intensity of a photon echo created using intense incoherent pulses. A series of experiments is underway to verify this theory.

A specific pulse sequence is required to create a photon echo, and each pulse in the sequence contributes to the echo. It is our goal to isolate uniquely the effects of each pulse involved in an echo experiment in order to understand how the incoherent light interacts with the atoms. The theory can be verified by studying how variations of the echo's constituent pulses effect the reulting echo signal. A number of different photon echo experiments must be performed to uniquely isolate the effects of each pulse. The parameters of interest will be the position in a pulse sequence of the incoherent pulses, the intensity of the incoherent pulse(s) and correlation between two pulses of a sequence. By permuting these parameters, 2, 3, and 4 pulse echo experiments can be designed to study different terms

from the theory and thus the theoretical and experimental results for the signal intensity can be compared. We are interested in studying how each pulse in an echo experiment contributes to the final signal.

The experiments underway consist of echo experiments involving 2, 3 and 4 laser pulses. For the sake of clarity only 2 and 3 pulse experiments will be explained; these will convey the essential ideas and points of theoretical interest. The goal of each experiment is to test the predictions of the theory concerning the contribution of each pulse to the final signal. This is achieved by permuting the order of the required pulses in a photon echo. If, for example, in one two pulse experiment $\mathbf{k}_1$ is incoherent and $\mathbf{k}_2$ is coherent (a laser pulse) and uncorrelated with $\mathbf{k}_1$, then, in another experiment $\mathbf{k}_2$ may be incoherent and $\mathbf{k}_1$ coherent. It is also possible that all the pulses in an experiment are incoherent. During a particular experiment the intensity of one incoherent pulse will be varied and the effect on the echo signal will be studied. This same procedure will be repeated with 3 and 4 pulse echo set ups.

The experimental set up requires a tunable dye laser and an incoherent source. Because we will be working in sodium at 5896 A, we use R610 (10^{-3}M in ethanol) in both dye cells, both sources are to be pumped by the 7 nanosecond long second harmonic pulse of a Quanta Ray DCR-1A yttrium aluminum garnet (YAG) laser. The incoherent source is made by removing the end mirror from a Hansch type dye laser and placing a 2400 grooves/mm diffraction grating in the littrow configuration, the output is the amplified spontaneous emission of the dye. A spectrometer is used to verify that the incoherent source has a width of 30-40 A which is to be centered around 5896 A. The correlation time of such a source is less than 1 picosecond. The lasers have widths of about 3 GHz, run in 1-2 modes, and are tuned to 5896 A. Each of the sources is amplified once by a longitudinal amplifier containing R610 in ethanol and pumped longitudinally by the YAG second harmonic. The output of each source is spatially filtered after amplification to ensure obtaining one spatial mode and to

insure uniform intensity throughout the beam. Several methods are being studied to vary the intensity of the beams. In a typical three pulse experiment, the output of one source is split into beams $\mathbf{k}_2$ and $\mathbf{k}_3$, and the output of the other source will be designated $\mathbf{k}_1$. Each pulse must be delayed from the previous pulse by more than 21 nsec. The three pulses are then sent into a sodium heat cell that has a temperature of about $413^{\circ}K$($L<1$). All three pulses are angled with respect to each other by a few milliradians allowing for the echo signal to be detected in the $\mathbf{k}_3+\mathbf{k}_2-\mathbf{k}_1$ phased matched direction with a photomultiplier tube after spatial filtering.

Currently predictions have been calculated from the theory and 2 and 3 pulse experiments are underway.

This research was also supported by the Office of Naval Research, Contracts N00014-78-C-0517 and N00014-86-G-0154.

References:

1 R. Friedberg and S. R. Hartmann, Journal of Physics (to be published).

2 N. Morita and T. Yajima, Phys. Rev. A30, 2525(1984).

3 R. Beach, D. DeBeer and S. R. Hartmann, Phys. Rev. A32, 6437(1987).

C. ATTOSECOND BEATS IN SODIUM VAPOR

(D. P. DeBeer, E. Usadi, and S. R. Hartmann)
(JSEP work unit 4, 1985 - 1988)
(Principal Investigator: S. R. Hartmann (212) 280-3272)

Research on ultrafast phenomena is characterized by a mixture of techniques and instrumentation of varied nature. Several practical schemes provide light pulses in the middle femtosecond regime and recent developments now yield excitation pulses with durations as short as six femtoseconds. Less direct methods using broadband light sources have the potential of exploiting short autocorrelation times in order to study ultrafast phenomena by way of transient four-wave mixing. These latter experiments have been shown to be capable of obtaining both spectroscopic and relaxation information in the pico- and femtosecond regimes. The extension of this technique to a much shorter time regime is promising. A potential difficulty which arises in the ultrafast regime is in establishing a well defined delay time because of the angling of the excitation beams with respect to each other. However, this is a problem only when making relaxation measurements, not when looking at modulation effects.

The observation of high frequency modulation effects in Time-Delayed Four-Wave Mixing (TDFWM) does not require the use of broadband excitation pulses when relaxation times are long. This is best seen by viewing the modulation process not as a consequence of superposition state modulation but rather as due to an interference of scattering processes from atomic gratings produced by exciting separate atomic optical transitions. In a previous study[1] outputs of two conventional lasers tuned separately to the two Na D lines were used to produce an excitation field of the form:

$$E = E_0\left\{e^{-i\Omega}\left[e^{ik_1\cdot r} + e^{ik_2\cdot r - i\Omega\tau}\right] + e^{-i\Omega' t}\left[e^{k'_1\cdot r} + e^{ik'_2\cdot r - i\Omega'\tau}\right]\right\} + c.c. \quad (1)$$

where the primed and unprimed k-vectors correspond to the frequencies Ω and Ω', τ is a variable relative delay between the prompt (1) and delayed (2) fields as indicated by the subscripts, and where the optics were adjusted so that $k_1 - k_2 = k'_1 - k'_2$. A mixing signal is generated with wavevector $2k_2 - k_1$ which modulates at the difference frequency $\Omega' - \Omega$ as a function of τ. In the case of the Na D-line excitations the difference frequency is 530 GHz resulting in a modulation with a period of 1.9 picoseconds. Similar results have been seen using broad-bandwidth excitations in both Na[2] and Rb[3]. In the case of Rb the splitting is much larger resulting in a difference-frequency beat with a period of 139 fs. To see such beats in the attosecond regime the difference frequency must be in the petahertz regime. Alternatively, attosecond beats can be realized by adjusting the beams so that $k_1 - k_2 = -(k'_1 - k'_2)$ whereupon the modulation frequency will be at the sum rather than at the difference of the individual excitation frequencies.

The origin of the sum frequency beats is easily understood in terms of a simple induced grating analysis. With the above double frequency excitation field, each resonant component generates an atomic grating with spacing $2\pi/|k_1 - k_2|$ which scatters the wave labeled k_2 by an angle $n\theta$ (for scattering order n) with respect to k_1, where θ is the angle between k_1 and k_2. The two gratings formed by the resonant excitations at Ω and Ω' are themselves separated by $(\Omega' + \Omega) / k_1 - k_2$ so that the phase shift $\Delta\phi$ in the two scattered waves at Ω along $n\theta$ is just $\Delta\Phi = n(\Omega' + \Omega)\tau$. Thus sum frequency modulations are expected in the interfering four-wave mixing signals as a function of τ. This simplified analysis is correct only for n=1 where it includes all scattering pathways. The correct expression for the modulation behavior for all n is obtained by directly calculating the induced polarization from a step function excitation field of the form of Eq. (1) on a three level system whose levels are sufficiently separated so that the resonant excitations are

effectively isolated. The time evolution of this polarization is given by

$$\mathcal{P}(t) = \left[P\Omega_R \sin\left(\Omega(t-\tau) - \mathbf{k}_2 \cdot \mathbf{r}\right) + P'\Omega'_R \sin\left(\Omega' t - \mathbf{k}'_1 \cdot \mathbf{r}\right)\right] \frac{\sin ft}{f} \tag{2}$$

where $$f^2 = 4\Omega_R^2 \left\{1 + \cos\left[\frac{\Omega + \Omega'}{2}\tau\right] \cos\left[\frac{\Omega' - \Omega}{2}\tau + (\mathbf{k}_2 - \mathbf{k}_1) \cdot \mathbf{r}\right]\right\},$$

P and P' are the dipole moments for the Ω and Ω' transitions, Ω_R and Ω'_R are the associated Rabi frequencies, and we have assumed the $\mathbf{k}_1 - \mathbf{k}_2 = -(\mathbf{k}'_1 - \mathbf{k}'_2)$ geometry. Working in the perturbation limit ($\Omega_R t, \Omega'_R t \ll 1$) and considering only the lowest-order terms phased to radiate in the directions $\mathbf{k}_2 + n(\mathbf{k}_2 - \mathbf{k}_1)(n>0)$ we find that the output signals have the same modulation whether one looks at Ω, Ω', or both simultaneously. The radiated intensity emitted into the n^{th} order signal is:

$$\begin{aligned} I_n &\propto \int \left(\mathcal{P}_n^* \cdot \mathcal{P}_n\right) dt \\ &\propto \cos^{2n}\left[\frac{\Omega + \Omega'}{2}\tau\right] \\ &\propto \left[\frac{1}{2} + \frac{1}{2}\cos((\Omega + \Omega')\tau)\right]^n \end{aligned} \tag{3}$$

The sum frequency beats therefore dominate to all orders of scattering. The effect of the higher order frequency terms is to sharpen the modulation pattern.

The experimental apparatus is shown in Figure 1. The dye-laser pulses were 7 ns in duration and were tuned to 589.6 and 589.0 nm, the wavelengths of the sodium $3S_{1/2}$-$3P_{1/2}$ and $3S_{1/2}$-$3P_{3/2}$ transitions, respectively. Each laser operated in four to five longitudinal modes, yielding an overall laser bandwidth of 5 GHz. The beam geometry, $\mathbf{k}_1 - \mathbf{k}_2 = -(\mathbf{k}'_1 - \mathbf{k}'_2)$, was imposed; since Ω and Ω' are nearly equal this can be satisfied (to within the beam divergence) by making $\mathbf{k}_1 \| \mathbf{k}'_2$ and $\mathbf{k}_2 \| \mathbf{k}'_1$. To accomplish this the dye-laser outputs were split and recombined to provide two double-frequency pulses in such a way that the 589.0 nm component was delayed by τ in one beam and the other frequency delayed by the same amount in the other beam. Since

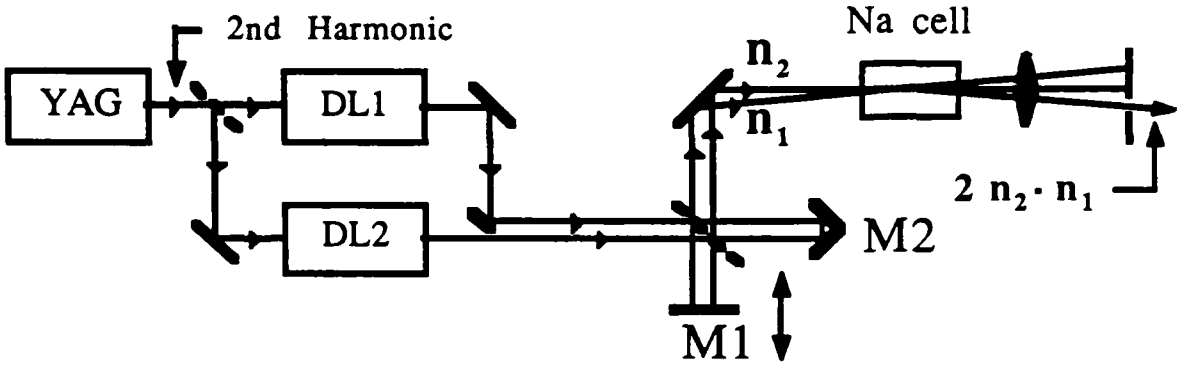

Figure 1. Schematic diagram of the experimental apparatus used to generate TDFWM in the sum-frequency geometry. Mirror M1 is mounted on a precision translation stage which provides variable relative delays of up to 30 fs in increments of < 100 as.

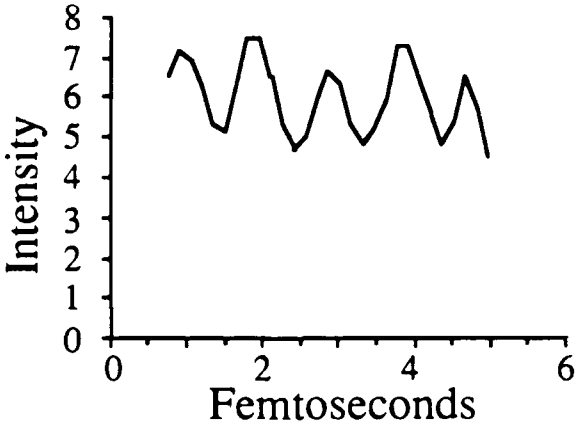

Figure 2. Typical set of data for the sum-frequency geometry plotting signal intensity vs relative pulse delay.

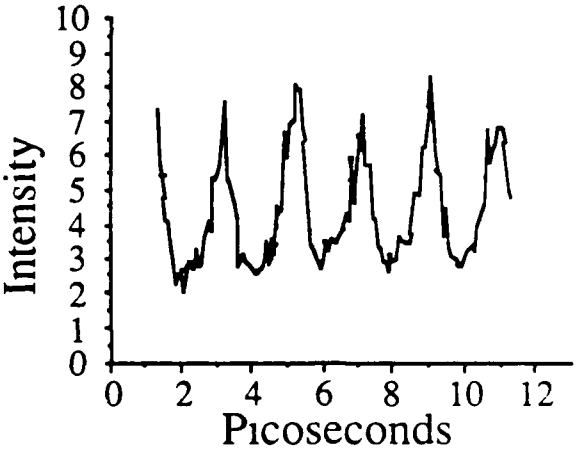

Figure 3. Data taken in the difference-frequency geometry showing the narrowing of the modulation in a high diffraction order (4th).

the delays introduced in the two beams must be stable compared to the period of the modulation, the beamsplitter, cornercube, and translating mirror shown in Figure 1 had to be stable to much better than a wavelength with respect to each other. Note also that this portion of the apparatus had to be enclosed to prevent air currents from changing the effective delay. The two double-frequency beams were angled at $\theta \approx 0.3$ mrad. These pulses overlapped spatially throughout a 100 mm long sodium cell which was held at 450 K. A pinhole in the focal plane of a 300 mm lens passed the TDFWM signal in the phase-matched $2k_2-k_1$ direction while blocking the excitation pulses. The signal was detected with an EG&G FND-100 photodiode and integrated over its full 7 ns duration. In a typical run the TDFWM signal was monitored as the relative delay was varied by moving mirror M1. The result of such a run is shown in Figure 2. The first order signal is harmonic in τ as predicted.

We have looked at signals emitted into higher orders but have not seen the narrowing of the peaks and flattening of the valleys expected from the above analysis. We believe this to be due to vibrational instabilities in our apparatus which average out the higher harmonic frequencies. However, to verify the existence of this effect we have redone the experiment in the difference-frequency geometry ($k_1-k_2=k'_1-k'_2$) of Reference 1. Here we have succeeded in observing the introduction of the higher harmonics and a representative set of data for the fourth order signal is shown in Figure 3. The data show the narrowing as expected.

As a spectroscopic tool this method of determining the sum frequency provides a useful complement to the difference-frequency technique, since taken together they can yield information on individual transition frequencies. Spectroscopy aside, this sum-frequency approach could find application as a position transducer. Using the first order signal, a device similar to a laser interferometer distance encoder could be constructed with the advantage that roughly twice the number of fringes would be observed for a given translation.

In summary, the new phenomenon of sum-frequency beats in a four-wave mixing experiment has been documented and its origin explained. This lays the groundwork for future spectroscopic and relaxation studies since as faster processes are studied shorter pulses will be used which will in turn couple several or many transitions, resulting in modulations in the observed signals. We hope that the present work will provide insight into the origin of those modulations.

This research was also supported by the Office of Naval Research, Contracts N00014-78-C-0517 and N00014-86-G-0154.

References:

1 D. DeBeer, L. G. Van Wagenen, R. Beach, and S. R. Hartmann, Phys. Rev. Lett. 56, 1131 (1986).

2 R. Beach, D. DeBeer, and S. R. Hartmann, Phys. Rev. A 32, 3467 (1985).

3 J. E. Golub and T. W. Mossberg, Opt. Lett. 11, 431 (1986).

D. LINE IMAGES

(M. Arend, S. R. Hartmann)
(JSEP work unit 4, 1985 - 1988)
(Principal Investigator: S. R. Hartmann (212) 280-3272)

The recent work of Durnin et. al.[1] on diffraction free beams has prompted us to investigate the effect of obstructing a collimated light beam with objects of cylindrical symmetry. Initial investigations have resulted in a comment on their paper[2], and indicate an improved method for generating line images or what they call "diffraction-free beams." Further studies have resulted in a more quantitative understanding of the phenomena of line images and suggest that a better theoretical description is needed.

One possible method for generating a line image is shown in Figure 1. Collimated light of wavelength λ illuminates a circular slit of diameter d and width Δ d located in the focal plane of a lens of radius R and focal length f. Light passing through the slit is diffracted both toward the axis and away from the axis. Figure 1A shows how the diverging rays can be thought of as originating from a virtual line object. Rays which are only slightly diverging are thought of as emerging from points which are far from the slit, and these points get imaged close to the focal point of the lens. Virtual object points close to the slit, corresponding to large angle diffraction, get imaged far from the lens. The segment of the line image between the lens and the focal point of the lens is due to light which is diffracted inward, as is shown in Figure 1B. As one recedes from the lens the transverse size of the line image remains constant and its diameter is given by $\delta = \frac{\lambda}{d} f$. If $R/f << \lambda/\Delta d$, then the on-axis intensity of the line image also remains constant as the observation point recedes from the lens. This is because the intensity of the diffracted light hardly varies as a function of

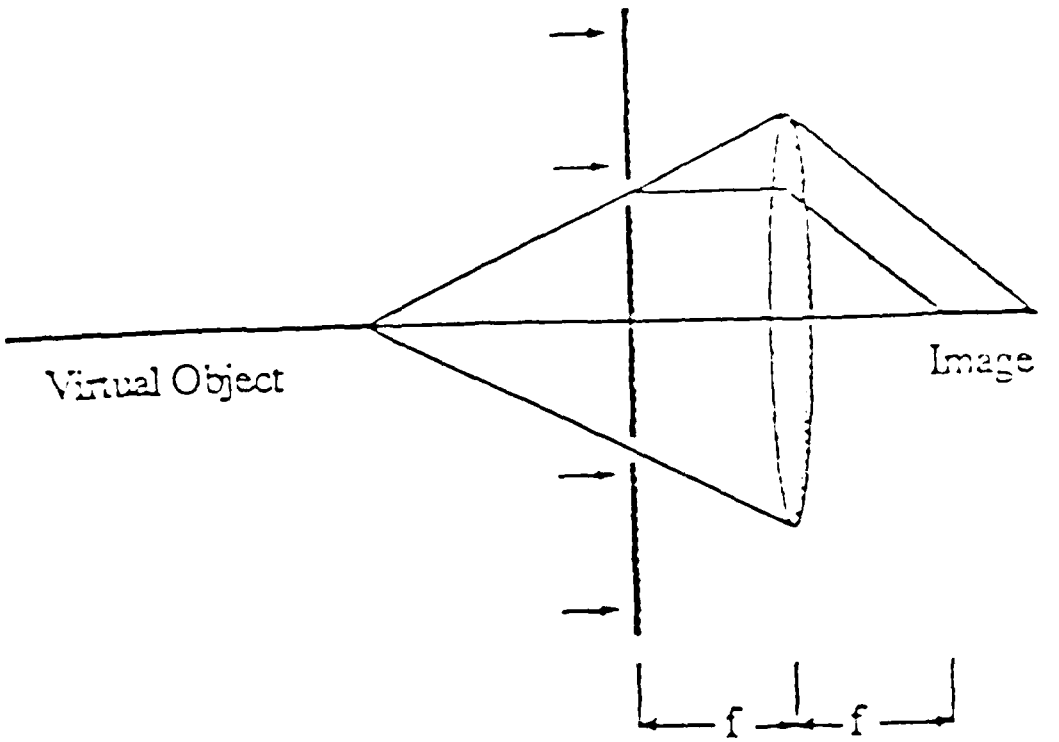

Figure 1A: Outward diffracting rays form a virtual line object which is imaged by the lens.

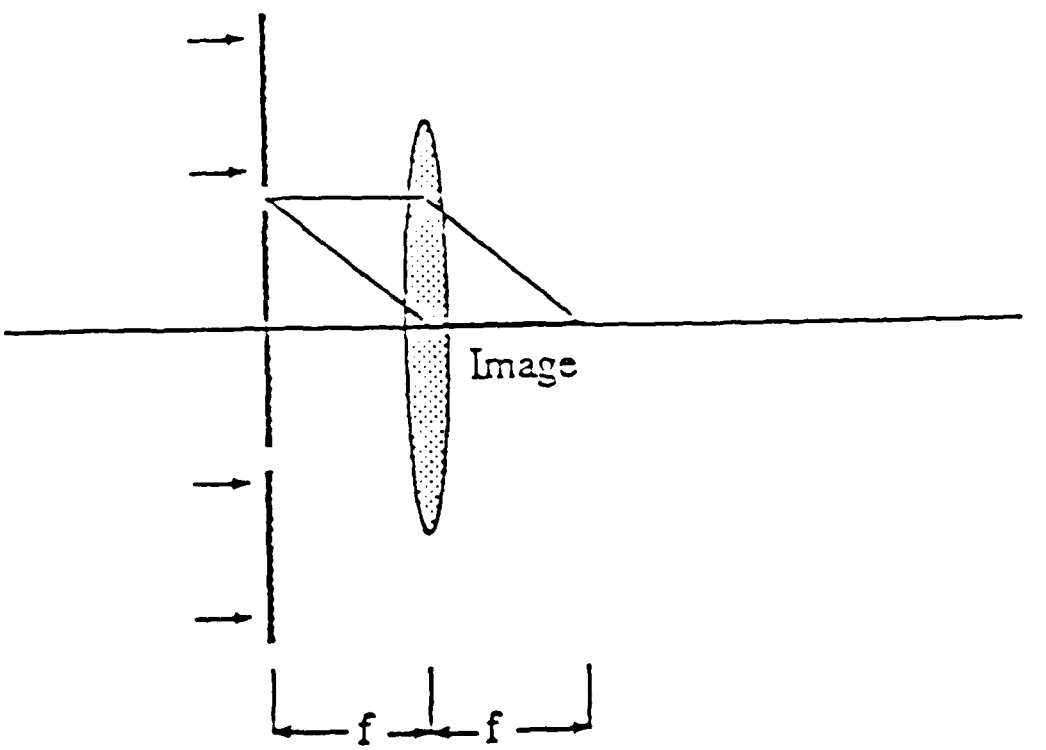

Figure 1B: Inward diffracting rays form a real line object extending to infinity. The lens forms an image of this line.

angle over the small range of angles $\theta \leq R/f$.

Using the setup described above, measurements of the intensity distribution in both the radial and axial directions have been performed by Durrin et. al.[1] The general characteristics of the intensity distribution mentioned above agree with their measurements. They claim that these measurements are evidence for the production of what they call a "diffraction-free beam." However, the setup of Figure 1 does not produce a beam. This is shown in Figure 2. In Figure 2A an attempt is made to block the central spot with a disk of diameter b and is unsuccessful, even when b is much larger than d. Conversely, Figure 2B demonstrates what happens when a pinhole is placed so as to "pass" only the central spot; a cone of light emerges at an angle $\tan^{-1}(d/f)$. The line image produced with the setup shown in Figure 1 may be quite useful though, since it is a way of continuously regenerating a small spot over a long distance; small and long, compared to a spot produced by what we normally think of as a beam.

A second method for producing a line image is shown in Figure 3. A ball bearing, which blocks the central portion of a collimated light beam, is placed before a lens, such that the center of the ball is in the focal plane of the lens. The primary effect of the ball is to cast a shadow region. Secondary effects include reflection from the surface of the ball and diffraction around the edge of the ball. These secondary effects are what form the line image as can be seen in Figure 3b. Rays which reflect or diffract from the ball at an angle θ can be thought of as emerging from a virtual point source a distance $R/\tan\theta$ behind the ball, and the argument is similar to earlier. The diameter of the spot is given by $\delta = \frac{\lambda}{d} f$ with d being the diameter of the ball. But the on-axis intensity is no longer constant with distance. There is an increase in intensity as one approaches the focal point from either direction as is shown by the data of Figure 4. These measurements represent the total flux of light passing through a 100 micron pinhole as a function of the pinhole's location on axis. The lens had a radius R=25mm

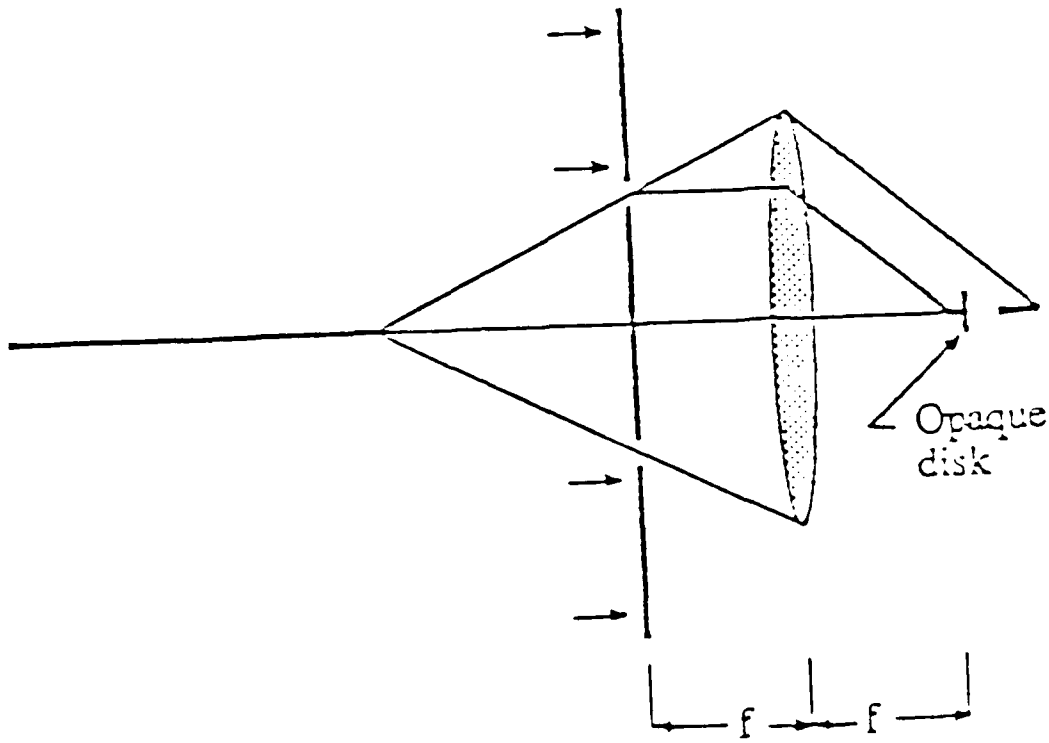

Figure 2A: Image reforms after the opaque disk.

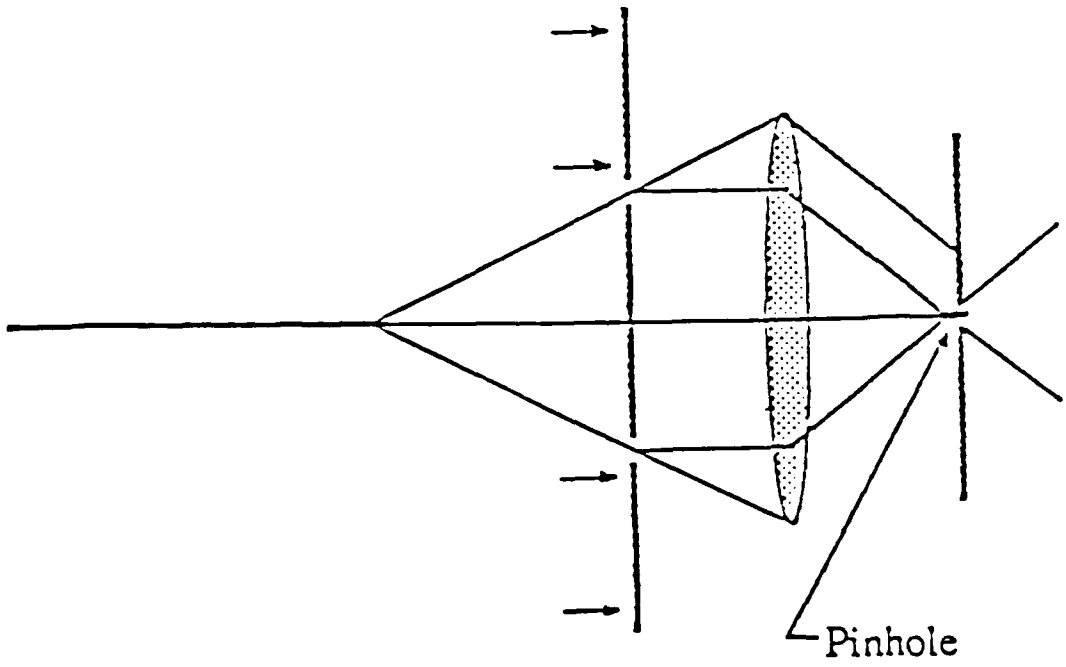

Figure 2B: "Diffractionless Beam" is blocked by a pinhole. Only a cone of light is passed.

Diagram of Apparatus

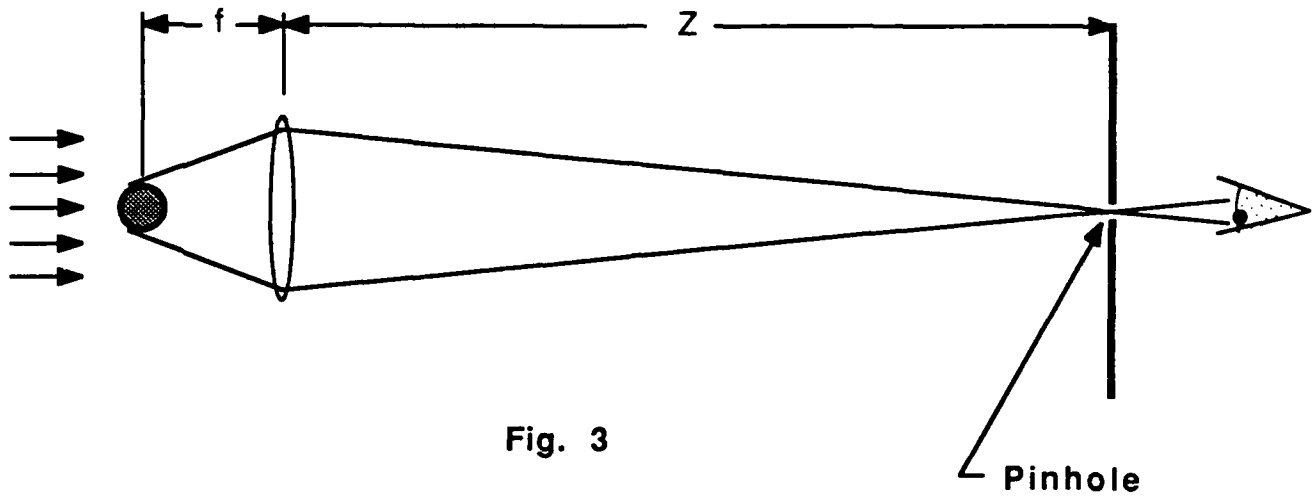

Fig. 3

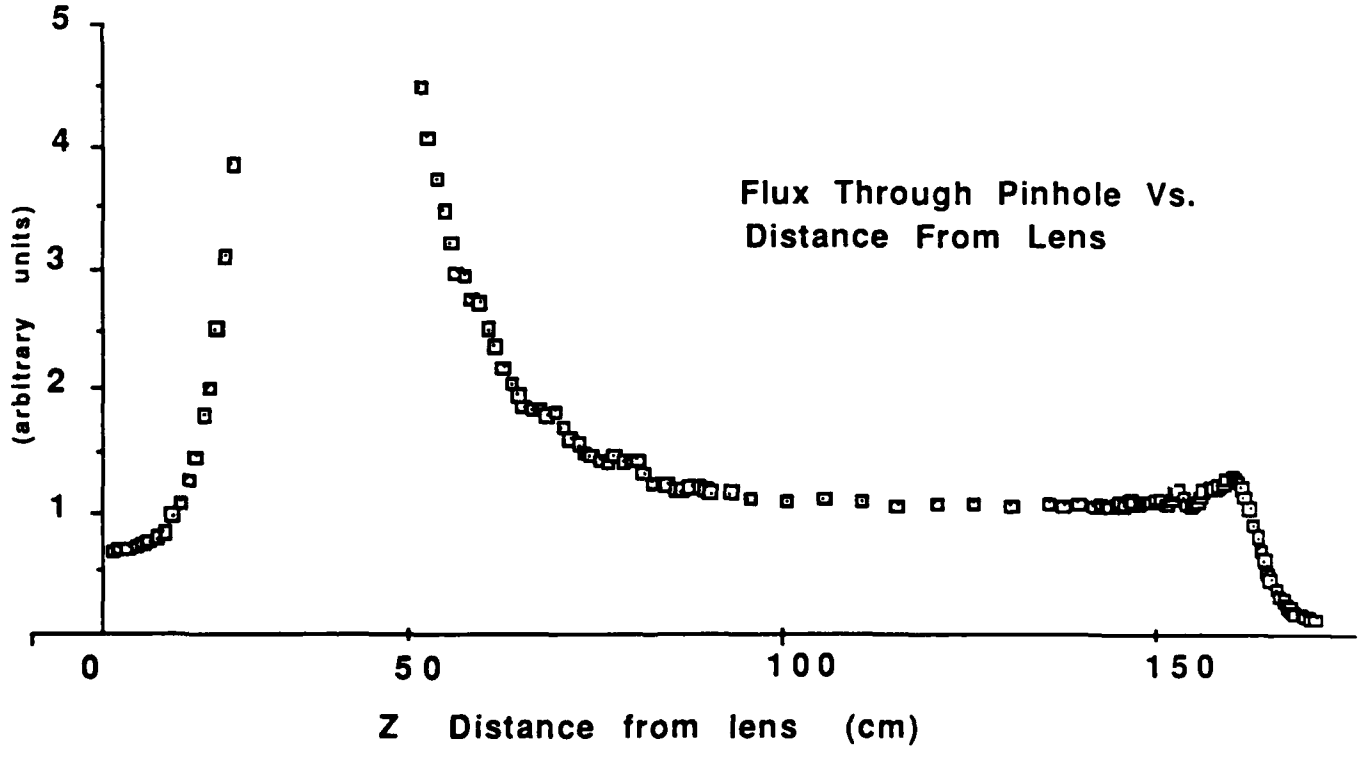

Fig. 4

and a focal length f=250mm. The diameter of the stainless steel ball was d=8mm. A 15mm diameter collimated helium neon laser (λ =6328) was used to illuminate the ball. The maximum range is seen to agree with the theoretical value of $Z_{max}=2Rf/d=156cm$. The plot also shows that the intensity is roughly constant over the latter half of the total range. This large range of constant intensity has not yet been explained. It should be noted that only rays reflecting or diffracting at an angle less than four degrees go through the imaging lens. For reflection, this corresponds to a narrow strip on the surface of the ball with an effective transverse width of about six wavelengths of light so that a geometric treatment of reflection is inappropriate. In future studies we will investigate the region farther away from the lens by modifying the apparatus so that rays with larger angles of reflection and diffraction go through the imaging lens.

The techniques mentioned above, for producing line images, may have several applications. The fact that a small spot persists over a large distance suggests applications in areas such as surveying and optical system alignment. The property of being able to continuously regenerate a spot on axis as one moves along the axis, may be used to align many small objects co-linearly. This same property has been suggested[3] as a mechanism for efficient energy transfer in an inverse free electron laser suggesting the possibility of a compact particle accelerator. It is not yet clear whether such a device can operate with a greater total efficiency than a similar device using a gaussian beam. A better understanding of line images is needed.

This research was also supported by the Office of Naval Research, Contracts N00014-78-C-0517 and N00014-86-G-0154.

References:

1 J. Durnin, J. J. Miceli Jr., and J. H. Eberly, Phys. Rev. Lett. 58, 1499 (1987).

2 D. DeBeer, S. R. Hartmann, and R. Friedberg, to be published

in Phys. Rev. Lett.

3 S. Y. Cai, A. Bhattacharjee, and T. C. Marshal, to be published in the proceedings for the 9th Interntional F.E.L. Conference.

SIGNIFICANT ACCOMPLISHMENTS AND TECHNOLOGY TRANSITION REPORTS

Significant Accomplishments

1. Professor Herman's Solid State Spectroscopy and Process Diagnostics Laboratory were completed this year, and studies of Si-Ge alloy depositions via lasers have begun.

2. Photoions were observed being ejected from Si surfaces under extremely low laser fluence. This phenomena has never been previously observed. The mechanism is now the subject of an intense study.

3. Charge particles have been found to play an unexpectedly important role in the laser etching of copper in a halogen atmosphere.

4. Recombination radiation from semiconductors has been found to produce photon-number-squeezed light if the current driving the device is thermal-noise limited.

5. A new technique for the measurement of interface capacitance has been developed. This technique overcomes the difficulties usually arising from the large diode conductance, so that it has significantly improved our measurement abilities and data accuracy.

6. The observation of negative capacitance reveals that the Shockley-Read recombination theory is inadequate to describe the occupancy of interface states under the influence of hot-carrier injection. In such circumstances, the impact ionization process must be taken into consideration.

7. The new phenomenon of sum-frequency beats in a time-delayed four-wave mixing experiment has been documented and its origin explained. These beats occur in a particular geometry of the excitation pulses where two transitions are exiled in the atomic sample. This lays the groundwork for future spectroscopic and relaxation studies.

8. Continued work towards expanding the technique of Broad-Band Incoherent Four-Wave-Mixing for spectroscopic and relaxation studies in the femtosecond time domain in glass doped with semiconductor (CdS_xSe_{1-x}) microcrystallites, indicates the possible existence of large inhomogeneous broadening for transitions near the conduction band edge, while a homogeneously broadened line shape is observed for excitations well into the conduction band. We believe that varying the optical thickness of our samples acts as a tuning element in the experiment, allowing the study of various parts of the absorption line. Relaxation rates observed by performing a single parameter fit to the theory in the case of low optical density (OD) samples of corning filter CS 2-59 yield T_2=30 fsec. The situation is more complicated for high OD samples where the extremely inhomogeneous line shape observed may be indicative of localized electronic transitions. In this regime T_2 seems to be approximately 45 fsec.

9. Diode lasers have been used to probe the recoil velocity of molecules undergoing collisions with high energy atoms. The Doppler profile of infrared molecular transitions is found to be broadened immediately after collisions occur.

10. A very efficient energy transfer process has been found which converts electronic excitation in VO_2 to vibrational excitation in CO_2.

11. Quantum state probing of photoproducts, chemical reaction products, and collisional product state distributions has been

dramatically improved and broadened through the use of infrared diode lasers.

Technology Transition Reports

1. Professor Flynn's work on the generation and chemical reaction of excited atomic oxygen atoms has become of interest to an industrial group for the purpose of etching organic thin film.

2. The observation of laser photoion emission from surfaces may provide an approach for making a high current electron source for free electron lasers.

3. The obervation of photoions ejected from surfaces by laser irradiation has shown that this ion emission can be supressed by using relatively long wavelength excimer lasers. This finding is important if charge particle emission is harmful as it might be in certain electronic device fabrication steps.

4. Professor Fossum's work in GaAs and silicon CCD's continues to attract industrial interest and support. He recently received funding from Analog Devices for this area of research.

PERSONNEL

Faculty

K. Eisenthal, Professor of Chemistry
G. Flynn, Professor of Chemistry, Co-Director
E. Fossum, Assistant Professor of Electrical Engineering
S. Hartmann, Professor of Physics
R. Osgood, Professor of Electrical Engineering and Applied Physics
P. Prucnal, Associate Professor of Electrical Engineering
M. Teich, Professor of Engineering Science
E. Yang, Professor of Electrical Engineering

Visiting Scientist

Dr. B. Brody

Research Associates

Dr. H. Evans
Dr. T. Kreutz
Dr. J. O'Neill
Dr. D. Podlesnik
Dr. E. Sitzmann
Dr. Z. Wu
Dr. C. F. Yu

Post-Doctoral Research Scientists

J. Hershberger
S. Sarkar
G. Pazionis (IBM Fellow at Columbia Radiation Laboratories)
S. Pang

Graduate Research Assistants

R. Ade
M. Arend
B. Burke
R. Bowman
T. Cacouris
R. Campos
E. Chen
L. Chen
J. Chou
R. Colbeth
D. DeBeer
E. Eid
E. Fu
L. Ge
U. Genser
N. Hakim
S. Hewitt
B. Jalali
J. Jiang
S. Keilson
S. Kemeny
F. Khan
T. Khorsandi
C. Knapp
J. Langan
T. Li
V. Liberman
T. Licata
K. Luo
Q.Y. Ma
F. Moshary
J. Piao
B. Quiniou
D. Rossi
M. Ruberto
E. Sanchez
M. Schmidt
P. Shaw
C. Shu
F. Singer
J. I. Sung
T. Tanabe
H. Tang
S. Todorov
V. Treyz
A. Tuchman
E. Usadi
L. Van Wagenen
L. Welsh
A. Willner
X. Wu
E. Zhang

Administration

Ms. Barbara Blegen
Mr. Andrew Hale
Ms. Cynthia Leslie
Ms. Marie Santoro
Ms. Glady White
Ms. Karen Wingate

Technician

Dave Rivera

Undergraduate Technicians

A. Cubina
C. Delos-Reyes
D. Eiref
N. Joshi
P. Landsberg
M. Levy
A. Mehta
N. Ramlagan
S. Ross
S. Seshadri
S. Shillinger
N. Shoshilas
B. Wendemagegnehu
K. Wong
M. Yang
J. Yee
J. Yves

Dr. Jimmie R. Suttle
U. S. Army Research Office
P. O. Box 12211
Research Triangle Park, NC 27709

Mr. Charles Graff
U. S. Army Comm. - Electronics Command
ATTN: DRSEL-COM-RF-2
Fort Monmouth, NJ 07703

Mr. Edward Kerr
U. S. Army Comm. - Electronics Command
ATTN: DRSEL-COM-RX-2
Fort Monmouth, NJ 07703

Mr. Roland Wright
Night Vision & Electro-Optics Labs
Fort Belvoir, VA 22060

Dr. Robert Rohde
Night Vision & Electro-Optics Labs
Fort Belvoir, VA 22060

Dr. Donn V. Campbell
U. S. Army Comm. - Electronics Command
ATTN: DRSEL-COM-RN-2
Fort Monmouth, NJ 07703

Dr. Nick Karavianis
Harry Diamond Laboratories
ATTN: DELHD-RT-CA
2800 Powder Mill Road
Adelphi, MD 20783

Dr. T. N. Chin
U. S. Army ARRADCOM
ATTN: DRDAR-SCF-10
Dover, NJ 07801

Dr. John Malamus
Night Vision & Electro-Optics Labs
Fort Belvoir, VA 22060

Dr. Rudolf G. Buser
Night Vision & Electro-Optics Labs
ATTN: DELNL-L
Fort Belvoir, NJ 22060

Dr. W. Ealy
Night Vision & Electro-Optics Labs
ATTN: DELNV-AC
Fort Monmouth, NJ 22060

Dr. J. Hall
Night Vision & Electro-Optics Labs
ATTN: DELNV-AC
Fort Belvoir, NJ 22060

Dr. J. Burgess
Night Vision & Electro-Optics Labs
ATTN: DELNV-RM-RA
Fort Belvoir, NJ 22060

DEPARMENT OF THE AIR FORCE

Dr. E. Champagne
AFWAL/AADD-1
Wright-Patterson AFB, OH 45433

Mr. W. Edwards, Chief
AFWAL/AAD
Wright-Patterson AFB, OH 45433

Professor R. E. Fontana
Head, Department of Electrical Engineering
AFIT/ENC
Wright-Patterson AFB, OH 45433

Dr. Alan Garscadden
AFWAL/POOC-1
Air Force Aeronautical Labs
Wright-Patterson AFB, OH 45433

Mr. Alan R. Barnum (CO)
Rome Air Development Center
Griffiss AFB, NY 13441

Chief, Electronic Research Branch
AFWAL/AADR
Wright-Patterson AFB, OH 45433

Mr. John Mott-Smith (ESD/ECE)
HQ ESD (AFSC), Stop 36
Hanscom AFB, MA 01731

Dr. J. Ryles
Chief Scientist
AFWAL/AS
Wright-Patterson AFB, OH 45433

Dr. Allan Schell
RADC/EE
Hanscom AFB, MA 01731

Dr. J. Bram
AFOSR/NM
Bolling AFB, DC 20332

Dr. David W. Fox
AFOSR/NM
Bolling AFB, DC 20332

Dr. J. Neff
AFOSR/NE
Bolling AFB, DC 20332

Dr. N. H. DeAngelis
RADC/ESR
Hanscom AFB, MA 01731

Dr. Gerald L. Witt
Program Manager
Electronic & Material Sciences Directorate
Department of the Air Force
AFOSR
Bolling AFB, DC 20332

Mr. Allan Barnum
RADC/IS
Griffiss AFB, N.Y. 13441

Dr. Tom Walsh
AFOSR/NE
Bolling AFB, DC 20332

Dr. Edward Altshuler
RADC/EEP
Hanscom AFB, MA 01731

DEPARTMENT OF THE NAVY

Naval Surface Weapons Center
ATTN: Technical Library
Code DX-21
Dahlgren, VA 22448

Dr. Gernot M. R. Winkler
Director, Time Service
U. S. Naval Observatory
Massachusetts Avenue at 34th Street, NW
Washington, DC 20390

G. C. Dilworth, Jr.
Technical Director
Naval Coastal Systems Center
Panama City, FL 32407

Naval Air Development Center
ATTN: Code - 301 A. Witt
Technical Library
Warminster, PA 18974

R. S. Allgaier, R-33
Naval Surface Weapons Center
Silver Spring, MD 20910

Office of Naval Research
800 North Quincy Street
ATTN: Code 250
Arlington, VA 22217

Office of Naval Research
800 North Quincy Street
ATTN: Code 411
Arlington, VA 22217

Office of Naval Research
800 North Quincy Street
ATTN: Code 411MA
(Dr. Stuart L. Brodsky)
Arlington, VA 22217

Commanding Officer
Naval Research Laboratory
ATTN: Dr. S. Teitler, Code 7601
Washington, DC 20375

Commanding Officer
Naval Research Laboratory
ATTN: Mrs. D. Folen, Code 2627
Washington, DC 20375

Commanding Officer
Naval Research Laboratory
ATTN: Mr. A. Brodzinsky, Code 5230
Washington, DC 20375

Commanding Officer
Naval Research Laboratory
ATTN: Mr. J. E. Davey, Code 5510
Washington, DC 20375

Commanding Officer
Naval Research Laboratory
ATTN: Mr. B. D. McCombe, Code [illegible]
Washington, DC 20375

Commanding Officer
Naval Research Laboratory
ATTN: Mr. W. L. Faust, Code 6504
Washington, DC 20375

Technical Director
Naval Underwater Systems Center
New London, CT 06320

Naval Research Laboratory
Underwater Sound Reference Detachment
Technical Library
P.O. Box 8337
Orlando, FL 32856

Naval Ocean Systems Center
ATTN: Dr. P. C. Fletcher, Code 92
San Diego, CA 92152

Naval Ocean Systems Center
ATTN: Mr. W. J. Dejka, Code 9302
San Diego, CA 92152

Naval Ocean Systems Center
ATTN: Dr. Alfred K. Nedoluha,
Code 922
San Diego, CA 92152

Naval Weapons Center
ATTN: Dr. G. H. Winkler, Code 381
China Lake, CA 93555

Dr. Donald E. Kirk (62)
Professor and Chairman, Electrical
Engineering
SP-304
Naval Postgraduate School
Monterey, CA 93940

Dr. D. F. Dence
Naval Underwater Systems Center
New London Laboratory
ATTN: Code 34
New London, CT 06320

Director, Technology Assessment
Division (OP-987)
Office of the Chief of Naval Oper.
Navy Department
Washington, DC 20350

Mr. J. W. Willis
Naval Air Systems Command
AIR-310
Washington, DC 20361

Naval Electronics Systems Command
NC #1
ATTN: Code 61R
2511 Jefferson Davis Highway
Arlington, VA 20360

Department of the Navy
Naval Sea Systems Command
ATTN: J. W. Blaine (SEA-09R)
Washington, DC 20362

David Taylor Naval Ship Research
and Development Center
ATTN: Mr. G. H. Gleissner, Code 18
Bethesda, MD 20084

Mr. Martin Mandelberg
Coast Guard R&D Center
Avery Point
Groton, CT 06340

Naval Underwater Systems Center
New London Laboratory
ATTN: 101E (Dr. Edward S. Eby)
New London, CT 06320

Mr. Thomas J. Manuccia, Head
Chemistry and Application Section
Code 6543
Naval Research Laboratory
Washington, DC 20375

Dr. Stephen G. Bishop, Head
Semiconductor Branch
Code 6870
Naval Research Laboratory
Washington, DC 20375

Dr. John W. Rockway
Comm. Technology Prog. Off.
Code 8105
Naval Ocean Systems Center
San Diego, CA 92152

Dr. Barry P. Shay
Joint Program Office,
ODUSD(P)
The Pentagon, Rm 40825
Washington, DC 20301

Dr. Sydney R. Parker
Professor, Electrical Engineering
Code 62PX
Naval Postgraduate School
Monterey, CA 93940

Dr. George B. Wright
Office of Naval Research
Code 427
Arlington, VA 22217

OTHER GOVERNMENT AGENCIES

Dr. Ronald E. Kagarise
Director
Division of Materials Research
National Science Foundation
1800 G Street
Washington, DC 20550

Director
Division of Electrical, Computer
and Systems Engineering
National Science Foundation
Washington, DC 20550

Dr. Dean C. Mitchell
Section Head
Condensed Matter Sciences Section
Division of Materials Research
National Science Foundation
1800 G Street, N. W.
Washington, DC 20550

Judson C. French, Director
Center for Electronics and Electrical
Engineering
B 358 Metrology Building
National Bureau of Standards
Washington, DC 20234

NON-GOVERNMENT AGENCIES

Director
Columbia Radiation Laboratory
Columbia University
538 West 120th Street
New York, NY 10027

Director
Coordinated Science Laboratory
University of Illinois
Urbana, IL 61801

Associate Director of Materials
and Electronics Research
Division of Applied Sciences
McKay Laboratory 107
Harvard University
Cambridge, MA 02138

Director
Electronics Research Center
University of Texas
P. O. Box 7728
Austin, TX 78712

Director
Electronics Research Laboratory
University of California
Berkeley, CA 94720

Director
Electronics Sciences Laboratory
University of Southern California
Los Angeles, CA 90007

Director
Microwave Research Institute
Polytechnic Institute of New York
333 Jay Street
Brooklyn, NY 11201

Director
Research Laboratory of Electronics
Massachusetts Institute of Technology
Cambridge, MA 02139

Director
Stanford Electronics Laboratory
Stanford University
Stanford, CA 94305

Director
Edward L. Ginzton Lab
Stanford University
Stanford, CA 94305

END

DATE

FILMED

DTIC

4/88